Wireless Channel Modeling, Simulation, and Estimation

A Thesis
Presented to
The Academic Faculty

by

Chirag S. Patel

In Partial Fulfillment
of the Requirements for the Degree
Doctor of Philosophy in Electrical and Computer Engineering

School of Electrical and Computer Engineering
Georgia Institute of Technology
May 2006

Wireless Channel Modeling, Simulation, and Estimation

Approved by:

Professor Gordon L. Stüber, Advisor
School of Electrical and Computer Engineering
Georgia Institute of Technology

Professor Gregory Durgin
School of Electrical and Computer Engineering
Georgia Institute of Technology

Professor Mary Ann Ingram
School of Electrical and Computer Engineering
Georgia Institute of Technology

Professor Alfred Andrew
School of Mathematics
Georgia Institute of Technology

Professor Geoffrey Li
School of Electrical and Computer Engineering
Georgia Institute of Technology

Date Approved: March 28, 2006

To my parents

Meeta and Suresh Patel

ACKNOWLEDGEMENTS

My five years at Georgia Tech have been a heady mix of anxiety and excitement. The rewards in waiting to see this day are undoubtedly sweet. Today, I am brimming with a sense of achievement and, more importantly, immense self-satisfaction. I owe this to my family, friends, Professors, and Georgia Tech.

It has been an honor to have Prof. Gordon L. Stüber as my thesis advisor. He has steadily and patiently encouraged my research by providing insightful suggestions and witty criticism. I value the freedom he gave me to pursue different research areas. His influence in shaping me and my career will be ever-lasting.

I also acknowledge the efforts of my dissertation proposal and defense committee members - Prof. Mary Ann Ingram (PhD proposal committee Chair), Prof. Geoffrey Li, and Prof. Gregory Durgin. Their encouragement and feedback during the proposal stage has proved valuable in improving the thesis. I am grateful to Prof. Alfred Andrew of the School of Mathematics for serving as an external committee member. I still remember the great time I had while taking Complex Analysis course under his guidance.

Simultaneously, I have enjoyed working with Dr. Thomas Pratt of Georgia Tech Research Institute. I extend my thanks to him for cooperating in my research efforts.

I have had wonderful lab-mates at the Wireless Systems Lab. Heewon has always been there to lend a patient ear to all my questions. It has been a pleasure to share ideas as well as jokes with Apurva, Joon Beom, Galib, Qing, and Kihong. It has been fascinating to learn the Chinese and the Korean cultures from some of these lab-mates.

The friendship of Shanti, Yogi, Vijay, Sriram, Amol, and Suraj has made these

last five years fly by memorably.

Finally, I thank my parents and other relatives for sharing their love all these years and being there when I needed them most. I owe all my success to their blessings and encouragement.

This work was supported by the Army Research Lab (ARL) and the "Robert J Shackelford Graduate Student Fellowship" provided by the Georgia Tech Research Institute (GTRI). I am indebted to ARL and GTRI for providing me this vital financial support.

TABLE OF CONTENTS

LIST OF TABLES

LIST OF FIGURES

ABBREVIATIONS

AF	Amplify and Forward
AFD	Average Fade Duration
AOD	Average Outage Duration
AR	Auto-regressive
BER	Bit Error Rate
BPSK	Binary Phase Shift Keying
BS	Base Station
CE	Channel Estimation
DF	Decode and Forward
FoO	Frequency of Outage
IFFT	Inverse Fast Fourier Transform
LCR	Level Crossing Rate
LMMSE	Linear Minimum Mean Square Error
LOS	Line of Sight
MEDS	Method of Exact Doppler Spread
MIMO	Multiple-input multiple-output
MMSE	Minimum Mean Square Error
MS	Mobile Station
PSAM	Pilot Symbol Aided Modulation
Rx	Receiver
SoS	Sum-of-sinusoids
SNR	Singal-to-noise Ratio
STBC	Space Time Block Code
Tx	Transmitter

SUMMARY

Several emerging wireless communication systems require direct transmission between mobile terminals to support efficient data transfer and user mobility. Such mobile-to-mobile communication systems differ from the conventional cellular systems where only the user unit is mobile. In addition, there might be a relay, also called a repeater, between the original transmitter and the final receiver to improve the network range and coverage. Potential applications for mobile-to-mobile systems include Intelligent Highways for coordinated traffic control and ad-hoc networks meant for military and disaster management. Relays may be deployed in cellular networks and IEEE 802.16 mesh networks for wireless broadband access.

Extensive research in cellular radio channels has led to the successful deployment of cellular networks. However, our knowledge of the radio channels encountered in mobile-to-mobile and relay-based systems is still inadequate. This forms the primary motivation behind our research in addressing wireless channel modeling, simulation, and estimation issues for these systems.

Specifically, we investigate frequency-flat mobile-to-mobile channels and develop simulation models by using the "sum-of-sinusoids" method, which is widely used for cellular channels. In addition, we present the properties of "amplify and forward" relay channels via theoretical analysis. This analysis, to the best of our knowledge, is the first of its kind. Further, we address the unique challenges, which arise because of the different underlying channel model, for channel estimation in amplify and forward relay systems.

Our work would provide other researchers the necessary tools for the design and testing of these emerging communication systems.

CHAPTER I

INTRODUCTION

1.1 Mobile-to-mobile Communication Systems

Cellular telephony has forever changed the way people communicate with one another, being one of those exciting technologies that has directly and significantly influenced our everyday life. Cellular networks enable people to stay connected with the world from almost anywhere and everywhere, even while "on the move" [42, 73]. Having seen the potential of cellular networks, consumers are demanding better quality of service (QOS), new applications, and increased mobility support from these networks. Fueled by this demand and supported strongly by the advances in semiconductor and signal processing technologies, new communication architectures are being envisioned to improve as well as complement current cellular networks to meet future communication needs. These architectures include ad-hoc and relay based cellular networks of the future [48, 76]. The goals behind using these architectures are to provide increased mobility to users while increasing network coverage, capacity, efficiency, and revenue for the service provider.

A typical cellular network connects different mobile users to one another via a fixed, i.e., stationary Base Station (BS) [42]. In this sense, all present day cellular radio links are mobile at one end only - the user end, while the service provider end is stationary. In contrast, ad-hoc networks are envisioned to eliminate the need for central BSs by directly connecting mobile users to one another [3, 48]. Therefore, they are also referred to as "mobile-to-mobile" or "doubly mobile" networks [82]. In such networks, all the nodes are mobile and data is routed by relaying from one node to another. Sometimes a mobile BS might be present as a central controller.

Mobile-to-mobile communications find applications in commercial as well as military arenas. The walkie-talkies or two way radios that have been in use for a long time are a simple example of mobile-to-mobile communication systems. But, traditionally, they employ analog modulation such as frequency modulation (FM). In contrast, future systems will need digital modulation formats to meet high data rate, QOS, and higher user mobility requirements. Therefore, the emphasis is toward research and design of digital mobile-to-mobile communication systems. Several applications such as Intelligent Highway Vehicular Systems (IHVS) for automated traffic control on highways, broadband audio and multimedia content delivery to mobile users, and emergency rescue operations [4, 24, 25, 30] are currently being explored. Efforts are being made to standardize technologies for the IHVS through the IEEE Dedicated Short Range Communication (DSRC) standard [1]. On the military front, ad-hoc networks offer the advantage of on-the-fly installation in battlefield environments without the need of a burdensome and inflexible fixed BS infrastructure. Some of the benefits of ad-hoc networks can be harvested by cellular networks by deploying intermediate relays that connect the mobile station (MS) to the fixed BS. The relay can be fixed or mobile. Such relay-based cellular networks promise increased reach and capacity of the existing networks [48].

As we observe, mobile-to-mobile communication is likely to become more prevalent in future communication systems. Being a relatively new area of research, it poses numerous interesting research problems. The first and perhaps the most important task to be carried out while designing a wireless communication system is to understand the nature of the wireless channel involved in communicating between two ends of the link. Only sound knowledge of the radio propagation channel can enable efficient, in-time, and practical design and testing of communication systems. Channel knowledge is required to understand various impairments such as attenuation, multipath fading, and time variations in the channel, which are discussed in

detail in Chapter II. Using this knowledge, communication systems can be designed to obtain optimal or near optimal performance. This philosophy has been the driving force behind more than four decades of research on wireless channels for applications like terrestrial and satellite broadcast and cellular networks.

Cellular (fixed BS to MS) channels have generated a considerable interest among the researchers owing to the challenges posed by the user terminal's mobility. Traditional research topics include: i) developing theoretical channel models , ii) conducting real-world channel measurements and deriving channel models from these measurements [12, 45], iii) developing simulation models for computer simulation of communication systems [35], and iv) developing hardware based channel emulators for real-time system testing. This research has led to standardized channel models for cellular systems in the form of COST 207, COST 231, IMT-2000, and 3GPP channel models [2, 6, 7]. The advent of multiple-input multiple-output (MIMO) antenna systems has led to extension of these models to incorporate spatial dimension into these models [22]. Numerous techniques available in the literature for simulating cellular channels in software are complemented by commercial hardware based real world channel emulators [5, 19, 36, 56, 57, 58, 59, 60, 61]. Such simulation capabilities enable the design, testing, and optimization of systems without conducting time consuming and expensive field trials before actual system deployment. Thus, the research in cellular channels has a rich and fascinating history. Unfortunately, the same is not true for mobile-to-mobile radio channels.

Though narrow bandwidth mobile-to-mobile fading channels were theoretically studied by Akki and Haber in the '80s [9, 10], no particular attention was paid to them due to lack of compelling applications. However, the new interest in mobile-to-mobile communications has led to some theoretical research on these channels as described in [43, 80, 81]. Real world channel measurements have been provided in [8, 31, 39, 46]. However, standardized narrowband or wideband mobile-to-mobile

channel models or methods to simulate them are yet to be developed. Therefore, our research focuses on the study and simulation of narrowband mobile-to-mobile wireless channels. We develop "sum-of-sinusoids" (SoS) models to simulate mobile-to-mobile channels by using the SoS modeling framework widely used for cellular channels [36, 56]. Statistical as well as deterministic simulation models are developed to provide a performance vs. complexity trade-off to the system designer. The properties and the performance of these models are rigorously verified by applying theoretical and simulation tools. This work improves upon the work in [81] and serves as an extension of the work presented by the author in [55].

1.2 Relay-based Communication Systems

In a relay-based communication system, transmission between the source and the destination is achieved through an intermediate transceiver unit called a relay or a repeater. Often, large distances between the source and the destination preclude direct communication between them due to high attenuation in the propagation medium. In such scenarios, a repeater is placed between the source and the destination to achieve end-to-end communication. Such use of relays is widely prevalent in fiber optic networks [64]. Satellite transponders used for a wide range of commercial and military applications are also examples of relay-based systems. But, implementation complexity and other practical constraints have prevented the use of relays for mobile communications until now. However, with advances in electronics and semiconductor technologies, their use for wireless, mobile communications seems feasible. As a result, relay-based systems have become a hot research topic in the wireless research community in recent years. They are proposed under different names such as "cooperation diversity" [41, 69, 70], "virtual antenna arrays" [20] or multihop networks [48]. Potential application areas of cooperation diversity are the next generation cellular networks, mobile wireless ad-hoc networks, and mesh networks for wireless broadband

access. Besides increasing the network coverage, relays can provide additional diversity to combat the effects of the wireless fading channel. Such diversity schemes are discussed further in Chapter II. These interesting capabilities offered by relay-based systems motivate us to study the propagation medium encountered in such systems. While mobile-to-mobile radio channels have two mobile nodes involved, relay channels with three nodes effectively have two links cascaded together: the link from the MS to the relay and the link from the relay to the fixed BS [32, 48, 88]. Depending on the mobility of the relay, the overall channel is either a cascade of mobile-to-mobile and mobile-to-fixed links or mobile-to-fixed and fixed-to-fixed links, as illustrated in Figure 1. It is logical to assume that the cascading of different links causes the relay channel to have characteristics that are very different from the individual fixed-to-mobile link or the mobile-to-mobile link. However, fading relay channels have not been studied yet in detail. There is no known reference that describes the fading and time-domain behavior of relay fading channels.

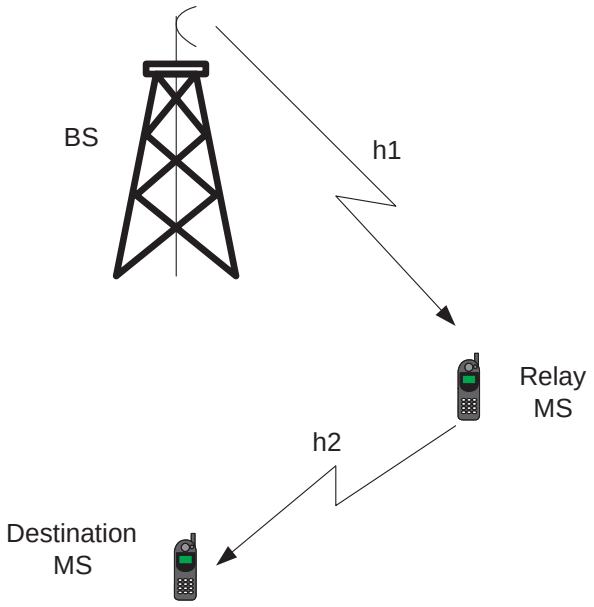

Figure 1: Relay channel example.

Therefore, we evaluate the properties of relay channels via theoretical analysis. We concentrate on "amplify and forward" relay channels, where the relay simply amplifies the signal received from the transmitter and forwards it to the final receiver.

1.3 Channel Estimation

As mentioned earlier, the propagation channel induces various impairments in the transmitted signal. Such impairments include time varying attenuation and phase changes that distort the transmitted data. Typically, a receiver mitigates these distortions for reliable demodulation of the transmitted data. This reception strategy is called coherent demodulation [63]. It should be noted that data demodulation is possible even without compensating the channel distortions by suitably adapting the transmission modulation. But, the performance of this reception scheme, termed non-coherent demodulation, is inferior compared to that of coherent demodulation in terms of the bit error rate (BER) achieved for a given amount of transmit power [74]. Therefore, most modern communication systems prefer coherent reception.

Coherent reception requires the receiver to acquire channel knowledge to compensate for the channel induced distortions. The process of acquiring the channel knowledge is called channel estimation and is an integral part of most communication receivers. Apart from the knowledge of channel statistics, the channel estimator also requires knowledge of the instantaneous channel values to track the channel fading and compensate it. Typically, known symbols called "pilot" symbols are multiplexed along with the data to aid the receiver in channel estimation [17]. This estimation scheme is called pilot symbol aided modulation (PSAM). Sophisticated signal processing algorithms are then applied by the estimator to acquire the channel knowledge and track it using pilot symbols.

The problem of channel estimation for cellular channels has been widely and successfully addressed in the literature. Estimation schemes capable of tracking the

fading channel in cellular systems are an integral part of standardized systems such as GSM and cdma2000. A detailed description of various estimation schemes can be found in the excellent survey paper [77] and the references therein. However, channel estimation in relay-based systems is still an open problem. Whether the existing estimation schemes can cope up with the different underlying channel model in relay-based systems is not known yet. Mobile-to-mobile channels undergo faster fading compared to cellular channels due to the increased mobility. Estimation schemes that can track this fast fading are required for mobile-to-mobile systems. On the other hand, for amplify and forward relay systems the cascading of two channels poses unique questions such as i) how to estimate the overall channel?; and ii) can existing estimation schemes be applied to estimate the cascaded channel without any sacrifice in performance? These issues have not been explored so far. Therefore, we address the problem of channel estimation for amplify and forward relay systems. Different estimation strategies such as Linear Minimum Mean Square Error (LMMSE) estimation and linear interpolation using pilot symbols are evaluated using the channel models we develop in our work. These and other research contributions are briefly summarized below.

1.4 Research Contributions

- Comprehensive analysis of statistical simulation models for cellular channels [52].
- Development of novel simulation models for mobile-to-mobile channels by introducing "double ring" scattering environment model [51, 53].
- Derivation of the properties of amplify and forward relay channels and their simulation [54].

- Evaluation of LMMSE channel estimation for amplify and forward relay systems. We also present approximate theoretical analysis to evaluate the impact of estimation errors on the BER [50].

1.5 Thesis Outline

The remainder of the thesis is divided into five additional chapters. In Chapter II, we review the theory of cellular and mobile-to-mobile channels and describe common radio channel impairments like multipath fading and path loss. We also describe important channel simulation philosophies in Chapter II. Chapter III presents our analytical results that compare different statistical simulation models used for cellular channels. These results provide guidelines to develop simulation models, which are presented in Chapter IV, for mobile-to-mobile channels. In Chapter V, we turn our attention to results describing the properties of amplify and forward relay channels. Chapter VI presents results pertaining to channel estimation for relay systems. Finally, in Chapter VII, we conclude by summarizing our research contributions and open areas of research in wireless channel modeling, simulation, and estimation.

CHAPTER II

BACKGROUND

The importance of understanding the radio propagation channel for successful design of communication systems can never be overstated. All wireless communication textbooks invariably begin with a brief discussion on the properties of the radio channel. Earlier, the wireless medium was viewed as an obstacle or a limiting factor in designing reliable communication links. However, decades of research and subsequent insights have changed this paradigm. Modern day communication systems rather tend to exploit the channel knowledge for increasing system reliability and capacity by employing techniques such as diversity and MIMO [78]. Schemes such as multi-user diversity are being employed in third generation (3G) cellular networks to optimally serve different users depending on their channel conditions. Thus, a good understanding of the wireless channel is the key for extending the limits of existing communication systems. With this view in mind, we discuss important concepts like path loss, shadow fading, multipath propagation, types of fading, and time-frequency selectivity of mobile radio channels in this chapter. This discussion is followed by a description of cellular, mobile-to-mobile, and amplify and forward relay channels that form the basis of our research. It must be noted that with a slight abuse of notation, we use the terms wireless channels and mobile channels interchangeably because all wireless channels of interest in this work have some degree of mobility in them.

- **Path loss**

  Path loss refers to the attenuation in the transmitted signal while propagating from the transmitter (Tx) to the receiver (Rx). Path loss is caused by dissipation of the radiated power as well as effects of the propagation channel such as absorption due to moisture. Typical path loss models assume a distance

dependence attenuation, i.e., the received power is a function of the distance between the Tx and the Rx. Significant variations in the path loss are observed over distances of several hundred to thousand wavelengths.

The simplest path loss model corresponds to propagation in free space, i.e., line-of-sight (LOS) link between the transmitter and receiver. Under this model, the received signal power is given as

$$P_R = P_T G_T G_R \frac{\lambda^2}{4\pi d^2}, \tag{1}$$

where P_T is the transmitted power, G_T and G_R are the transmit and receive antennas gains, respectively, λ is the transmitted carrier wavelength, and d is the distance between the Tx and the Rx. Thus, the received power decreases with a factor of distance-squared under free space propagation. We also observe the path loss dependency on the transmitter wavelength. Shorter the wavelength or equivalently higher the transmitter frequency, higher the path loss.

Though simple, the free space path loss model cannot capture all the propagation scenarios encountered in the real world. Therefore, several different models such as Okumura, Hata, Walfish-Ikegami, etc., [74] have been proposed to model path loss in different propagation environments such as urban, rural, and indoor areas. Experiments show that typical path loss exponents, i.e., the power of the distance dependence in (1) is around 3-5, thus suggesting higher attenuation than free space propagation conditions. In addition, these models also capture the path loss dependence on factors such as the heights of antennas and surrounding structures as well as seasonal variations. A detailed description on different path loss models can be found in [27, 74].

- **Shadow fading**

  The path loss model described above assumes the path loss to be constant at a given distance. However, the presence of obstacles such as buildings and

tress results in random variations of the received power at a given distance. These variations also arise due to change in scattering and reflecting surfaces in the propagation environment. This effect is termed shadow fading. The shadow fading variations are observed over distances of tens to hundreds of wavelengths. In the presence of shadow fading, the received signal power can be written as

$$P_R = P_T G_T G_R P_L S, \tag{2}$$

where P_L and S correspond to the path loss and the shadow fading contributions, respectively.

Experimental results show that the shadow fading can be fairly accurately modeled as a log-normal random variable. In other words, the shadow fading behaves as a Normal (Gaussian) random variable when S is expressed in the dB domain. Thus, the shadow fading distribution is given by

$$f_S(s) = \frac{10}{s\sigma_s\sqrt{2\pi}\ln 10} \exp\left[-\frac{(10\log s - \mu_{PL})^2}{2\sigma_s^2}\right], \tag{3}$$

where μ_{PL} is the path loss expressed in dB and σ_s is the shadow fading standard deviation. Typical σ_s values range from 5-10 dB. Thus, shadow fading (in dB) behaves as a Gaussian random variable with mean and standard deviation determined by the average path loss and σ_s, respectively.

Measurements show that the shadow fading exhibits spatial correlation, i.e., shadow fading is correlated over short distances. The spatial correlation is given by the exponential correlation model proposed by Gudmundson [29] based upon an approximate fitting of empirical data. According to this model, the spatial correlation is quantified as

$$R_S(\Delta x) = \sigma_s^2 \exp\left(-|\Delta x|/d_c\right), \tag{4}$$

where Δx is the spatial separation between points at which the correlation is measured and d_c is the spatial de-correlation distance. Typically, the shadow

fading de-correlation distance d_c ranges from 10-50 m. It must be noted that though theoretical results preclude an exponential correlation model for shadow fading, it is still widely used because it provides a reasonably good fit to experimental data [44].

When the Rx is mobile, these spatial correlation translates into time correlation. Therefore, the shadow fading behaves as a correlated, time-varying process. The time auto-correlation can be obtained from (4) by substituting $\Delta x = vt$, where v is the Rx speed and t is the time variable.

The above discussion suggests that path loss and shadow fading variations become significant when the receiver moves over distances greater than several tens of the carrier wavelength. As a result, these effects are often called large scale effects. Large scale effects play an important role in the system design at the network level. For example, the cell coverage area, outage, and handoffs are influenced by these effects. On the other hand, small scale fading caused by multipath propagation, which is described below, determines the link level performance in terms of the BER, average fade durations, etc.

- **Multipath propagation and fading**

  Figure 2 depicts a typical transmission scenario encountered in mobile radio channels. Either the Tx or the Rx or both may be in motion depending on the application. Figure 2 depicts the Tx and the Rx surrounded by local scatterers, a natural scenario for mobile-to-mobile channels owing to low elevation antennas at both the Tx and the Rx. However, for cellular radio, where the BSs have high elevation antennas, the BSs may be free from local scatterers. The presence of local scattering objects, either natural, such as foliage, mountains, or man-made, such as buildings, obstructs a direct radio wave path between the Tx

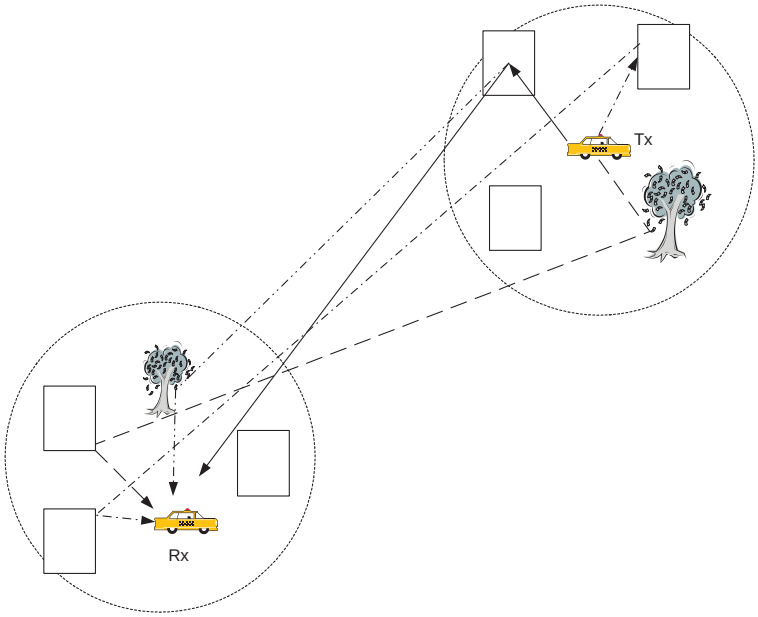

Figure 2: Example of scattering environment in mobile radio channels.

and the Rx giving rise to non line-of-sight propagation (NLOS). The transmitted radio waves suffer reflection, diffraction, and/or scattering on falling upon various obstacles. As a result, the received signal is a combination of several different waves, also termed paths, arriving from different directions with random delays due to different path lengths traveled by them. This propagation mechanism is called multipath propagation, which is discussed below from a physics viewpoint.

Let us consider the local area scattering conditions, i.e., assume the receiver to be sufficiently far away from the scatterers so that only homogenous plane waves constitute the received signal [22]. When an impulse is transmitted through the channel, the received signal or, equivalently, the channel impulse response consisting of several homogeneous plane waves can be represented as

$$h(\overrightarrow{r}) = \sum_{n=1}^{N} V_n \exp\left\{ j \left(\frac{2\pi}{\lambda} \hat{k_n} \cdot \overrightarrow{r} + \phi_n \right) \right\}, \tag{5}$$

where $\overrightarrow{r}$ is the vector representing the receiver translation in the spatial dimension, V_n and ϕ_n are the amplitude and the phase, respectively, of the n^{th}

wave component while $\hat{k_n}$ is the unit vector in the direction of the propagation of the n^{th} component. The phase ϕ_n captures the phases changes introduced by interaction with the scatterers as well as those due to the distance traveled by the wave from the Tx to the Rx. A reasonable assumption is that the phases are uniformly distributed over $[-\pi,\pi)$. Typically, for NLOS propagation the amplitudes of the wave components are of the same order and have magnitude very small compared to the total average power in the received signal. Such wave components are called diffuse wave components. Because of their random phases, these diffuse components combine vectorially giving rise to constructive and destructive interference, thereby forming a resultant signal whose amplitude varies in the spatial dimension. When the Rx is mobile, this amplitude variations along the space translate into amplitude variations with time. This phenomenon is called multipath fading. This spatial to time domain translation is easily observed by substituting $\overrightarrow{r} = \overrightarrow{v}t$, where $\overrightarrow{v}$ is the Rx velocity vector. We can re-write equation (5) in time domain as

$$\begin{aligned} h(t) &= \sum_{n=1}^{N} V_n \exp\left\{ j\left(\frac{2\pi}{\lambda} \hat{k_n} \cdot \overrightarrow{v}t + \phi_n \right) \right\} \\ &= \sum_{n=1}^{N} V_n \exp\left\{ j\left(\frac{2\pi}{\lambda} v\cos(\alpha_n)t + \phi_n \right) \right\}, \end{aligned} \tag{6}$$

where v is the speed of the Rx and α_n is the angle between the direction of wave propagation $\hat{k_n}$ and the Rx velocity vector $\overrightarrow{v}$. Note that $f_n = (2\pi v\cos(\alpha_n))/\lambda$ is the Doppler shift produced by the Rx moving at a speed v.

In the presence of such diffuse components, the fading is described by a Rayleigh distribution. Figure 3 plots the received signal envelope under these Rayleigh fading conditions. It is evident that the mobile Rx can experience fades as deep as 20-30 dB below the mean power level within a fraction of a second (or equivalently over a distance of one wavelength because of fading).

Diffuse wave components arise under NLOS propagation due to the presence

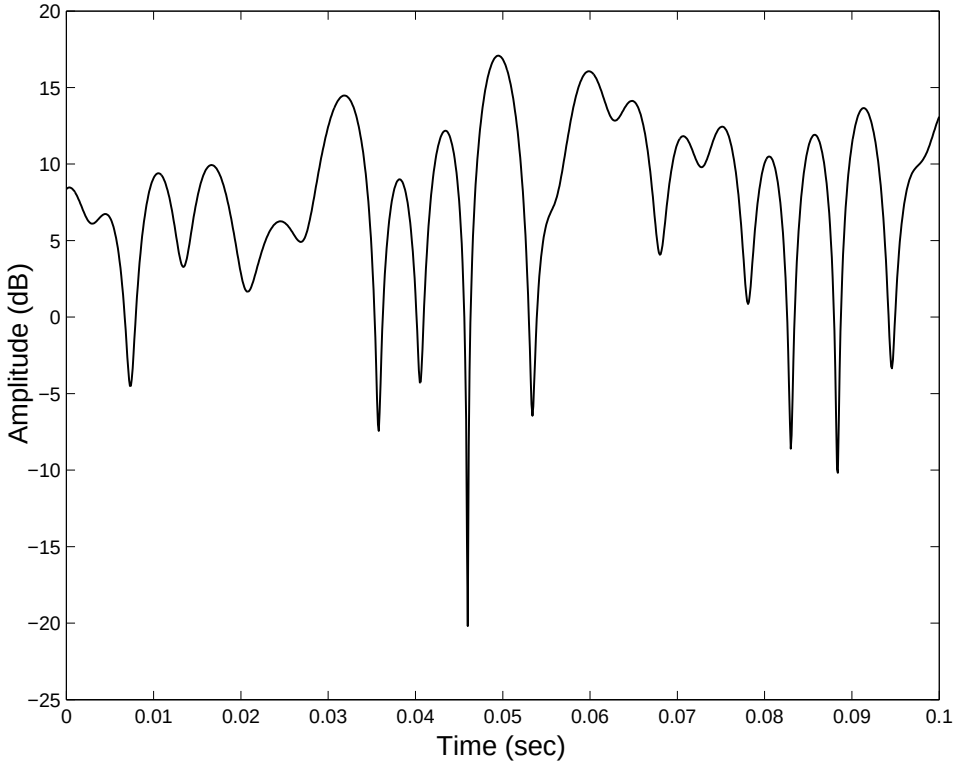

Figure 3: Rayleigh faded signal envelope.

of several scatterers in the environment. However, when a LOS or a strong reflected path, termed specular component, also arrives at the receiver, the fading is more appropriately modeled by a Rician distribution [74]. A detailed analysis on these multipath channels can be found in [36, 73]. The interested reader is also referred to [22] for a detailed discussion on fading and the physics behind it.

- **Time and frequency selectivity**

  The above discussion implicitly assumed the Rx bandwidth to be small enough so that multipath arriving at different delays cannot be resolved. However, if the Rx bandwidth is sufficiently large, then multipath arriving with different delays can be resolved at the receiver, the resolution being inversely proportional to the Rx bandwidth. Under such circumstances, the impulse response in (6) should be modified to to incorporate multipaths arriving at different resolvable

delays. This delay-resolved channel impulse response is given by

$$h(t,\tau) = \sum_{l=0}^{L-1} g_l(t)\delta(\tau - \tau_l), \tag{7}$$

where L is the total number of resolvable multipath components, $g_l(t)$ is the time-varying complex envelope associated with the l^{th} resolvable multipath arriving with an average time delay τ_l. Note that each $g_l(t)$ is of the form (6) and consists of all non-resolvable multipaths arriving within delay $\tau_l - 1/(2B)$ to $\tau_l + 1/(2B)$, B being the receiver bandwidth. Thus, each $g_l(t)$ is either Rayleigh or Rician faded. With this channel impulse response, if a signal $s(t)$ is transmitted, the received signal is given by

$$r(t) = s(t) * h(t,\tau) = \sum_{l=0}^{L-1} g_l(t)s(t - \tau_l), \tag{8}$$

where $*$ is the linear convolution operator. Therefore, we can interpret $h(t,\tau)$ as the channel impulse response at time t corresponding to an impulse applied at time $t - \tau$. Two important properties stand out from the above channel impulse response - time selectivity and frequency selectivity.

Time selectivity refers to the change in the channel impulse response with time. The motion of the Tx, the Rx or the scatterers results in change in the scattering objects in the environment due to which the impulse response also changes. For example, an impulse applied at time $t_1 - \tau$ will experience a different channel compared to an impulse applied at some other time $t_2 - \tau$, i.e., the impulse response is time-variant or time selective. When viewed in the frequency domain, time selectivity appears as Doppler shifts in the transmitted signal causing a broadening of the transmitted signal spectrum. This effect is also called frequency dispersion. Based on the rate with which the channel impulse response changes relative to the signal transmission rate, channels may be classified as fast fading or slow fading. Fast fading implies that the channel changes within

the transmitted symbol duration, while slow fading implies that the channel is approximately constant within a symbol duration. A good measure of channel selectivity is given by the channel coherence time or, equivalently, the Doppler spread, i.e., the time duration for which the channel can be considered to be approximately time-invariant. The Doppler spread depends on the maximum Doppler frequency shift f_d arising from the mobility in the environment. The higher the maximum Doppler shift, the higher the Doppler spread. Equivalently, coherence time is inversely proportional to the Doppler spread.

The multipath delay spread due to multipaths arriving at different time delays leads to frequency selectivity of channels. Frequency selectivity causes different transmitted frequencies to undergo different amplitude and phases changes and requires equalization at the receiver to remove these effects for data recovery. To make the notion of frequency selectivity explicit, we express the time-varying impulse response $h(t, \tau)$ in the frequency domain by taking the Fourier transform with respect to the variable τ to obtain the channel transfer function

$$\begin{aligned} H(t, f) &= \mathcal{F}_{\tau}[h(t, \tau)] \\ &= \sum_{l=0}^{L-1} g_l(t) \exp\left(-j2\pi f \tau_l\right). \end{aligned} \tag{9}$$

Thus, we observe that different frequencies (f's) will have different amplitude and phase determined by the multipath time delays. This effect is termed frequency selective fading. Based on their degree of frequency selectivity, channels may be classified as frequency-flat or frequency selective channels. If all the transmitted frequencies undergo approximately identical amplitude and phase changes, the channel is termed frequency flat. However, if they experience different amplitude and phase changes, the channel is termed frequency selective. Frequency selectivity is measured in terms of the coherence bandwidth, i.e, the

bandwidth over which channel's frequency response remains constant. Approximately, the coherence bandwidth is inversely proportional to the multipath delay spread. Thus, if the transmission bandwidth is less than the channel's coherence bandwidth, the channel appears as frequency flat.

Frequency selective channels have a minimum of two resolvable multipath components, i.e. $L \geq 2$ while for frequency non-selective channels $L = 1$. Applying (8), we notice that for frequency non-selective channels the received signal is simply the multiplication of the transmitted signal with the complex channel envelope $g_0(t)$, i.e.,

$$r(t) = g_0(t)s(t). \tag{10}$$

The above description suggests that a frequency-flat form is the most basic representation of mobile radio channels. By combining several frequency-flat channels at different delays, a frequency non-selective channel can be characterized in the form of a tapped delay line model with the aid of power-delay profile data [74]. Owing to this fundamental importance of frequency-flat channels, we concentrate on modeling and simulating frequency-flat channels throughout the thesis. Our frequency-flat models can then be extended to the case of frequency-selective channels. Our assumption of frequency-flat channel nature is valid if the transmission is narrowband compared to the channel's coherence bandwidth.

2.1 Cellular Channels

A cellular channel refers to the channel between a fixed BS to a MS (or vice versa) in current cellular networks. A tremendous amount of research has been conducted on cellular channels in the past four decades resulting in several modeling and simulation approaches for cellular channels. The pioneering work done by Clarke provides a theoretical reference model for narrowband cellular channels [19]. The model is

mathematically convenient and has also been validated by extensive measurements resulting in its incorporation into standard channel models [6]. We discuss the properties of this model below, assuming transmission from a BS to a MS.

Clarke's model defines the complex channel gain under narrowband, frequency flat fading, and NLOS propagation assumptions as [19]

$$g(t) = \sqrt{\frac{2}{N}} \sum_{n=1}^{N} \exp\{j[\omega_d t \cos(\alpha_n) + \phi_n]\}, \tag{11}$$

where N is the number of propagation paths and ϕ_n is the random phase of the n^{th} multipath component, uniformly distributed over $[-\pi, \pi)$.[1] The maximum angular Doppler frequency, ω_d, is determined by the carrier wavelength λ and the vehicle speed v as $\omega_d = 2\pi f_d = (2\pi v)/\lambda$, where f_d is the maximum Doppler frequency in Hertz. The angle of arrival α_n depends on the scattering environment and the antenna radiation pattern. An often used assumption for cellular channels is that the BS is free of local scatterers because of its high elevation antennas, while the MS is uniformly surrounded by scatterers in the horizontal plane. Then, assuming omni-directional transmit and receive antennas and two-dimensional (2-D) isotropic scattering around the MS, the angle of arrival $\alpha_n \sim U[-\pi, \pi)$ and is independent of the ϕ_n's. For sufficiently large N, the Central Limit Theorem [49] can be invoked to show that the in-phase (I) component $g_i(t) = \Re\{g(t)\}$ and the quadrature (Q) phase component $g_q(t) = \Im\{g(t)\}$ of the complex envelope are zero-mean Gaussian. The I and Q components are also independent if the 2-D isotropic scattering assumption is satisfied. Therefore, the envelope $|g(t)|$ is Rayleigh distributed. As a result, the received power level undergoes significant fluctuations with time, thus making reliable communication a challenging task. Nevertheless, sufficient knowledge of the fading properties can be exploited to the system's advantage [74]. We briefly discuss some properties of the fading channel here.

[1] Henceforth, a uniform distribution over the interval $[a,b)$ will be denoted as $\sim U[a,b)$.

Properties of cellular channels

Let the I and Q components be zero mean, independent Gaussian random variables with unit variance. The probability density functions (pdf) of the channel envelope, phase, and the squared envelope are given as follows:

- The pdf of the channel envelope $\alpha_e = |g(t)|$:

$$f(\alpha_e) = \alpha_e \exp\left\{-\frac{\alpha_e^2}{2}\right\} \qquad \alpha_e \geq 0, \tag{12}$$

  which corresponds to a Rayleigh distributed envelope.

- The pdf of the channel phase $\Phi = \arg\{g(t)\}$:

$$f(\Phi) = \frac{1}{2\pi} \qquad -\pi \leq \Phi \leq \pi, \tag{13}$$

  i.e., the phase of the complex channel $g(t)$ is uniformly distributed of [-π,π).

- The pdf of the squared envelope $\beta = \alpha_e^2$

$$f(\beta) = \frac{1}{2}\exp\left\{-\frac{\beta}{2}\right\} \qquad \beta \geq 0. \tag{14}$$

  Thus, the channel power α_e^2 follows an exponential distribution.

Assuming the channel is wide-sense stationary (wss), the correlations in the time-domain for the I and Q components as well as the channel complex envelope and squared envelope are given by

$$\begin{aligned}
R_{g_{i/q}g_{i/q}}(\tau) &= \mathrm{E}[g_{i/q}(t+\tau)g_{i/q}(t)] = J_0(\omega_d\tau) && (15)\\
R_{g_ig_q}(\tau) &= R_{g_qg_i}(\tau) = 0 && (16)\\
R_{gg}(\tau) &= \frac{1}{2}\mathrm{E}[g(t+\tau)g^*(t)] = J_0(\omega_d\tau) && (17)\\
R_{|g|^2|g|^2}(\tau) &= \mathrm{E}[|g(t+\tau)|^2|g(t)|^2] \\
&= 4 + 4J_0^2(\omega_d\tau), && (18)
\end{aligned}$$

where E[·] is the statistical expectation operator, $*$ is the complex conjugate operator, and $J_0(\cdot)$ is the zeroth order Bessel function of the first kind. The corresponding Doppler spectrum is represented as

$$\begin{aligned} S_{gg}(f) &= \frac{1}{\pi f_d} \frac{1}{\sqrt{1-(f/f_d)^2}} && 0 \leq |f| \leq f_d \\ &= 0 && \text{otherwise.} \end{aligned} \tag{19}$$

The above equation defines the well-known U-shaped spectrum of cellular channels, which is plotted in a later section.

Besides these properties, higher order statistics such as the level crossing rate (LCR) and the average fade duration (AFD) are also important.

LCR: The LCR is defined as the rate at which the channel envelope $\alpha_e = |g(t)|$ crosses a specified level with a positive (or negative) slope. The LCR affects handoff probability and outage statistics and therefore it is of interest in system design [74]. For cellular channels with 2-D isotropic scattering, the LCR of the envelope α_e at level R is given by

$$L_{\alpha_e=R} = \sqrt{2\pi} f_d \rho \exp(-\rho^2), \tag{20}$$

$$\rho = \frac{R}{\sqrt{\mathrm{E}[\alpha_e^2]}}. \tag{21}$$

AFD: The AFD, which is the average time duration the envelope spends below a specified threshold, is given by

$$T_{\alpha_e=R} = \frac{1}{\sqrt{2\pi} f_d \rho}(\exp(\rho^2) - 1). \tag{22}$$

The knowledge of these statistical properties enables the system designer to make informed decisions regarding the choice of modulation, interleaving, and coding scheme to be used at the transmitting end and the type of channel estimator and decoder to be used at the receiving end. This is achieved by simulating the entire system along with the underlying channel model in software to assess system performance. Therefore, channel simulation is an important component in the design cycle.

The goal of any channel simulator is to reproduce the channel's desired properties in simulations to recreate real world propagation effects. Several simulation models are available in the literature for cellular channels. A brief introduction to these models is provided in Section 2.4. However, literature survey shows that comprehensive analysis comparing these models is not available. Issues such as relative performance, complexity, and feasibility for practical applications of these models have not been addressed thoroughly. Therefore, in Chapter III we address these important issues to provide a better understanding of cellular channels' simulation models. This analysis also provides insights for developing simulation models for mobile-to-mobile channels.

2.2 Mobile-to-mobile Channels

Mobile-to-mobile wireless communication channels have characteristics that are widely different from cellular channels. A detailed description of mobile-to-mobile channels can be obtained from [43, 9, 10]. Here, we provide a brief comparison between the statistical properties of mobile-to-mobile channels and cellular channels to demonstrate the need for developing new methods to simulate mobile-to-mobile channels.

Consider transmission from a mobile Tx to a mobile Rx. The propagation path between the Tx and the Rx is obstructed by buildings, foliage, etc. resulting in NLOS propagation conditions. The transmitted signal undergoes reflection, diffuse scattering, and diffraction on encountering the obstacles. As a result, the received signal is a sum of several different scattered or reflected paths. Each path has its own amplitude, random phase, and a Doppler shift induced by the motion of the Tx and the Rx. For narrowband transmission, the complex envelope resulting from the addition of N multipaths is given by [10]

$$g(t) = \sqrt{\frac{2}{N}} \sum_{n=1}^{N} \exp[j(2\pi f_1 \cos(\alpha_n)t + 2\pi f_2 \cos(\beta_n)t + \theta_n)], \tag{23}$$

where $\theta_n \sim U[-\pi,\pi)$ is the random phase and $f_n = f_1 \cos(\alpha_n) + f_2 \cos(\beta_n)$ is the

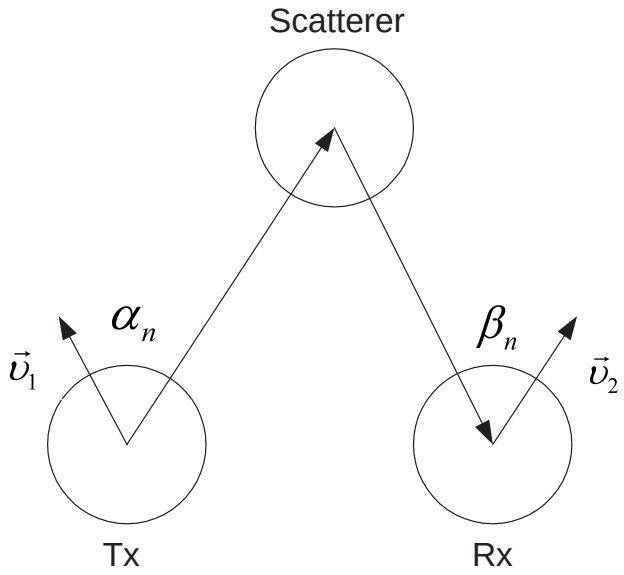

Figure 4: A typical propagation path from the Tx to the Rx.

Doppler shift associated with the n^{th} path. Here, α_n and β_n are the angle of departure and the angle of arrival of the n^{th} path measured with respect to the Tx and the Rx velocity vectors $\overrightarrow{v_1}$ and $\overrightarrow{v_2}$, respectively, as illustrated in Figure 4. Also, $f_1 = (2\pi v_1)/(\lambda)$ and $f_2 = (2\pi v_2)/(\lambda)$ are the maximum Doppler frequencies due to the motion of the Tx and the Rx, respectively, with λ being the carrier wavelength and v_1 and v_2 being the Tx and the Rx speeds, respectively. When sufficiently large multipaths combine, the channel behaves as a complex Gaussian random process. Therefore, a mobile-to-mobile channel is Rayleigh faded similar to a cellular channel. However, in contrast to cellular channels, both stations here carry low elevation antennas. As a result, the Tx as well as the Rx are likely to be surrounded by scatterers. Then, assuming omni-directional transmit and receive antennas and a 2-D isotropic scattering environment in the horizontal plane of the antennas, α_n and β_n are uniformly distributed over $[-\pi, \pi)$. Under these assumptions, the time auto-correlation of the channel envelope is given by [10]

$$\Re_{gg}(\tau) = J_o(2\pi f_1 \tau) J_o(2\pi f_2 \tau)$$

$$= J_o(2\pi f_1 \tau) J_o(2\pi a f_1 \tau), \quad (24)$$

where $a = (f_2)/(f_1)$ is the ratio of the two maximum Doppler frequencies with $0 \leq a \leq 1$, assuming $f_2 \leq f_1$.

Comparison of (17) with the above equation shows that the auto-correlation for mobile-to-mobile channels is a product of two Bessel functions rather than a single Bessel function that characterizes cellular channels. The auto-correlation of cellular channels can be obtained from (24) by setting 'a' = 0. This shows that mobile-to-mobile channels can be considered a set of generalized channels, with cellular channels being a special case where the scattering and mobility are restricted to the MS end alone. Taking the Fourier transform of the auto-correlation, we obtain the Doppler spectrum $S(f)$ at frequency f as

$$S(f) = \frac{1}{\pi^2 f_1 \sqrt{a}} K \left[\frac{1+a}{2\sqrt{a}} \sqrt{1 - \left(\frac{f}{(1+a) f_1} \right)^2} \right], \quad (25)$$

where $K[\ \cdot\ ]$ is the complete elliptic integral of the first kind.

Figure 5 shows Doppler spectra encountered in mobile-to-mobile channels, which clearly differ from the U-shaped spectrum of cellular channels. The higher order statistics such as level crossing rates and average fade durations are also different [9]. The LCR is given by

$$L_{\alpha_e = R} = \sqrt{2\pi} \sqrt{1 + a^2} f_1 \rho \exp(-\rho^2), \quad (26)$$

$$\rho = \frac{R}{\sqrt{E[\alpha_e^2]}}, \quad (27)$$

while the AFD is given by

$$T_{\alpha_e = R} = \frac{1}{\sqrt{2\pi} \sqrt{1 + a^2} f_1 \rho} (\exp(\rho^2) - 1). \quad (28)$$

Comparing (22) and (28) by assuming $f_d = f_1$ and $a = 1$, we observe that the average fade durations are smaller for mobile-to-mobile channels than those in cellular

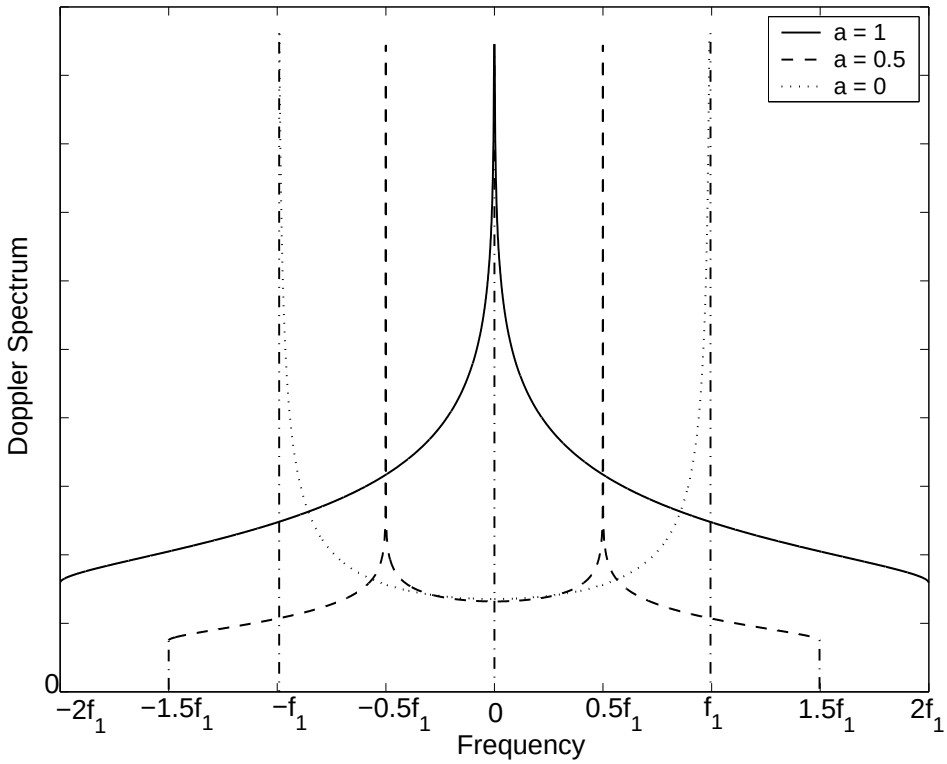

Figure 5: Doppler spectrum of mobile-to-mobile and cellular channels.

channels. This is also shown in Figure 6 , where we plot the average fade durations normalized with respect to the Doppler shift f_1 for cellular and mobile-to-mobile channels. The reduction in fade durations for mobile-to-mobile channels is due to the faster fading caused by the increased mobility. With faster fading, the channel is less likely to remain in a fade for a longer duration, thereby resulting in smaller average fade durations. The difference in the properties of mobile-to-mobile channels compared to those of cellular channels makes it necessary to modify existing methods or develop new methods to simulate mobile-to-mobile channels. Double mobility, which is the distinguishing feature of such channels, should be taken into account while simulating these channels. One such attempt was made by Wang and Cox in [81]. Though the model in [81] attacks the problem of obtaining a simulation model for mobile-to-mobile channels, it has certain drawbacks, which are discussed in Chapter IV. The author of the thesis provided a statistical simulation model for

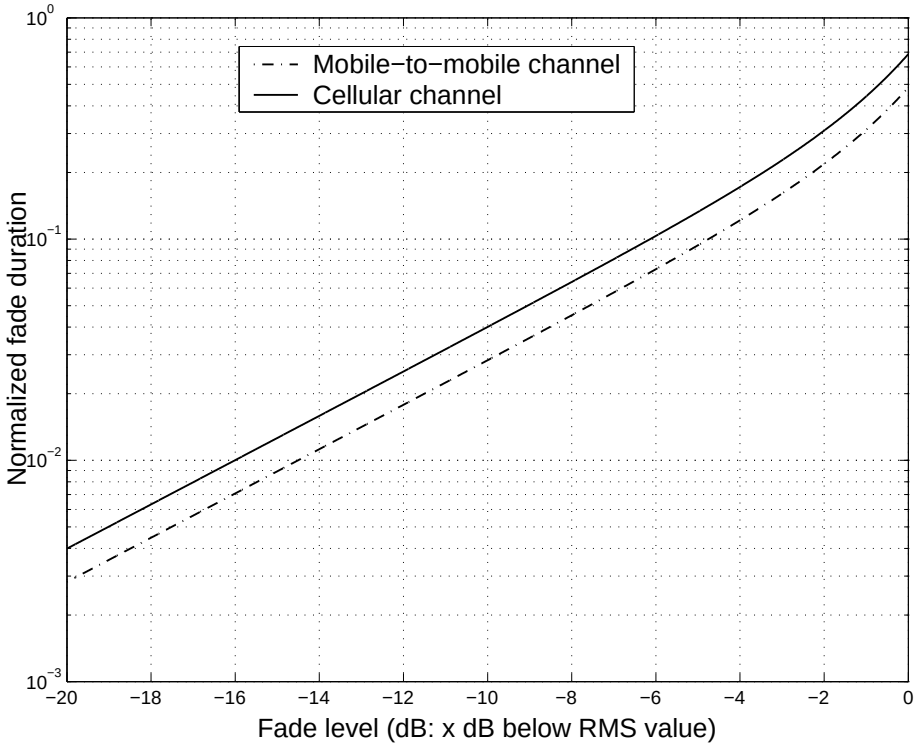

Figure 6: Average fade durations of mobile-to-mobile channels and cellular channels.

mobile-to-mobile channels in [55]. The performance of this model was chiefly assessed by simulations. A rigorous theoretical analysis was not provided. Here we extend our earlier work in [55] by developing different simulation models and verifying their performance through theoretical and simulation results.

2.3 Amplify and Forward Relay Channels

Having understood the various impairments suffered by a signal transmitted through a wireless channel, let us now consider how relays can help in mitigating some of these effects. The deep fades caused by Rayleigh fading in mobile applications reduce the reliability of the transmission and limit the capacity of the channel. To increase reliability under such fading conditions, diversity schemes are often employed. In general, the goal of a diversity scheme is to provide multiple, preferably independent replicas of the transmitted signal so that the receiver can mitigate fading by means

of signal processing. For example, if two copies of the signal are received via independently faded channels, the probability that both the channels are in deep fade is less compared to the probability of a single channel being in a deep fade. As a result, the receiver can demodulate the signal with greater reliability.

It is well-known that diversity can be achieved by employing multiple transmit or receive antennas. Such schemes are called spatial diversity schemes. Further, if multiple antennas are used at both the Tx and the Rx, the system capacity can be increased as shown by the pioneering work of Telatar on MIMO antenna systems [23, 75]. The motivation behind using the relay concept in mobile communications stems from this promise of increased reliability and system capacity offered by MIMO systems. Typically, MSs cannot be equipped with multiple antennas due to size constraints. Hence, a new form of spatial diversity known as "cooperation diversity" has been proposed in [41, 69, 70] to reap spatial diversity benefits in MSs. In a cooperation diversity scheme, a MS "partners" with another MS to send (or receive) its signal to (from) the BS or some other final destination. The partner station serves as a relay and forwards the signal from the source to the destination. This arrangement provides antenna diversity in a virtual fashion - virtual because the multiple transmit or receive antennas are not geographically co-located. Therefore, this scheme is also called "Virtual Antenna Arrays". To understand this concept better, we now illustrate how transmit diversity is achieved in traditional systems as well as in relay based cooperation diversity systems.

2.3.1 Cooperation diversity example

- **Traditional transmit diversity using Alamouti scheme**:

  The Alamouti space-time block code (STBC) scheme is widely used in current systems to achieve transmit antenna diversity [11]. The STBC scheme employs two co-located transmit antennas to send specially structured codewords to the

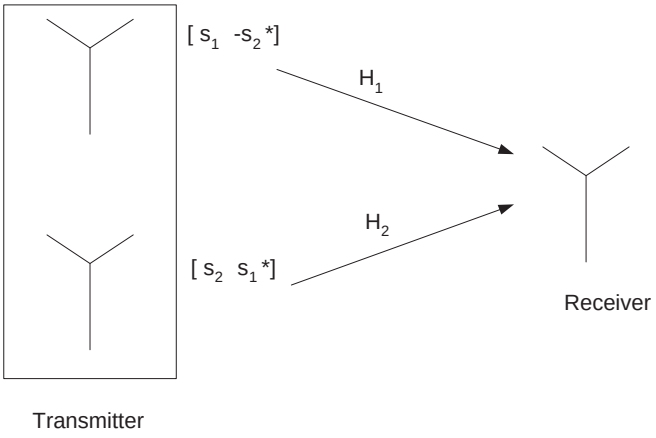

Figure 7: Alamouti STBC scheme with two co-located transmit antennas.

Rx and provide a diversity order of two, i.e., provide two independent replicas of the same signal. Figure 7 illustrates this concept. The transmitted codeword is given by the following matrix:

$$\begin{pmatrix} s_1 & -{s_2}^* \\ s_2 & {s_1}^* \end{pmatrix} \tag{29}$$

According to this scheme, the first antenna transmits the symbols of the first row of the code matrix successively over two time slots and the second antenna transmits the second row of the code matrix over two time slots. The channels H_1 and H_2 from the first and second transmit antenna to the receive antenna, respectively, fade independently when the transmit antennas are spaced sufficiently far apart. Thus, with STBC, same symbol is transmitted over two different channels over two time slots. By using signal processing, the Rx combines these replicas of a given symbol to achieve a diversity order of two.

- **Cooperation transmit diversity using relays**:

  By using a relay, space-time coding similar to Alamouti scheme can be achieved in a distributed fashion. Consider the transmission protocol discussed in [47], where the Tx transmits to the relay in the first time block and the Tx and relay both communicate with the Rx in the second time block. We assume both the

Tx and the relay have single transmit antennas. To achieve spatial diversity, the Tx transmits the first row of the above space-time code matrix to the relay in the first time block. During the second time block, the Tx transmits the second row of the code matrix to the Rx. Simultaneously, the relay forwards the first row that is received from the Tx to the Rx. Thus, two replicas of the same symbol are received at the Rx over two independent channels - the direct Tx-Rx channel and the Tx-relay-Rx channel, thereby achieving a spatial diversity order of two. Since space-time coding is achieved by using distributed (not co-located) antennas, this scheme is also called distributed STBC.

The above example highlights the diversity benefits that can be reaped with relay based cooperation diversity schemes. This has led to significant research on cooperation diversity, its implementation, and performance issues, which is evident from the work in [15, 47, 48, 69, 70].

2.3.2 Amplify and forward relay system model

Typically, the relays can be non-regenerative or regenerative. In a non-regenerative system, the relay simply amplifies and forwards the received signal, while in a regenerative system the relay decodes, re-encodes, and forwards the received signal. The amplify and forward (AF) mode puts less processing burden on the relay and therefore it is often preferable when complexity is an issue. The relay channel consisting of the BS (or a source Tx), the mobile relay, and the MS (or a destination Rx) involves a fixed-to-mobile channel and a mobile-to-mobile channel leading to temporal characteristics that are quite different from the cellular channel. These AF relay channels with their unique nature are not well understood today. It should be noted that for decode and forward (DF) relays, channel modeling is not an issue since each individual link's characteristics are known. Therefore, we focus on studying the properties of AF relay fading channels in our work. We briefly provide the AF system model

here, which is utilized in Chapter V and VI.

Consider the downlink relay channel from a BS to a destination MS via a mobile relay, as shown in Figure 1. Assuming frequency non-selective fading, the signal received by the relay at time t is

$$r_1(t) = h_1(t)s(t) + n_1(t), \tag{30}$$

where $s(t)$ is the transmitted signal, $h_1(t)$ is the channel between the BS and the relay modeled as a wss zero mean complex Gaussian (ZMCG) random process with power σ_1^2, and $n_1(t)$ is the zero mean complex additive white Gaussian noise (AWGN) with power σ_n^2. The relay amplifies $r_1(t)$ and retransmits it to the destination MS, which receives

$$\begin{aligned} r_2(t) &= A(t)h_2(t)r_1(t) + n_2(t) \\ &= A(t)h_2(t)h_1(t)s(t) + A(t)h_2(t)n_1(t) + n_2(t) \\ &= h(t)s(t) + A(t)h_2(t)n_1(t) + n_2(t). \end{aligned} \tag{31}$$

In the above equations, $A(t)$ is the amplification factor controling the power transmitted by the relay, $h_2(t)$ is the relay-MS channel modeled as a wss ZMCG process with power σ_2^2, $h(t) = A(t)h_1(t)h_2(t)$ is the overall relay channel, and $n_2(t)$ is the receiver AWGN with power σ_n^2. Here, we assume that the relay and the destination receiver chains have identical noise properties resulting in the same AWGN noise power.

Though both links $h_1(t)$ and $h_2(t)$ are individually Rayleigh faded, the overall channel $h(t) = A(t)h_1(t)h_2(t)$ is likely to have properties very different from the individual channels. To the best of our knowledge, there is little work that addresses AF relay channels. Therefore, we present the characteristics of these channels in Chapter V.

2.4 Simulation Models for Fading Channels

The importance of simulating communication systems in software for system design and verification is well recognized by designers of these systems. Simulation offers cost effective and time saving alternative to real-time system testing in the field. The prime requirement of the simulation set-up is to capture the fading effects created by a radio channel. As a result, efforts have been made to develop efficient models to simulate the actual radio propagation environment in software and test various communications algorithms. Models such as Jakes' SoS [36] model, filtered noise models [84] and their refinements have been widely accepted for simulating cellular channels [58, 85]. Our goal is to extend this work to the case of mobile-to-mobile channels and relay channels. Before we discuss our contributions in this area, it is necessary to understand different simulation philosophies commonly employed to simulate fading channels. Therefore, we provide an overview of different simulation techniques in this section. Specifically, we discuss the SoS models and different kinds of filtered noise models along with their pros and cons.

2.4.1 Sum-of-sinusoids model

Our discussion on multipath propagation and the physics behind it showed that the complex channel envelope can be represented as a sum of homogeneous wave components, as shown in (5). Each homogenous component is represented by a complex sinusoid with certain amplitude, frequency, and phase. The overall channel waveform is the sum of several sinusoids. Therefore, this channel description is often called a "sum-of-sinusoids" model. Being a natural representation of the channel waveform, several SoS models have been presented in the past to simulate cellular channels. Rather than simulating the channel by directly applying the Clarke's reference model of (11), specialized SoS models are proposed to efficiently simulate the channel by using a finite number of sinusoids. The SoS modeling philosophy has been made

popular by the pioneering work of Jakes [36], which is discussed below.

For convenience, we repeat the Clarke's reference model. Clarke's model defines the complex channel gain under NLOS, frequency flat fading, and 2-D isotropic scattering assumptions as [19]

$$g(t) = \sqrt{\frac{2}{N}} \sum_{n=1}^{N} \exp\{j[\omega_d t \cos(\alpha_n) + \phi_n]\}, \tag{32}$$

where N is the number of propagation paths, $\phi_n \sim U[\text{-}\pi,\pi)$ and $\alpha_n \sim U[\text{-}\pi,\pi)$ are the random phase and angle of arrival of the n^{th} multipath component, and ω_d is the maximum angular Doppler frequency due to the receiver mobility. To simulate the cellular channel, this SoS model can be directly applied by generating the random variables involved in the model. However, as we show in Chapter III, this high degree of randomness is not desirable for efficient simulation. Therefore, Jakes proposed the following SoS model:

$$g_I(t) = \sqrt{2}\cos(\omega_d t) + 2\sum_{n=1}^{M} \cos\left(\frac{2\pi n}{M}\right) \cos\left(\omega_d \cos\left[\frac{2\pi n}{4M+2}\right] t\right) \tag{33}$$

$$g_Q(t) = 2\sum_{n=1}^{M} \sin\left(\frac{2\pi n}{M}\right) \cos\left(\omega_d \cos\left[\frac{2\pi n}{4M+2}\right] t\right) \tag{34}$$

A detailed discussion on the derivation of the model parameters can be found in [36, 74]. The intuition behind this model is the fact that under 2-D isotropic scattering, the symmetry in the environment can be exploited to reduce the number of sinusoids. For example, while the Clarke's model distributes the angles of arrival over [-π,π) resulting in negative as well as positive Doppler frequencies in the model, the Jakes' model simulates only the positive Doppler frequencies to reduce the number of sinusoids M. The amplitudes of these sinusoids, i.e., $\cos(\alpha_n)$ and $\sin(\alpha_n)$ are chosen to produce zero cross-correlation between the I and Q components, a constraint imposed by the Clarke's model to generate Rayleigh faded envelope.

The Jakes' model has been the de-facto simulation model for a long time. However, recent studies have highlighted several drawbacks of this model [62, 85]. For

example, since all the parameters in the model are fixed (deterministic), the channel waveform simulated in each simulation run is identical. Therefore, statistical averaging or Monte Carlo simulation results cannot be obtained while computing metrics such as BER. Several authors have proposed "statistical" simulation models for cellular channels to remove this drawback. In contrast to a "deterministic" model like the Jakes' model, which has fixed, non-random Doppler frequencies, the statistical models use random Doppler frequencies for each simulation trial. Note that both the deterministic as well as statistical models can have random phases. If a deterministic model uses random phases, different channel waveforms are simulated for different trials. However, properties like time-averaged correlations are identical for all the trials. Therefore, with such deterministic models statistical averaging of these properties is not possible. In contrast, the time-averaged correlations of statistical models vary with simulation trials due to random Doppler frequencies [85]. These properties converge to the properties of the reference model in the statistical sense, i.e., over several simulation trials. Therefore, the parameters of the statistical models are chosen carefully to reduce the number of trials required for convergence. These and other issues such as complexity and performance of statistical models for cellular channels are analyzed further in Chapter III.

2.4.2 Filtered noise models

Eventually, the goal of any simulation model is to reproduce the channel properties. Therefore, in contrast to SoS models, filtered noise models are tailored to simulate the channel properties by means of signal processing techniques without considering the underlying propagation mechanism. Instead of adding multipaths to generate fading, these models filter noise to generate the channel waveform. The underlying principle is that on filtering Gaussian noise through appropriately designed filters, the channel power spectral density (psd or the Doppler spectrum) can be simulated,

thereby capturing the important first and second order channel statistics.

To understand the working of filtered noise models, we first mention an important result from the linear time-invariant filtering theory. Given a filter with frequency response $H(f)$, if a signal $x(n)$ with psd $P_{xx}(f)$ is filtered through this filter, the output $y(n)$ has psd given by

$$P_{yy}(f) = P_{xx}(f)|H(f)|^2. \tag{35}$$

This suggests that to generate Gaussian I or Q phase components of the channel envelope, each having a Doppler spectrum $P_{yy}(f) = S(f)$, we can filter a white Gaussian random process with psd $N_o/2$ through a filter $H(f)$ whose frequency response is chosen to be

$$H(f) = \sqrt{\frac{2}{N_o} S(f)}. \tag{36}$$

Then, the output random process will also be Gaussian and with a psd $S(f)$, thereby reproducing the properties of the complex Gaussian channel. The next goal in the simulation model is to implement the filter $H(f)$. We describe two such implementation schemes below - the Inverse Fast Fourier Transform (IFFT) filter model and the Auto-regressive (AR) filter model. The former is designed in the frequency domain while the later is designed in the time domain to provide an approximation of the Doppler spectrum that we desire.

2.4.2.1 IFFT filter model

Since it is easy to discuss the IFFT operation in discrete time, and our ultimate goal is to simulate discrete time waveforms, we deal with discrete time-domain sequences in this section. A block diagram of this method is shown in Figure 8.

To generate a discrete time sequence $y[n]$ of N complex Gaussian variables with a given Doppler spectrum, the Doppler spectrum is sampled at N equi-spaced frequencies $f_k = (kf_s)/(N), k = 0, 1, ...N-1$, where f_s is the sampling frequency. This

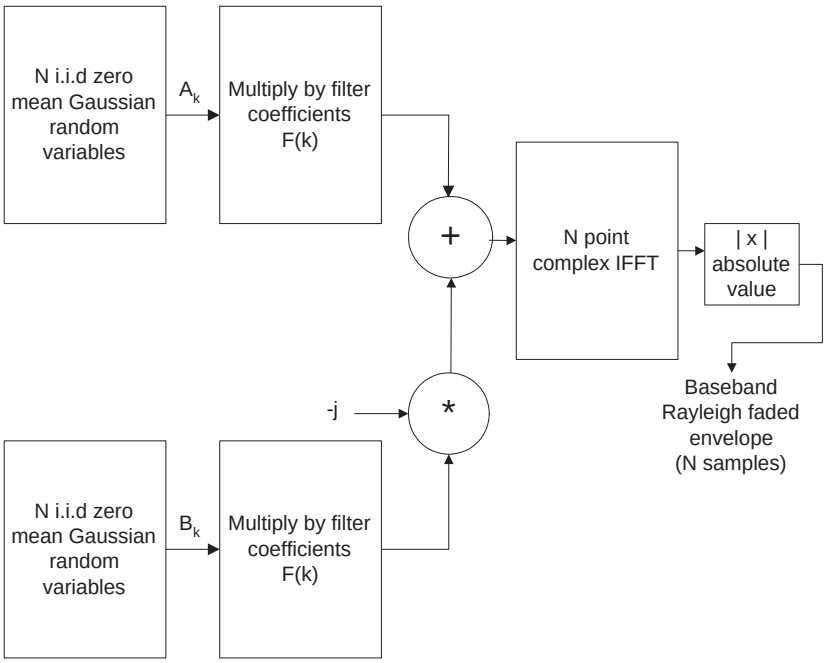

Figure 8: Block diagram for generating Rayleigh faded envelope using IFFT filtering

provides the filter coefficients $F_c[f_k] \equiv F_c[k]$ [84],

$$\begin{aligned} F_c[k] &= \sqrt{F_s[0]} && k = 0 \\ &= \sqrt{\frac{F_s[k]}{2}} && k = 1, 2, ... \left(\frac{N}{2} - 1\right) \\ &= \sqrt{F_s[k]} && k = \frac{N}{2} \\ &= \sqrt{\frac{F_s[N-k]}{2}} && k = \left(\frac{N}{2} + 1\right), ...(N-1). \end{aligned} \tag{37}$$

In the above equation, $F_s[k]$ are obtained by sampling Doppler spectrum in (19) at frequencies f_k. In addition, two sequences $A[k]$ and $B[k]$, each having N i.i.d real Gaussian random variables with zero mean and variance σ^2 are generated. Then, the desired signal $y[n]$ is obtained as

$$y[n] = IFFT\{A[k]F_c[k] - jB[k]F_c[k]\}_{k=0}^{N-1}. \tag{38}$$

2.4.2.2 Auto-regressive filter model

The AR model imposes an all-pole structure on the filter $H(f)$ and determines the AR filter coefficients in the time-domain by using the knowledge of channel auto-correlation function. However, it must be noted that the underlying principle of filtering Gaussian noise to produce an output with the desired psd remains the same.

Let $x(n)$ be a white, Gaussian random process filtered through a p^{th} order (p poles) AR filter $H(z) = 1/A_p(z) = 1/(1 + \sum_{k=1}^{p} a_p(k)z^{-1})$. Then, the output $y(n)$ is given by the difference equation

$$y(n) = -\sum_{k=1}^{p} a_p(k)x(n-k) + x(n). \tag{39}$$

If the auto-correlation, $r_{yy}(n)$, of $y(n)$ is known for the delays ranging from $n = 0$ to $n = p$, the filter coefficients a_ps can be chosen to exactly reproduce these auto-correlation values in the output signal $y(n)$. The necessary filter coefficients obey the well-known Yule-Walker equation [33]

$$\begin{pmatrix} r_{yy}(0) & r_{yy}(1) & \dots & r_{yy}(p-1) \\ r_{yy}(1) & r_{yy}(0) & \dots & r_{yy}(p-2) \\ \vdots & \vdots & \vdots & \ddots \\ r_{yy}(p-1) & r_{yy}(p-2) & \cdots & r_{yy}(0) \end{pmatrix} \begin{pmatrix} a_p(1) \\ a_p(2) \\ a_p(3) \\ a_p(4) \end{pmatrix} = - \begin{pmatrix} r_{yy}(1) \\ r_{yy}(2) \\ \vdots \\ r_{yy}(p) \end{pmatrix}, \tag{40}$$

which can be written in the matrix form as

$$\begin{aligned} \mathbf{R_{yy}a_p} &= -\mathbf{r} \quad \text{and} \\ \mathbf{a_p} &= -\mathbf{R_{yy}}^{-1} \quad \mathbf{r}. \end{aligned} \tag{41}$$

However, an exact solution to the Yule-Walker equation does not exist if the auto-correlation matrix R_{yy} is non-singular and therefore non-invertible. This is especially the case for R_{yy}s encountered in mobile channel simulation [14]. In such cases, a solution is obtained by using a technique called "diagonal loading" or "matrix stabilization" [67], where we artificially introduce some noise variance into R_{yy} to make it

stable, non-singular and thus invertible matrix. The a_ps are then obtained as

$$\mathbf{a_p} = -(\mathbf{R_{yy}} + \epsilon\mathbf{I})^{-1} \quad \mathbf{r}, \tag{42}$$

where $\mathbf{I}$ is a p x p identity matrix and $\epsilon \neq 0$ is a suitable diagonal loading parameter that renders $(\mathbf{R_{xx}} + \epsilon\mathbf{I})$ non-singular and invertible.

The above discussion shows that fading channels can be simulated by several different methods. Both SoS models and filtered noise models have found acceptance in academia and industry. Several authors have pointed out the pros and cons of these models. The filtered noise models can simulate any arbitrary Doppler spectrum provided the spectrum is known. But, the IFFT filter method suffers from the drawback that large size IFFT capability and memory requirements are needed because the IFFT filter processes all the required N samples at a time. The AR model can provide good accuracy if a high order filter is used. However, the spectrum is not band-limited because, in practice, filters with sharp stop-bands are difficult to implement. In general, SoS models produce channel waveforms that have high accuracy and perfectly-band limited spectrum. The complexity of SoS models is typically reduced by cleverly choosing the model parameters and thereafter using a look-up table technique for simulation. This technique stores the samples of a single period of the sinusoids in a look-up table to avoid repetitive computations, thereby reducing computation load. In addition, SoS models can be easily extended to develop spatial channel models for directional or MIMO antenna systems because they explicitly include the spatial information like multipath angles of arrivals and departures. Owing to these advantages, we develop different SoS models for mobile-to-mobile channels in our work.

CHAPTER III

ANALYSIS OF SIMULATION MODELS FOR CELLULAR CHANNELS

3.1 Overview

The primary goal of this thesis is to develop theoretical and simulation models for mobile-to-mobile and amplify and forward relay channels. However, it is also essential that cellular channels and their simulation models be properly studied to gain insights into the modeling problem. These insights can provide us guidelines to develop simulation models for other channels. With this aim, we provide a comprehensive analysis of different statistical simulation models commonly used for cellular channels.

The background section pointed out the rich body of existing literature devoted to developing and evaluating simulation models for cellular channels. However, we found a lack of coherent and comprehensive analysis that compares these different models scattered all over the literature. Therefore, in this chapter, different statistical models are compared in terms of their complexity and performance. These models are based on the "sum-of-sinusoids" philosophy described earlier. Since these SoS models converge statistically to the desired properties, they are also called Monte Carlo (MC) models. Owing to their statistical nature, it is important to determine the number of simulation trials needed to achieve a desired convergence level. This is directly related to the variation in the time average properties of a single simulation trial from the desired ensemble average properties. Hence, we use these variations as a performance metric to compare properties such as the auto-correlation, the cross-correlation, and the level crossing rate of different models. Further, we investigate the convergence of these models in terms of their squared envelope correlation. Our analysis shows that the squared envelope correlations derived in [83, 85, 86, 87] are incorrect. Hence,

we present the correct expressions for the squared envelope correlation and compare different methods on this basis. Moreover, one of the SoS models previously believed to produce the desired channel properties turns out to be non-stationary [86]. It exhibits problems in reproducing the Gaussian statistics in the complex envelope and is non-stationary in terms of the squared envelope correlation. Based on our analysis, we identify a particular model that gives desired performance. This model forms the basis of a statistical simulation model for mobile-to-mobile channels, which is presented in Chapter IV.

Before we describe the statistical models used in our analysis, we repeat the reference cellular channel model of Chapter II because it is often referred in the later sections.

3.2 The Mathematical Reference Model

Under frequency-flat fading and 2-D isotropic scattering assumptions, the properties of a Rayleigh faded cellular channel are summarized below [36, 74]:
For the complex envelope, $g(t) = g_i(t) + jg_q(t)$, the in-phase (I) and quadrature (Q) components have a zero-mean unit variance Gaussian distribution with auto-correlation and cross-correlation properties

$$\begin{aligned} R_{g_{i/q}g_{i/q}}(\tau) &= \mathrm{E}[g_{i/q}(t+\tau)g_{i/q}(t)] = J_0(\omega_d\tau) && (43)\\ R_{g_ig_q}(\tau) &= R_{g_qg_i}(\tau) = 0 && (44)\\ R_{gg}(\tau) &= \frac{1}{2}\mathrm{E}[g(t+\tau)g^*(t)] = J_0(\omega_d\tau) && (45)\\ R_{|g|^2|g|^2}(\tau) &= \mathrm{E}[|g|^2(t+\tau)|g|^2(t)] \\ &= 4 + 4J_0^2(\omega_d\tau). && (46) \end{aligned}$$

Note that the properties of the reference model do not depend on the number of multipaths, i.e., the number of sinusoids that constitute the model. However, when finite number of sinusoids are used in a simulation model, the properties of the

simulation model are likely to deviate from those of the reference model. Therefore, the goal of any simulation model is to choose the sinusoid frequencies, amplitudes, and phases as optimally as possible to simulate the reference channel properties accurately and efficiently.

3.3 Statistical Simulation Models

3.3.1 Clarke's model

An obvious simulation model is the Clarke's reference model provided in Chapter II. We use finite number of sinusoids (finite N) in (11) to simulate the channel. Based on these assumptions, the statistical properties of Clarke's model for a finite N are given by (43), (44), and (45) [87], while the squared envelope correlation is given by

$$R_{|g|^2|g|^2}(\tau) \;=\; \mathrm{E}[|g|^2(t+\tau)|g|^2(t)] = 4 + 4\frac{N-1}{N}J_0^2(\omega_d\tau). \tag{47}$$

Equation (47) can be derived in a manner similar to the expression derived in Appendix 3.2. Note that for the Clarke's model with finite N, the auto- and cross-correlation of the quadrature components match those of the reference model while the squared envelope auto-correlation reaches the desired value $4 + 4J_0^2(\omega_d\tau)$ asymptotically as $N \to \infty$. Also, (47) gives the correct squared envelope auto-correlation expression for finite N. (the expression in [87], Eqn. (2f) is incorrect).

The time average correlations $\hat{R}(\cdot)$ (all time averaged quantities are distinguished from the statistical averages with a ' $\hat{}$ ' here onwards) are random and depend on a specific realization of the random parameters in a given simulation trial [87]. The variances of these correlations, defined as $\mathrm{Var}[R(\cdot)]$=$\mathrm{E}[|\hat{R}(\cdot) - \lim_{N\to\infty} R(\cdot)|^2]$, have been derived in [87] and are repeated here for convenience.

$$\begin{aligned}
\mathrm{Var}[R_{g_ig_i}(\tau)] &= \mathrm{Var}[R_{g_qg_q}(\tau)] \\
&= \frac{1 + J_0(2\omega_d\tau) - 2J_0^2(\omega_d\tau)}{2N} \\
\mathrm{Var}[R_{g_ig_q}(\tau)] &= \mathrm{Var}[R_{g_qg_i}(\tau)]
\end{aligned} \tag{48}$$

$$= \frac{1 - J_0(2\omega_d\tau)}{2N} \tag{49}$$

$$\mathrm{Var}[R_{gg}(\tau)] = \frac{1 - J_0^2(\omega_d\tau)}{N} \tag{50}$$

Using these variances, we later compare the performance of Clarke's model for finite N with several other models.

3.3.2 Modified Hoeher's model - Model I

Consider the channel model [56]

$$g(t) = g_i(t) + jg_q(t) \tag{51}$$

$$g_i(t) = \sqrt{\frac{2}{N}} \sum_{n=1}^{N_i} \cos(\omega_d t f_{i,n} + \phi_{i,n}) \tag{52}$$

$$g_q(t) = \sqrt{\frac{2}{N}} \sum_{m=1}^{N_q} \cos(\omega_d t f_{q,m} + \phi_{q,m}) \tag{53}$$

$$f_{i/q,n/m} = \sin\left(\frac{\pi}{2} u_{i/q,n/m}\right), \tag{54}$$

where the Doppler frequencies $f_{i/q,n/m}$ for the I and Q components are determined by $u_{i/q,n/m}$, where $u_{i/q,n/m} \sim U[0,1)$ and are mutually independent for all n and m. The random phases $\phi_{i/q,n/m} \sim U[-\pi,\pi)$ are mutually independent, for all n and m, and are also independent of $u_{i/q,n/m}$'s. For convenience, the number of sinusoids in the quadrature components are set equal, i.e., $N_i = N_q = N$. This model is derived from the Hoeher's model in [35] by considering only the positive Doppler frequencies in the simulation. Therefore, we refer to it as the modified Hoeher's model. The performance of this model was compared with several deterministic simulation models in [57]. Here, we compare it against statistical simulation models for finite N with the aid of several statistical and time average correlations, along with the variances of the latter. The statistical averages given by (43), (44), and (45) are valid for this model, while the squared envelope correlation is (proof is analogous to the derivation

given in Appendix 3.2)

$$R_{|g|^2|g|^2}(\tau) = 4 + 4\frac{N-1}{N}J_0^2(\omega_d\tau) + \frac{1}{N}J_0(2\omega_d\tau), \tag{55}$$

which for finite N differs from the reference model. The time averaged correlations can be derived as follows (proofs are simple and therefore omitted here):

$$\begin{aligned}
\hat{R}_{g_ig_i}(\tau) &= \lim_{T\to\infty}\frac{1}{2T}\int_{-T}^{T} g_i(t+\tau)g_i(t)dt \\
&= \frac{1}{N}\sum_{n=1}^{N}\cos(\omega_d f_{i,n}\tau) && (56)\\
\hat{R}_{g_qg_q}(\tau) &= \frac{1}{N}\sum_{n=1}^{N}\cos(\omega_d f_{q,n}\tau) && (57)\\
\hat{R}_{g_ig_q}(\tau) &= \hat{R}_{g_qg_i}(\tau) = 0 && (58)\\
\hat{R}_{gg}(\tau) &= \frac{1}{2}\lim_{T\to\infty}\frac{1}{2T}\int_{-T}^{T} g(t+\tau)g^*(t)dt \\
&= \frac{1}{2N}\sum_{n=1}^{N}\left[\cos(\omega_d f_{i,n}\tau) + \cos(\omega_d f_{q,n}\tau)\right] && (59)
\end{aligned}$$

The variances of these time-averaged properties are quantified by the following theorem.

Theorem 1 *The variances of the auto-correlation and cross-correlation of the quadrature components, and the variance of the auto-correlation of the complex envelope $g(t)$, as defined by Model I in (51), are*

$$\begin{aligned}
\mathrm{Var}[R_{g_ig_i}(\tau)] &= \mathrm{Var}[R_{g_qg_q}(\tau)] \\
&= \frac{1 + J_0(2\omega_d\tau) - 2J_0^2(\omega_d\tau)}{2N} && (60)\\
\mathrm{Var}[R_{g_ig_q}(\tau)] &= \mathrm{Var}[R_{g_qg_i}(\tau)] = 0 && (61)\\
\mathrm{Var}R_{gg}(\tau) &= \frac{1 + J_0(2\omega_d\tau) - 2J_0^2(\omega_d\tau)}{4N}. && (62)
\end{aligned}$$

Proof: Proof of (60) is provided in Appendix 3.1. (61) and (62) can be derived in a similar manner. ■

3.3.3 Zheng and Xiao's models

Recently, Zheng and Xiao have proposed several new statistical models to simulate Rayleigh fading channels [83, 85, 86, 87]. These models differ from one another in terms of the model parameters and therefore they have different time-average properties. We provide a detailed analysis of the statistical and time-average properties of these models in the present section. We distinguish the models by naming them Model II, Model III, and Model IV, with Model I being the modified Hoeher's model.

Model II

From [85],

$$
\begin{aligned}
g(t) &= g_i(t) + jg_q(t) && (63)\\
g_i(t) &= \sqrt{\frac{2}{N}} \sum_{n=1}^{N} \cos[\omega_d t \cos(\alpha_n) + \phi_{i,n}] && (64)\\
g_q(t) &= \sqrt{\frac{2}{N}} \sum_{n=1}^{N} \cos[\omega_d t \sin(\alpha_n) + \phi_{q,n}] && (65)\\
\alpha_n &= \frac{2\pi n - \pi + \theta}{4N} \qquad n = 1, 2..., N && (66)
\end{aligned}
$$

where $\theta \sim U[-\pi, \pi)$, $\phi_{i,n} \sim U[-\pi, \pi)$ and $\phi_{q,n} \sim U[-\pi, \pi)$ for all n, and all values are mutually independent.

Model III

From [83, 87],

$$
\begin{aligned}
g_i(t) &= \sqrt{\frac{2}{N}} \sum_{n=1}^{N} \cos[\omega_d t \cos(\alpha_n) + \phi_n] && (67)\\
g_q(t) &= \sqrt{\frac{2}{N}} \sum_{n=1}^{N} \sin[\omega_d t \cos(\alpha_n) + \phi_n] && (68)\\
\alpha_n &= \frac{2\pi n + \theta_n}{N} \qquad n = 1, 2..., N, && (69)
\end{aligned}
$$

where $\theta_n \sim U[-\pi, \pi)$ and $\phi_n \sim U[-\pi, \pi)$ for all n, and all values are mutually independent. For Model III, we also consider a slight modification[1] to Zheng and Xiao's model by using

$$\alpha_n = \frac{2\pi n - \pi + \theta_n}{2N} \qquad n = 1, 2..., N \tag{70}$$

In Zheng and Xiao's original model, the α_ns vary over the range [0,2π). It is intuitive that if the range of the α_n is reduced, the statistical properties of the resulting new model will vary less from the desired properties. Hence, we consider the α_ns described above which vary over a range [0,π). We call this model the modified Model III and study its performance in the next section.

Model IV

From [86],

$$g_i(t) = \frac{2}{\sqrt{N}} \sum_{n=1}^{N} \cos(\xi_n) \cos[\omega_d t \cos(\alpha_n) + \phi] \tag{71}$$

$$g_q(t) = \frac{2}{\sqrt{N}} \sum_{n=1}^{N} \sin(\xi_n) \cos[\omega_d t \cos(\alpha_n) + \phi] \tag{72}$$

$$\alpha_n = \frac{2\pi n - \pi + \theta}{4N} \qquad n = 1, 2..., N, \tag{73}$$

where $\xi_n \sim U[-\pi, \pi)$, $\theta \sim U[-\pi, \pi)$, and $\phi \sim U[-\pi, \pi)$. These random variables being mutually independent. For a sufficiently large number of sinusoids, N, all of the above models produce Gaussian quadrature components and hence a Rayleigh faded envelope [85, 87, 86]. However, a closer inspection of Model IV reveals that the probability density function (pdf) of the quadrature components is non-stationary as stated below:

Theorem 2 *The pdfs of the quadrature components of the complex envelope $g(t)$ produced by Model IV are non-stationary, i.e., they are a function of time t and tend*

[1]It has recently come to our notice that this model has been proposed earlier in a different form (even before Zheng and Xiao's independent and original models) in [34]. Therefore, we also refer the interested reader to [34] for further details on the model and its performance.

to the desired Gaussian distribution only for sufficiently large time t, even in the asymptotic case when $N \to \infty$.

Proof: Consider the in-phase component $g_i(t)$ given in (71). Assume that θ and ϕ are known. Then, for N sufficiently large, the application of the Central Limit Theorem [49] to $x{=}g_i(t)$ (assume time t is fixed) shows that the distribution of x conditioned on ϕ and θ is zero-mean Gaussian with variance σ^2, i.e.,

$$\begin{aligned} f_X(x|\theta,\phi) &= \frac{1}{\sqrt{2\pi\sigma^2}} \exp\left(-\frac{x^2}{2\sigma^2}\right) && (74)\\ \sigma^2 &= \frac{2}{N}\sum_{n=1}^{N} \cos^2[\omega_d t \cos(\alpha_n) + \phi] && (75)\\ \sigma^2 &\overset{N\to\infty}{=} 1 + J_0(2\omega_d t)\cos(\phi) - H_0(2\omega_d t)\sin(\phi), && (76) \end{aligned}$$

where $H_0(\cdot)$ is the zeroth order StruveH function [28]. Since σ^2 is a function of ϕ and/or θ, it is a random variable. Moreover, it depends on the time variable t which suggests that the pdf $f_X(x)$ is non-Gaussian and time varying. Although a closed form expression for $f_X(x)$ cannot be obtained, it can be evaluated numerically by averaging the conditional pdf $f_X(x|\theta,\phi)$ over θ and ϕ, i.e.,

$$\begin{aligned} f_X(x) &= \int_\theta \int_\phi \frac{1}{\sqrt{2\pi\sigma^2}} \exp\left(-\frac{x^2}{2\sigma^2}\right) f_{\Theta,\Phi}(\theta,\phi)\, d\theta\, d\phi \\ &= \frac{1}{(2\pi)^{5/2}} \int_{-\pi}^{\pi}\int_{-\pi}^{\pi} \frac{1}{\sqrt{\sigma^2}} \exp\left(-\frac{x^2}{2\sigma^2}\right) d\theta\, d\phi, && (77) \end{aligned}$$

where we used the fact that θ and ϕ are mutually independent and uniformly distributed over $[-\pi,\pi)$. Using this equation with $N{=}50$, we evaluate the pdf of x at different time values (ts) and plot the results in Figure 9. To facilitate comparison, the pdf of a standard Gaussian random variable $N(0,1)$ is also plotted in Figure 9. The pdf is clearly time varying and approaches the desired pdf only for sufficiently large t. Simulation results, though not presented in Figure 9 to retain clarity, also confirm this fact. This proves the non-stationary nature of the pdf of the in-phase component (and analogously of the quadrature component) of the complex envelope $g(t)$. ■

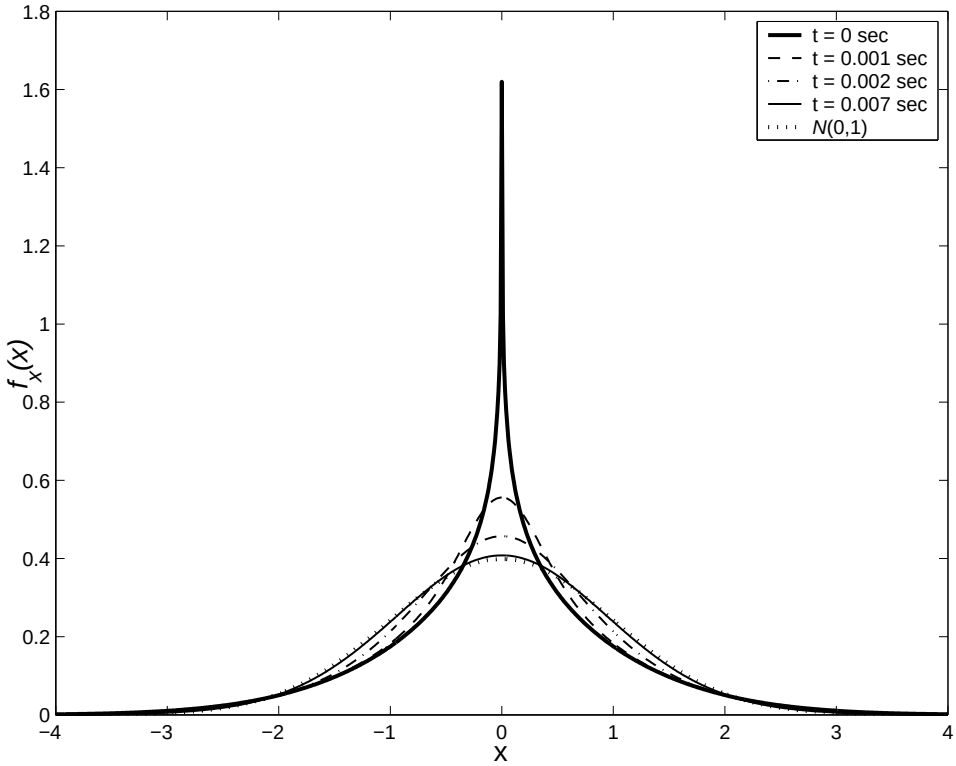

Figure 9: Pdf of Model IV's I-phase component.

Owing to the non-stationary, non-Gaussian, nature exhibited by Model IV, it is not a good candidate for channel simulation purposes. Model IV is also non-stationary with respect to the properties of the squared envelope as discussed below. The statistical correlation functions of the quadrature components for Models II, III, and IV have been computed by Zheng and Xiao and match the desired functions in (43), (44), and (45). The time-average correlations are easy to derive and therefore are not provided here. Besides, unlike the earlier methods, closed form expressions for the variances of the time-average correlations do not exist for Zheng and Xiao's models. These variances are computed via simulations in Section 3.4. Here, we only present the statistical squared envelope correlation expressions since they represent the corrected versions of expressions given in [85] (eqn. $5f$), [87](eqn. $8f$) and [86] (eqn. $16f$) for Models II, III, and IV, respectively.

Theorem 3 *The auto-correlation functions of the squared envelope obtained with Models II, III, and IV are given by (78), (79), and (80), respectively.*

Model II :

$$R_{|g|^2|g|^2}(\tau) = 4 + \frac{J_0(2\omega_d\tau)}{N} + \frac{4}{N^2}\sum_{n=1}^{N}\sum_{m(\neq n)=1}^{N} \mathrm{E}\{\cos[\omega_d\tau\cos(\alpha_n)]\cos[\omega_d\tau\cos(\alpha_m)]\} \tag{78}$$

Model III :

$$R_{|g|^2|g|^2}(\tau) = 4 + 4J_0^2(\omega_d\tau) - \frac{4}{N^2}\sum_{n=1}^{N}\left([\mathrm{E}\{\cos[\omega_d\tau\cos(\alpha_n)]\}]^2 + [\mathrm{E}\{\sin[\omega_d\tau\cos(\alpha_n)]\}]^2\right) \tag{79}$$

Model IV :

$$\begin{aligned} R_{|g|^2|g|^2}(\tau) = {} & 4 + \frac{2J_0(2\omega_d\tau)}{N} + \\ & \frac{4}{N^2}\sum_{n=1}^{N}\sum_{m(\neq n)=1}^{N} \mathrm{E}\{\cos[\omega_d\tau\cos(\alpha_n)]\cos[\omega_d\tau\cos(\alpha_m)]\} + \\ & \frac{2}{N^2}\sum_{n=1}^{N}\sum_{m(\neq n)=1}^{N} \mathrm{E}\{\cos[2\omega_d(t+\tau)\cos(\alpha_n) - 2\omega_d t\cos(\alpha_m)]\} + \\ & \frac{2}{N^2}\sum_{n=1}^{N}\sum_{m(\neq n)=1}^{N} \mathrm{E}\{\cos[\omega_d(2t+\tau)\cos(\alpha_n) - \omega_d(2t+\tau)\cos(\alpha_m)] \end{aligned} \tag{80}$$

Proof: A brief outline of the proofs of (79) and (80) are provided in Section 3.7 and 3.8, respectively. (78) can be obtained in a similar manner. ■

Note that there are no closed form expressions for the squared envelope correlation because the last term in (78), (79), and (80) cannot be simplified further; they must be evaluated numerically. It is important to note that for Model IV, the squared envelope correlation is a function of both the time variable t and the delay variable τ,

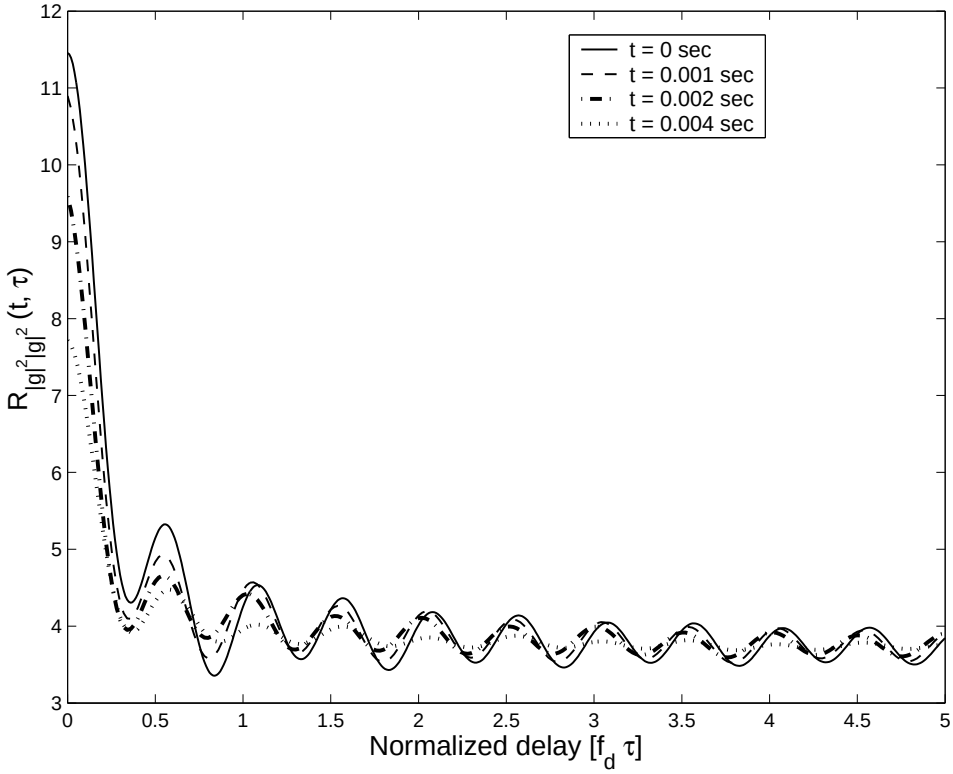

Figure 10: Auto-correlation of Model IV's squared envelope.

exposing the non-stationary nature of the squared envelope. This is further verified in Figure 10, where the squared envelope correlation is plotted for different time values (ts) by numerically evaluating (80), using $N = 11$. It is clear from Figure 10 that the squared envelope correlation varies with time t. Owing to the non-stationarity problems exhibited by Model IV, we exclude it from further analysis.

3.4 Analysis and Simulation Results

This section combines the analysis of earlier sections to compare different simulation models. We begin by comparing their relative complexity in terms of the number of computations required and the simulation time.

3.4.1 Complexity analysis

Table 1 summarizes the number of operations needed to generate one sample of the complex envelope $g(t)$ for different models. Here, we count the frequently executed operations only, neglecting operations that are performed only once during a simulation trial such as the generation of random variables.[2] The relative simulation times needed to generate 10^5 samples of $g(t)$ in Matlab on a Pentium III laptop are also tabulated in Table 1. From Table 1, it is evident that Clarke's model and Model III require the least simulation time owing to their low complexity.

Table 1: Complexity of different models

Model	Computations needed to generate 1 sample of $g(t)$	Relative simulation time
Clarke	$2N$ cosine, N additions	T_x
Model I	$2N$ cosine, $2N$ additions	$1.20T_x$
Model II	$2N$ cosine, $2N$ additions	$1.20T_x$
Model III	$2N$ cosine, N additions	T_x

3.4.2 Auto-correlation/cross-correlation analysis

We now investigate the performance of these models in terms of their auto- and cross-correlation functions. All the results presented here are obtained using N=11 and a normalized sampling period f_dT_s of 0.001 (f_d is the maximum Doppler frequency and T_s is the sampling period). The variances are computed by averaging over 10^4 simulation trials for each value of time delay τ. Figure 11 presents the variance in the auto-correlation of the in-phase component $g_I(t)$. The quadrature component is similar.

Figure 12 compares the variance in the cross-correlation between the quadrature

[2]The number of random variables required by all models is almost the same ($2N$), except Model I which requires double the number of random variables ($4N$).

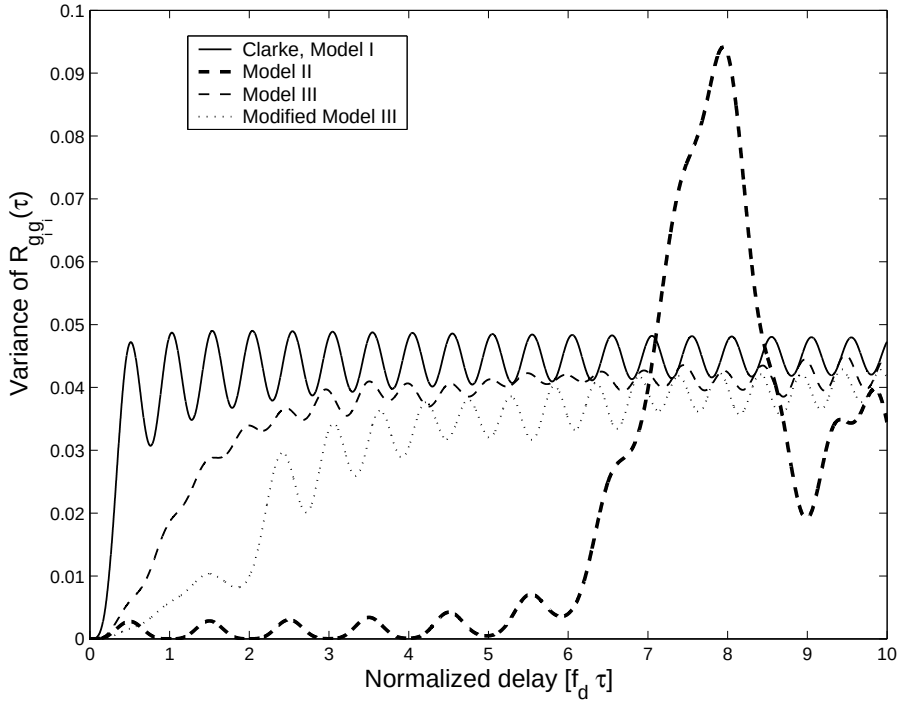

Figure 11: Variance of the auto-correlation of the I component.

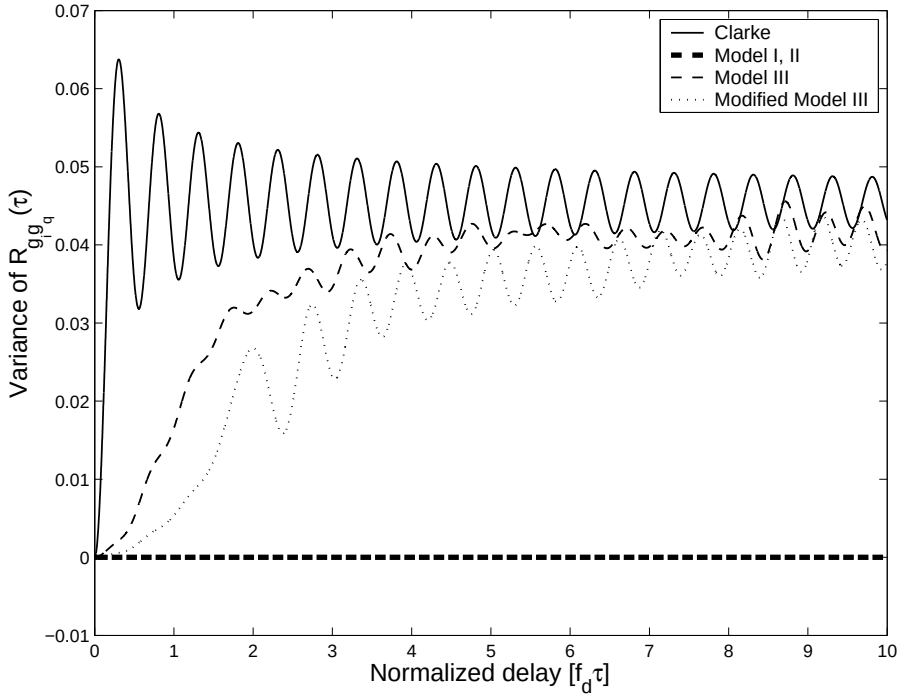

Figure 12: Variance of the cross-correlation between the quadrature components.

components while Figure 13 depicts the variance in the auto-correlation of the complex envelope $g(t)$. From Figure 11 and Figure 13 it is interesting to note that the variances for Model II increase for longer time delays [$\tau \geq N/(2f_d)$]. However, for shorter time delays (and even longer time delays, see Figure 13), which are of more interest for most communication systems [34], the variance of correlation functions of Model II are lower than the variances for all (or most) other models. Hence, Model II is the best among all models for a finite N. Moreover, Model II always produces uncorrelated in-phase and quadrature components, a property which is necessary to yield a Rayleigh distributed envelope. Interestingly, Model II performs better than Model I in spite of their same relative operational complexity. This can be attributed to the proper selection of the simulation parameters in Model II given by (63). Model II achieves superior performance by adding "just the right amount of randomness" in the simulations. This can be observed by comparing (54) and (63), which determine

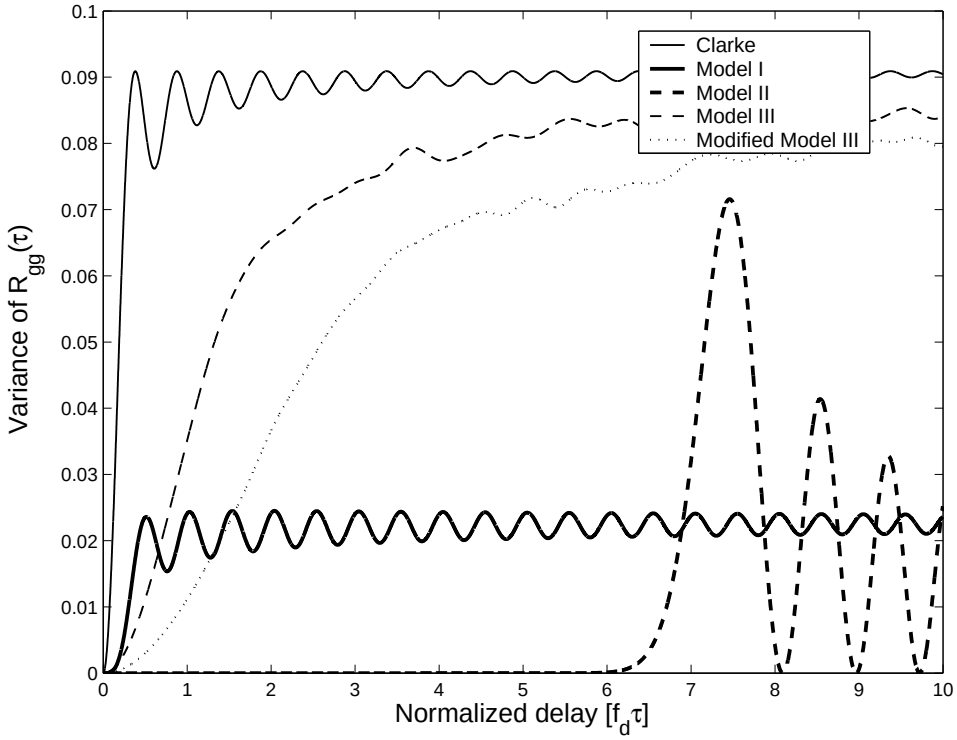

Figure 13: Variance of the auto-correlation of the complex envelope.

the Doppler frequencies used in Model I and Model II, respectively. In Model I, all the Doppler frequencies are chosen randomly and independently of one another. However, in Model II the frequencies are random, but inter-related because the same random parameter θ in (63) defines all the Doppler frequencies. Due to this controlled randomness in Model II, it shows smaller error variance. We can also see that the modified Model III proposed here performs better than the original Model III because we reduced the randomness in this modified Model III.

Further, the statistical squared envelope correlations exhibited by Zheng and Xiao's models are compared in Figure 14 based on the analytical expressions derived earlier. Simulation curves are obtained by averaging the time-averaged squared envelope correlation over 50 simulation trials. Here, we do not consider their variances since neither of them gives the exact desired correlation. Instead, we look for a model which approximates the desired correlation as closely as possible in a statistical sense. From Figure 14, we find that all the models give a fairly good approximation

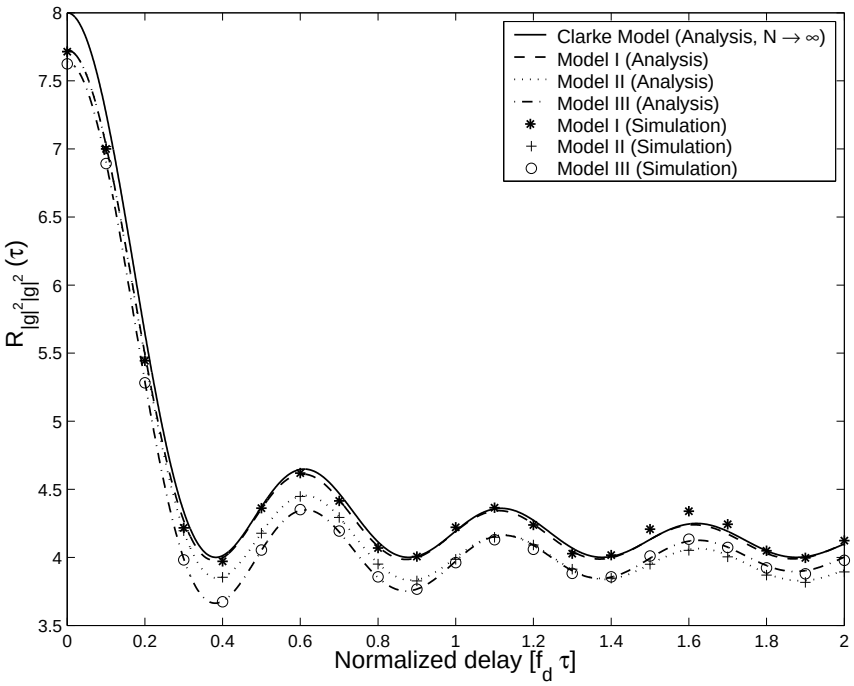

Figure 14: Squared envelope auto-correlation.

of the desired correlation with Model I being the most accurate.

3.4.3 Level crossing rate analysis

Now, we evaluate the various models in terms of their higher order statistics. Specifically, we focus on the level crossing rate. Zheng and Xiao used simulations to evaluate the level crossing rate, while in our work we use an analytical approach. An analytical approach enables us to compare the different models easily and precisely.

Under the assumption that the Gaussian approximation of the channel holds even with finite number of sinusoids, we determine the LCR by utilizing the analysis provided in [56]. Since the LCR for each simulation trial varies randomly, we quantify the variance in the error between the LCR produced by a simulation trial and the desired LCR. Before proceeding further, a note on the notation used. We need to consider two cases separately as described below:

Case I: The quadrature components of $g(t)$ are uncorrelated, i.e., the time average correlation $\hat{R}_{g_i g_q}(\tau)$=0 for all τ, and $\hat{\beta}_i \neq \hat{\beta}_q$, where

$$\hat{\beta}_i = -\left[\frac{d^2 \hat{R}_{g_i g_i}(\tau)}{d\tau^2}\right]_{\tau=0}, \qquad \hat{\beta}_q = -\left[\frac{d^2 \hat{R}_{g_q g_q}(\tau)}{d\tau^2}\right]_{\tau=0} . \tag{81}$$

Then, the LCR at signal envelope level R is [56]

$$\hat{L}_R = \sqrt{\frac{\hat{\beta}_i}{2\pi}} \left(\frac{2}{\pi}\mathbf{E}(\hat{\mathrm{k}})\right) P_R(r), \tag{82}$$

$$\hat{k} = \sqrt{\frac{\hat{\beta}_i - \hat{\beta}_q}{\hat{\beta}_i}} \qquad \hat{\beta}_i \geq \hat{\beta}_q, \tag{83}$$

where $\mathbf{E}$ is the complete elliptic integral of the second kind and $P_R(r)$ represents the cumulative distribution function of the envelope $|g(t)|$=R. The desired LCR value at level R is obtained by substituting the statistical averaged quantities in the above equation by using $\hat{\beta}_i = \hat{\beta}_q = \beta$. Then, the error in the simulated LCR is

$$e_R = \frac{L_R - \hat{L}_R}{L_R} = 1 - \sqrt{\frac{\hat{\beta}_i}{\beta}} \left(\frac{2}{\pi}\right) \mathbf{E}(\hat{\mathrm{k}}) \ . \tag{84}$$

This analysis is valid for Models I and II since they satisfy the assumptions made earlier[3].

Case II: The quadrature components of $g(t)$ are correlated, i.e., the time average correlation $\hat{R}_{g_i g_q}(\tau) \neq 0$ for all τ, and $\hat{\beta}_i = \hat{\beta}_q = \hat{\beta}$. Then,

$$\hat{L}_R = \sqrt{\frac{b_0 b_2 - b_1^2}{2\pi b_0}} P_R(R) \tag{85}$$

$$e_R = 1 - \sqrt{\frac{b_0 b_2 - b_1^2}{b_0 \beta}}, \tag{86}$$

where b_0, b_1, and b_2 are defined as [74]

$$b_n = (j)^n \left[\frac{d^n \hat{R}_{gg}(\tau)}{d\tau^2} \right]_{\tau=0}. \tag{87}$$

Case II holds for the Clarke's model and Model III since they generate correlated quadrature components.

Using this analysis, we compute the errors in the LCRs of different models via simulations by assuming $N = 11$ and a maximum Doppler frequency of 100 Hz. The error variance calculated from these errors by averaging over 50000 simulations are tabulated in in Table 2. We can conclude from this analysis that Model II is the best

Table 2: LCR analysis

Model	Error mean	Error variance
Clarke	5.4e-2	1.56e-2
Model I	4.2e-3	5.8e-3
Model II	2e-4	1e-8
Model III	2e-3	1.2e-3

even in terms of LCR, followed by Model III.

3.4.4 Comparison with other models

Finally, it is worth comparing the MC models discussed here with other popular models such as the Method of Exact Doppler Spread (MEDS) [56].As the name suggests

[3]This can be easily verified by computing time average auto-correlations for different models.

this model reproduces the Doppler spread exactly in simulations. The MEDS model for cellular channels is given by the following set of equations:

$$g(t) = g_I(t) + jg_Q(t) \tag{88}$$

$$g_I(t) = \sqrt{\frac{2}{N}} \sum_{n=1}^{N} \cos\left[\omega_d \cos\left(\frac{\pi(n-1)}{2N}\right) + \phi_{i,n}\right] \tag{89}$$

$$g_Q(t) = \sqrt{\frac{2}{N+1}} \sum_{n=1}^{N+1} \cos\left[\omega_d \cos\left(\frac{\pi(n-1)}{2(N+1)}\right) + \phi_{q,n}\right] \tag{90}$$

Note that only the phases $\phi_{i/q,n}$ are random while the Doppler frequencies are non-random. Due to random phases, the model produces different channel waveforms for different simulation trials. But, it can be proved [56] that due to non-random frequencies, properties like time average auto-correlation do not vary with simulation trials. In this sense, the MEDS is a deterministic model, as discussed in Chapter II. A single simulation trial is representative of the MEDS model properties. This along with the fact that it reproduces desired properties with good accuracy [56] has led to widespread acceptance of this model. In contrast to the MEDS, the MC models discussed earlier are complex since they require several simulation trials for convergence. However, to partly overcome the complexity problem, "multiple parameter set Monte Carlo" (MPS-MC) simulation method has been introduced in [34]. The MPS-MC method divides a simulation trial into several frames and generates random Doppler frequencies and phases for each frame. With this method, the performance of MC models is considerably improved and found to be even better than the MEDS method. A detailed discussion on the MEDS and the MPS-MC methods can be found in [56] and [34], respectively. For completeness, we provide a brief comparison of the performance between the MEDS method and the MPS-MC method applied to Model II. Note, that MPS-MC is not applied to MEDS since its properties do not vary over simulation trials.

For MPS-MC 10 sinusoids are used for simulation of both the I and Q phase components. 10^6 samples are generated by dividing them into 10^2 frames of length

10^4 samples each to get time average auto-correlation results. The MEDS model given in (89) and (90) is used with $N = 10$ and 11 sinusoids for the I and Q components, respectively.

Figure 15 shows the auto-correlation of the complex envelope obtained with a single simulation trial using the two methods for $f_d T_s = 0.01$. Clearly, MPS-MC Model II provides a better fit over a wide range of time delays than the MEDS method. Results over numerous simulation trials showed the same trend. It should also be noted here that the auto-correlation with the MPS-MC model is zero if the time delay exceeds the frame length. Hence, the frame length should be sufficiently long to cover the time delays of interest to get meaningful results. Finally, in Figure 16, we

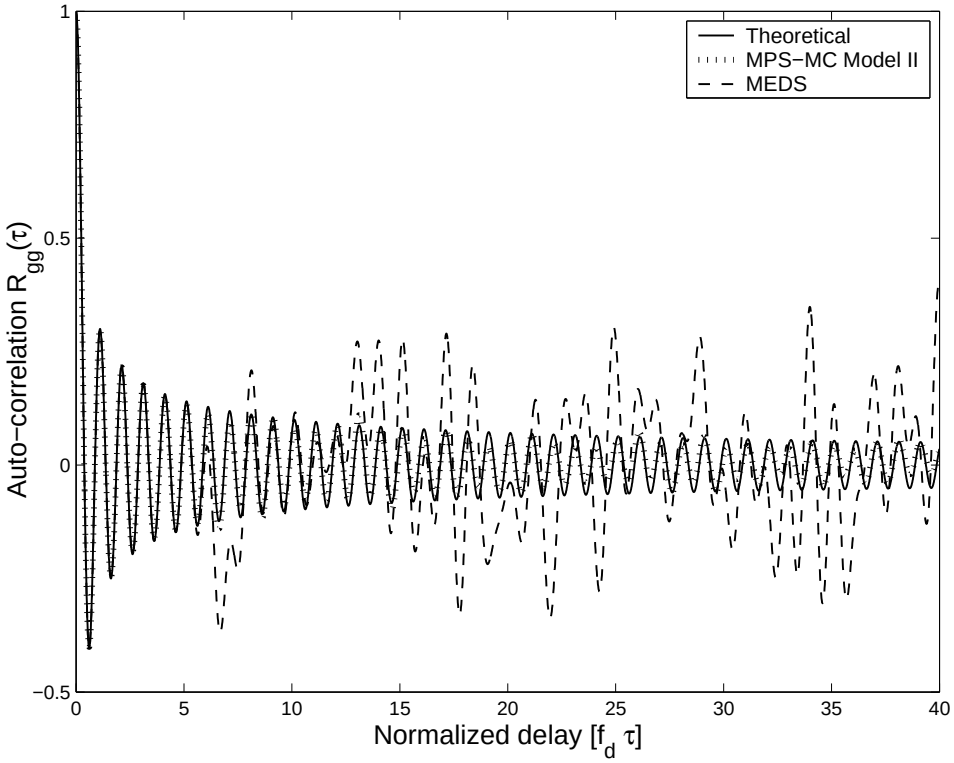

Figure 15: Comparison between the auto-correlation function of the MPS-MC Model II vs. the MEDS model.

compare the BER performance of non-coherent differential BPSK (D-BPSK) modulation. Non-coherent D-BPSK was chosen since its performance depends on the

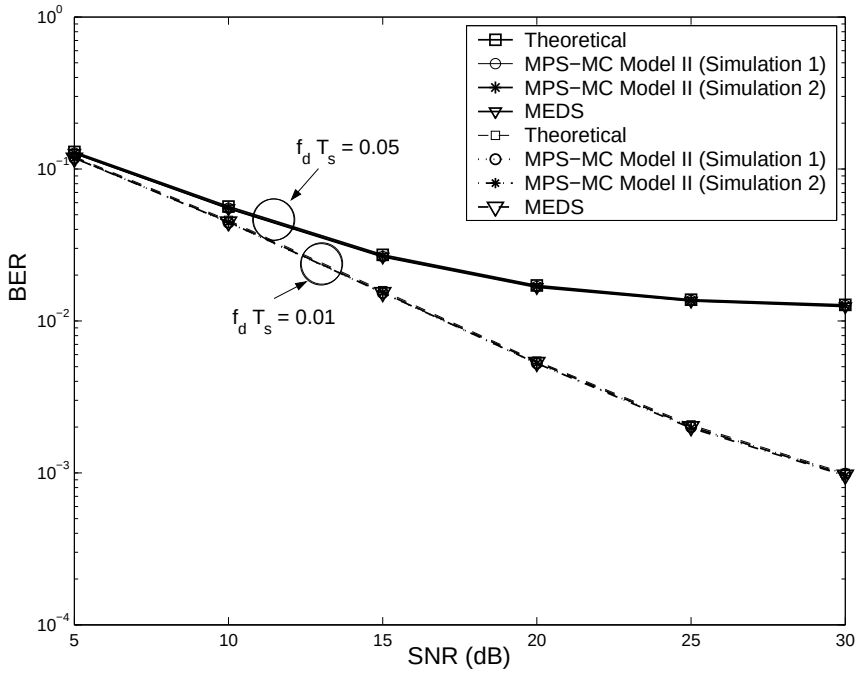

Figure 16: Comparison between the BER of non-coherent DPSK for the MPS-MC Model II vs. the MEDS model.

channel auto-correlation [63] and hence provides a better understanding as to which model is better. BER results were obtained by averaging over 10^7 bits (samples) consisting of 10^4 frames for the MPS-MC model for two different values of the normalized maximum Doppler frequency f_d. Figure 16 shows that the BER obtained using both the MPS-MC Model II and the MEDS model matches the theoretical BER [63]. Further, the undesirable variation of the BER over several simulation trials for the MC method observed in [56] is eliminated by the MPS-MC method, which is evident from the results of two simulation trials. Though 20 simulation trials were conducted to confirm this, results of all 20 trials are not shown to preserve clarity.

Finally, it must be noted that the MC models discussed in earlier sections can provide better performance compared to MEDS at the expense of somewhat increased complexity. A detailed comparison between the MPS-MC method and the MEDS method can be a topic of further study. Issues such as the effect of simulating different frames independently on channel estimation, synchronization, and Viterbi decoding

should be addressed in such a study.

3.5 Summary

In this chapter, we presented a rigorous analysis comparing various SoS statistical models available in the literature for simulating Rayleigh faded cellular channels. We addressed performance as well as complexity issues to identify an appropriate model for simulation purposes. From our analysis, we conclude that Model II, though slightly more complex than some of the other models, is the best for simulating cellular channels. Depending on the complexity constraints and desired performance, we can select other models by using the analysis presented here. In particular, the modified Model III can provide a good trade-off between complexity and performance.

Appendix 3.1: Derivation of (60)

In this section, we provide the derivation of (60), which quantifies the variance of auto-correlation of Modified Hoeher model's I component $g_I(t)$.The variance is defined as

$$\mathrm{Var}[R_{g_ig_i}(\tau)] \;=\; E[\{R_{g_ig_i}(\tau) - \hat{R}_{g_ig_i}(\tau)\}^2]. \tag{91}$$

Using (56), we can re-write the above equation as

$$\begin{aligned}\mathrm{Var}[R_{g_ig_i}(\tau)] \;=\;& R_{g_ig_i}(\tau)^2 - 2R_{g_ig_i}(\tau)\frac{1}{N}E[\sum_{n=1}^{N}\cos(\omega_d f_{i,n}\tau)] + \\ & \frac{1}{N^2}\sum_{n=1}^{N}\sum_{m=1}^{N}E[\cos(\omega_d f_{i,n}\tau)\cos(\omega_d f_{i,m}\tau)].\end{aligned} \tag{92}$$

Now, using the definition of $f_{i,n}$ provided in (54), we get

$$\begin{aligned}\frac{1}{N}E[\sum_{n=1}^{N}\cos(\omega_d f_{i,n}\tau)] \;&=\; \frac{1}{N}\sum_{n=1}^{N}E[\cos(\omega_d f_{i,n}\tau)] \\ &=\; \frac{1}{N}\sum_{n=1}^{N}\int_0^1 \cos\left(\omega_d sin\left(\frac{\pi}{2}u_{i,n}\right)\tau\right)du_{i,n} \\ &=\; \frac{1}{N}\sum_{n=1}^{N}\int_0^{\pi/2}\cos(\omega_d sin(x)\tau)dx\end{aligned}$$

$$
\begin{aligned}
&= \frac{1}{N}\sum_{n=1}^{N} J_0(\omega_d\tau) \\
&= J_0(\omega_d\tau). \qquad (93)
\end{aligned}
$$

Further,

$$
\begin{aligned}
\sum_{n=1}^{N}\sum_{m=1}^{N} E[\cos(\omega_d f_{i,n}\tau)\cos(\omega_d f_{i,m}\tau)] &= \sum_{n=1}^{N} E[\cos(\omega_d f_{i,n}\tau)^2] + \\
&\quad \sum_{n=1}^{N}\sum_{m(\neq n)=1}^{N} E[\cos(\omega_d f_{i,n}\tau)]E[\cos(\omega_d f_{i,m}\tau)] \\
&= \sum_{n=1}^{N} \frac{1+E[\cos(2\omega_d f_{i,n}\tau)]}{2} + \\
&\quad N(N-1)J_0(\omega_d\tau)^2 \\
&= \frac{N+NJ_0(\omega_d\tau)}{2} + N(N-1)J_0(\omega_d\tau)^2. \qquad (94)
\end{aligned}
$$

After substituting (93) and (94) into (92) and making some simplifications, we get the desired expression in (60).

Appendix 3.2: Derivation of (79)

Here we derive the squared envelope correlation of Model III. Following this proof, the squared envelope correlation of other models may be derived. We follow a procedure similar to the one outlined in [86]. We have

$$
\begin{aligned}
R_{|g|^2|g|^2}(\tau) &= \mathrm{E}[|g(t+\tau)|^2|g(t)|^2] \\
&= \mathrm{E}[g_i^2(t+\tau)g_i^2(t)] + \mathrm{E}[g_q^2(t+\tau)g_q^2(t)] + \\
&\quad \mathrm{E}[g_i^2(t+\tau)g_q^2(t)] + \mathrm{E}[g_q^2(t+\tau)g_i^2(t)]. \qquad (95)
\end{aligned}
$$

We compute $\mathrm{E}[g_i^2(t+\tau)g_i^2(t)]$ in this equation as follows, with the remainder of the proof following a similar pattern:

$$
\begin{aligned}
\mathrm{E}[|g_i(t+\tau)|^2|g_i(t)|^2] &= \frac{4}{N^2}\sum_{n=1}^{N}\sum_{m=1}^{N}\sum_{k=1}^{N}\sum_{l=1}^{N} \mathrm{E}\left\{\cos[\omega_d(t+\tau)\cos(\alpha_n)+\phi_n]\times\right. \\
&\quad \cos[\omega_d(t+\tau)\cos(\alpha_m)+\phi_m]\cos[\omega_d t\cos(\alpha_k)+\phi_k]\times \\
&\quad \left.\cos[\omega_d t\cos(\alpha_l)+\phi_l]\right\}. \qquad (96)
\end{aligned}
$$

The mutual independence of the ϕ_i ensures that all terms in the above equation are zero, except the four terms with: 1) $n = m = k = l$; 2) $n = m$, $k = l$, $n \neq k$; 3) $n = k$, $m = l$, $n \neq m$; 4) $n = l$, $m = k$, $n \neq m$. We compute each of these terms individually to derive the overall expression.[4]

Term 1: $n = m = k = l$

$$\begin{aligned}
& \sum_{n=1}^{N} \mathrm{E}\{\cos^2[\omega_d(t+\tau)\cos(\alpha_n) + \phi_n] \times \cos^2[\omega_d t \cos(\alpha_n) + \phi_n]\} \\
= & \sum_{n=1}^{N} \mathrm{E}\{\frac{1}{2}(1 + \cos[2\omega_d(t+\tau)\cos(\alpha_n) + 2\phi_n]) \times \frac{1}{2}(1 + \cos[2\omega_d t \cos(\alpha_n) + 2\phi_n])\} \\
= & \frac{1}{4}\sum_{n=1}^{N}(1 + \frac{1}{2}\mathrm{E}\{\cos[2\omega_d \tau \cos(\alpha_n)]\}) \\
= & \frac{1}{4}[N + \frac{1}{2}NJ_0(2\omega_d\tau)] \qquad (97)
\end{aligned}$$

resulting from the fact that [28]

$$\sum_{n=1}^{N} \mathrm{E}\{\cos[2\omega_d \tau \cos(\alpha_n)]\} = NJ_0(2\omega_d\tau).$$

Term 2: $n = m$, $k = l$, $n \neq k$

$$\begin{aligned}
& \sum_{n=1}^{N}(\mathrm{E}\{\cos^2[\omega_d(t+\tau)\cos(\alpha_n) + \phi_n]\} \times \sum_{k=1,k\neq n}^{N} \mathrm{E}\{\cos^2[\omega_d t \cos(\alpha_k) + \phi_k]\}) \\
= & \sum_{n=1}^{N} \frac{1}{2} \sum_{k=1,k\neq n}^{N} \frac{1}{2} \\
= & \frac{N(N-1)}{4} \qquad (98)
\end{aligned}$$

Term 3: $n = k$, $m = l$, $n \neq m$

$$\begin{aligned}
& \sum_{n=1}^{N} \mathrm{E}\{\cos[\omega_d(t+\tau)\cos(\alpha_n) + \phi_n] \cdot \cos[\omega_d t \cos(\alpha_n) + \phi_n]\} \times \\
& \sum_{m=1,m\neq n}^{N} \mathrm{E}\{\cos[\omega_d(t+\tau)\cos(\alpha_m) + \phi_m] \cdot \cos[\omega_d t \cos(\alpha_m) + \phi_m]\} \\
= & \sum_{n=1}^{N} \frac{1}{2}\mathrm{E}\{\cos[\omega_d \tau \cos(\alpha_n)]\} \times \sum_{m=1,m\neq n}^{N} \frac{1}{2}\mathrm{E}\{\cos[\omega_d \tau \cos(\alpha_m)]\}
\end{aligned}$$

[4] We apply the constant $4/N^2$ factor at the end and, hence, omit it here.

$$
\begin{aligned}
&= \frac{1}{4}\left(\sum_{n=1}^{N}\mathrm{E}\{\cos[\omega_d\tau\cos(\alpha_n)]\}\right)^2 - \frac{1}{4}\sum_{n=1}^{N}[\mathrm{E}\{\cos[\omega_d\tau\cos(\alpha_n)]\}]^2 \\
&= \frac{1}{4}(N^2J_0^2(\omega_d\tau) - \sum_{n=1}^{N}[\mathrm{E}\{\cos[\omega_d\tau\cos(\alpha_n)]\}]^2) \qquad (99)
\end{aligned}
$$

Term 4 can be shown equal to Term 3. Then,

$$
\begin{aligned}
\mathrm{E}[g_i^2(t+\tau)g_i^2(t)] &= \frac{4}{N^2}(\mathrm{Term1} + \mathrm{Term2} + \mathrm{Term3} + \mathrm{Term4}) \\
&= 1 + \frac{1}{2N}J_0(2\omega_d\tau) + \\
&\quad 2J_0^2(\omega_d\tau) - \frac{2}{N^2}\sum_{n=1}^{N}[\mathrm{E}\{\cos[\omega_d\cos(\alpha_n)\tau]\}]^2 \qquad (100)
\end{aligned}
$$

Similarly, we can show that

$$
\begin{aligned}
\mathrm{E}[g_q^2(t+\tau)g_q^2(t)] &= \mathrm{E}[g_i^2(t+\tau)g_i^2(t)] \qquad (101) \\
\mathrm{E}[g_i^2(t+\tau)g_q^2(t)] &= 1 - \frac{1}{2N}J_0(2\omega_d\tau) - \frac{2}{N^2}\sum_{n=1}^{N}[\mathrm{E}\{\sin[\omega_d\cos(\alpha_n)\tau]\}]^2 \qquad (102) \\
\mathrm{E}[g_q^2(t+\tau)g_i^2(t)] &= \mathrm{E}[g_i^2(t+\tau)g_q^2(t)]. \qquad (103)
\end{aligned}
$$

Adding these terms together, gives (79) as

$$
\begin{aligned}
R_{|g|^2|g|^2}(\tau) &= 4 + 4J_0^2(\omega_d\tau) - \\
&\quad \frac{4}{N^2}\sum_{n=1}^{N}\left([\mathrm{E}\{\cos[\omega_d\tau\cos(\alpha_n)]\}]^2 + [\mathrm{E}\{\sin[\omega_d\tau\cos(\alpha_n)]\}]^2\right),
\end{aligned}
$$

which cannot be simplified further due to the presence of the last term and has to be evaluated numerically.

Appendix 3.3: Squared Envelope Correlation of Model IV

Analogous to the derivation of the squared envelope correlation of Model III provided in the earlier section, we derive the squared envelope correlation of Model IV. The proof reveals the non-stationary nature of the simulation model by providing the correct correlation expression in contrast to the expression derived in [86], thereby making our analysis more concrete.

Again, we consider the derivation of $\mathrm{E}[g_i^2(t+\tau)g_i^2(t)]$ term only. Analogous to Appendix 3.2, Term 1 can be shown to be:

Term 1: $n = m = k = l$

$$\begin{aligned} & \sum_{n=1}^{N} \mathrm{E}\{\cos^4(\xi_n)\cos^2[\omega_d(t+\tau)\cos(\alpha_n)+\phi]\cos^2[\omega_d t\cos(\alpha_n)+\phi]\} \\ = \; & \frac{3}{32}[N + \frac{1}{2}NJ_0(2\omega_d\tau)]. \end{aligned} \tag{104}$$

Term 2: $n = m$, $k = l$, $n \neq k$

$$\begin{aligned} & \sum_{n=1}^{N}\sum_{k=1,k\neq n}^{N} \mathrm{E}\{\cos^2(\xi_n)\cos^2(\xi_k)\cos^2[\omega_d(t+\tau)\cos(\alpha_n)+\phi]\cos^2[\omega_d t\cos(\alpha_k)+\phi]\} \\ = \; & \frac{1}{16}\sum_{n=1}^{N}\sum_{k=1,k\neq n}^{N} \mathrm{E}\{1+\cos[2\omega_d(t+\tau)\cos(\alpha_n)+2\phi]\times\cos[2\omega_d t\cos(\alpha_k)+2\phi]\} \\ = \; & \frac{1}{16}[N(N-1) + \frac{1}{2}\sum_{n=1}^{N}\sum_{k(\neq n)=1}^{N} \mathrm{E}\{\cos[2\omega_d(t+\tau)\cos(\alpha_n) - 2\omega_d t\cos(\alpha_k)]\}] \end{aligned} \tag{105}$$

Unlike the derivation of Term 2 in [86], the expectation of the product of the two cosine terms cannot be simplified into the product of the expectations of the individual cosine terms due to the presence of the random phase ϕ in both these terms. This leads to the correct expression given above in contrast to the expression provided in [86]. Further, it is clear that this term depends not only on the time difference τ but also the time variable t. Hence, the squared envelope correlation is non-stationary. Following a similar methodology, we can derive other terms to obtain (80), the squared envelope correlation for Model IV. The other terms in (80) that depend on t are also non-zero, thereby contributing to the non-stationarity of the model.

CHAPTER IV

NEW SIMULATION MODELS FOR MOBILE-TO-MOBILE CHANNELS

4.1 Overview

The previous chapter provided analysis of several different statistical SoS models for simulating cellular channels. In this chapter, we turn our attention to mobile-to-mobile channels. We first evaluate the existing models for mobile-to-mobile channels such as the Akki and Haber model and the Wang and Cox model. Our evaluation brings forth several drawbacks of these models. This motivates us to develop new SoS models for mobile-to-mobile channels. To this end, we introduce a "double ring" scattering model to simulate the mobile-to-mobile local scattering environment. Combining this model with our analysis on cellular channel models, we present models for mobile-to-mobile channels. We adapt Zheng and Xiao's Model II described in the previous chapter for mobile-to-mobile channel simulation. Further, we propose a reduced complexity alternative by modifying the Method of Exact Doppler Spread (MEDS), which was discussed in Chapter III, originally proposed for cellular channels [56]. Since the MEDS model is deterministic, a single simulation trial represents its properties. This avoids multiple simulation trials, thereby reducing complexity. Theoretical and simulation results are employed to verify the usefulness of the our models.

Before proceeding further, we briefly repeat the theoretical reference model for mobile-to-mobile channels for convenience.

4.2 The Mathematical Reference Model

Under frequency-flat fading and 2-D isotropic scattering assumptions around both the Tx and the Rx, the properties of a Rayleigh faded mobile-to-mobile channel are summarized below [10]:

For the complex envelope, $g(t) = g_i(t) + jg_q(t)$, the in-phase, I, and quadrature, Q, components have a zero-mean unit variance Gaussian distribution with auto-correlation and cross-correlation properties

$$\begin{aligned} R_{g_ig_i}(\tau) &= \mathrm{E}[g_i(t+\tau)g_i(t)] = J_0(2\pi f_1\tau)J_0(2\pi f_2\tau) && (106)\\ R_{g_qg_q}(\tau) &= \mathrm{E}[g_q(t+\tau)g_q(t)] = J_0(2\pi f_1\tau)J_0(2\pi f_2\tau) && (107)\\ R_{g_ig_q}(\tau) &= R_{g_qg_i}(\tau) = 0 && (108)\\ R_{gg}(\tau) &= \frac{1}{2}\mathrm{E}[g(t+\tau)g^*(t)] \\ &= J_0(2\pi f_1\tau)J_0(2\pi f_2\tau) = J_0(2\pi f_1\tau)J_0(2\pi a f_1\tau), && (109) \end{aligned}$$

where E[$\cdot$] is the statistical expectation operator, $*$ denotes the complex conjugate operator, $J_0(\cdot)$ is the zeroth order Bessel function of the first kind, $a = (f_2)/(f_1)$ is the ratio of the two maximum Doppler frequencies (or vehicle speeds), and $0 \leq a \leq 1$ assuming $f_2 \leq f_1$.

4.3 Existing Simulation Models

4.3.1 Akki and Haber's simulation model

An obvious simulation model is the one using (23), where we use finite number of paths or sinusoids, N, and generate random angle of departures and arrivals and random phases to simulate the channel. We refer to this model as Akki and Haber's simulation model because they originally proposed this reference model. Though the statistical correlations of this model, given in (106)-(109), do not depend on N, the time-average properties [denoted by $\hat{R}(\cdot)$] indeed depend on N. For example, the

time-average auto-correlation of the complex envelope is

$$\begin{aligned}\hat{R}_{gg}(\tau) &= \frac{1}{2}\lim_{T\to\infty}\frac{1}{2T}\int_{-T}^{T} g(t+\tau)g^*(t)dt \\ &= \frac{1}{N}\sum_{n=1}^{N}\exp[j\{2\pi f_1\cos(\alpha_n)\tau + 2\pi f_2\cos(\beta_n)\tau\}]. \end{aligned} \quad (110)$$

Further the time-average correlations are random due to the random angles of departure and arrival and therefore vary over simulation trials. In such a scenario, as pointed out in [87], the variance $\mathrm{Var}[R(\cdot)]$=$\mathrm{E}[|\hat{R}(\cdot) - \lim_{N\to\infty} R(\cdot)|^2]$ provides a measure of the usefulness of the model in simulating the desired channel waveform using a finite N. A lower variance means that a smaller number of simulation trials are needed to achieve desired properties statistically and, hence, the corresponding model is better. Therefore, we derive the variance of the auto-correlation and the cross-correlation of the I and Q components of the complex envelope, which are stated below:

$$\begin{aligned}\mathrm{Var}[R_{g_ig_i}(\tau)] &= \mathrm{Var}[R_{g_qg_q}(\tau)] \\ &= \frac{1 + J_0(4\pi f_1\tau)J_0(4\pi a f_1\tau) - 2J_0^2(2\pi f_1\tau)J_0^2(2\pi a f_1\tau)}{2N} \end{aligned} \quad (111)$$

$$\mathrm{Var}[R_{g_ig_q}(\tau)] = \mathrm{Var}[R_{g_qg_i}(\tau)] = \frac{1 - J_0(4\pi f_1\tau)J_0(4\pi a f_1\tau)}{2N} \quad (112)$$

$$\mathrm{Var}[R_{gg}(\tau)] = \frac{1 - J_0^2(2\pi f_1\tau)J_0^2(2\pi a f_1\tau)}{N} \quad (113)$$

The proofs of these equations follows the derivation provided in Appendix 3.1. We later utilize these variances to compare the performance of the proposed models with Akki and Haber's simulation model.

4.3.2 Discrete Line Spectrum Method

Wang and Cox [82] presented a modification to the well-known Spectrum Sampling method [65], where they approximate the continuous Doppler spectrum as a set of discrete frequencies to generate the received multipath signal as

$$g(t) = \frac{1}{A}\sum_{n=1}^{N}\sqrt{S(\hat{f}_n)}\exp\left[-j(2\pi\hat{f}_n t + \theta_n)\right]. \quad (114)$$

The model parameters are defined as

$$S(\hat{f}_n) = \sum_{n=1}^{N} \left(\int_{F_n}^{F_{n+1}} S(f)df \right) \delta(f - \hat{f}_n) \quad (115)$$

$$\hat{f}_n = \frac{\int_{F_n}^{F_{n+1}} fS(f)df}{\int_{F_n}^{F_{n+1}} S(f)df}. \quad (116)$$

Here, F_n's are equi-spaced frequencies, $F_1, F_2..., F_{N+1}$, with $F_1 = -(f_1 + f_2)$ and $F_{N+1} = (f_1 + f_2)$, and A is a normalization factor to make the signal envelope have unit power. Thus, $\hat{f}_n$ and $S(\hat{f}_n)$, referred to as the center of mass frequencies and the corresponding masses, respectively, are obtained by numerical integration over the Doppler spectrum given in (25).

Since Wang and Cox do not assess the model performance in terms of the auto-correlation and other properties, we extend their analysis to verify their method. The statistical and time-average properties of this model are given below.

- Statistical correlations:

$$R_{g_i g_i}(\tau) = R_{g_q g_q}(\tau) = \frac{1}{2A^2} \sum_{n=1}^{N} S(\hat{f}_n) \cos(2\pi \hat{f}_n \tau) \quad (117)$$

$$R_{g_i g_q}(\tau) = R_{g_q g_i}(\tau) = \frac{1}{2A^2} \sum_{n=1}^{N} S(\hat{f}_n) \sin(2\pi \hat{f}_n \tau) = 0 \quad (118)$$

$$R_{gg}(\tau) = \frac{1}{2A^2} \sum_{n=1}^{N} S(\hat{f}_n) \cos(2\pi \hat{f}_n \tau), \quad (119)$$

  where the last equality in (118) is obtained using the fact that the Doppler spectrum is symmetrical about the zero frequency. This symmetry gives a negative frequency component for every positive frequency in the set of $\hat{f}_n$'s in (116) such that for even N: $\hat{f}_n = -\hat{f}_{(N+1)-n}$, $S(\hat{f}_n) = S(\hat{f}_{(N+1)-n})$, $n = 1, 2, ..., N/2$, and for odd N: $\hat{f}_n = -\hat{f}_{(N+1)-n}$, $S(\hat{f}_n) = S(\hat{f}_{(N+1)-n})$, $n = 1, 2, ..., (N-1)/2$, $\hat{f}_{(N+1)/2} = 0$. This set of $\hat{f}_n$'s results in zero cross-correlation in (118) because *sine* is an odd function.

- Time-average correlations (for even N):

$$\hat{R}_{g_i g_i}(\tau) = \frac{1}{2A^2} \sum_{n=1}^{N} S(\hat{f}_n) \left[\cos(2\pi \hat{f}_n \tau) + \cos(2\pi \hat{f}_n \tau + \theta_n + \theta_{N+1-n}) \right] \quad (120)$$

$$\hat{R}_{g_q g_q}(\tau) = \frac{1}{2A^2}\sum_{n=1}^{N} S(\hat{f}_n)\left[\cos(2\pi\hat{f}_n\tau) - \cos(2\pi\hat{f}_n\tau + \theta_n + \theta_{N+1-n})\right] \quad (121)$$

$$\hat{R}_{g_i g_q}(\tau) = \hat{R}_{g_q g_i}(\tau)$$

$$= \frac{1}{2A^2}\sum_{n=1}^{N} S(\hat{f}_n)\sin(2\pi\hat{f}_n\tau + \theta_n + \theta_{N+1-n}) \quad (122)$$

$$\hat{R}_{gg}(\tau) = \frac{1}{2A^2}\sum_{n=1}^{N} S(\hat{f}_n)\cos(2\pi\hat{f}_n\tau). \quad (123)$$

The above expressions are also valid for odd N provided proper subscripts on the second θ dependent terms are used.

Some interesting inferences can be drawn from this analysis. First, (120), (121), and (122) show that the time-average correlations for the I and Q components vary with simulation trials since they are functions of random phases θ_n's. It should be noted that this drawback can be easily avoided by constraining the random phases so that θ_n = - θ_{N+1-n}, n = 1,2,...,$N/2$, for an even N or θ_n = - θ_{N+1-n}, n = 1,2,...,$(N-1)/2$, for an odd N. However, some other problems still exist, which are discussed below.

Though the I and Q components are statistically uncorrelated as prescribed by the reference model, they are correlated for a single simulation trial as evident in (122). Figure 17 plots the time-averaged cross-correlation between the I and Q components for two arbitrary simulation trials. We observe that cross-correlation is clearly not zero.

Now, consider the auto-correlation of the complex envelope shown in Figure 18 obtained using $N = 40$, $a = 1$, $f_1 = 100$ Hz, and a sampling time $T_s = 10^{-6}$ second. The simulated auto-correlation follows the desired auto-correlation closely but shows some form of periodicity, the period being determined by the separation between different $\hat{f}_n$. Though the separation between successive $\hat{f}_n$'s is not constant, numerical investigations show the difference to be very close to a constant. This combined with the loss of numerical precision in simulations causes the sinusoidal frequencies to be harmonically related leading to periodicity in the auto-correlation function. For

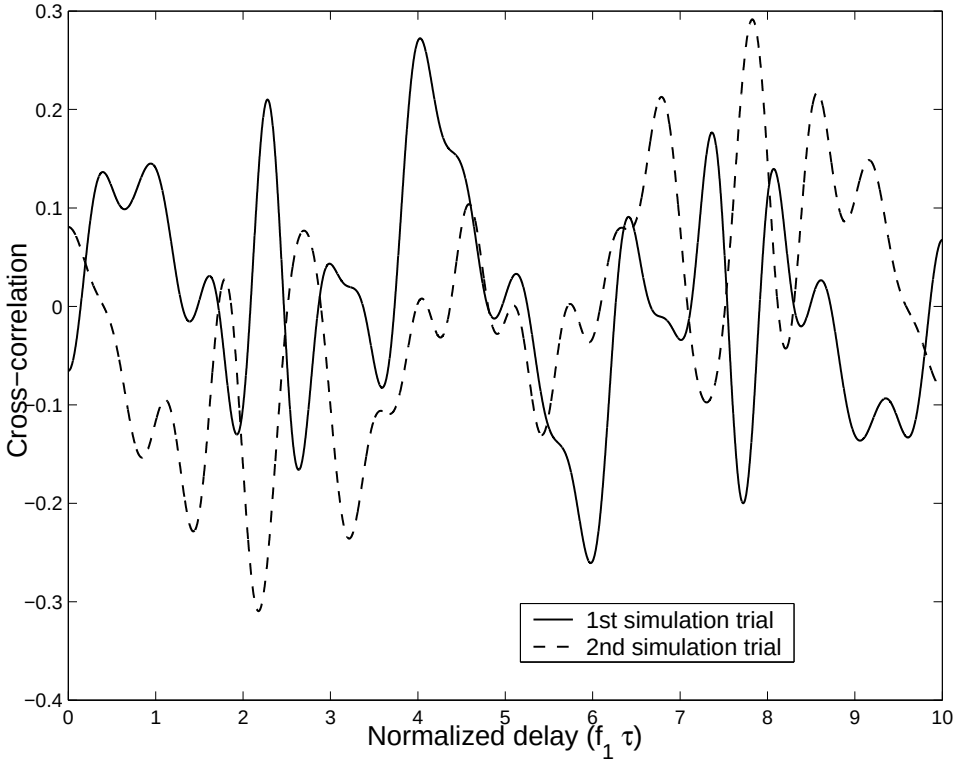

Figure 17: Cross-correlation between the quadrature components generated by the discrete line spectrum method.

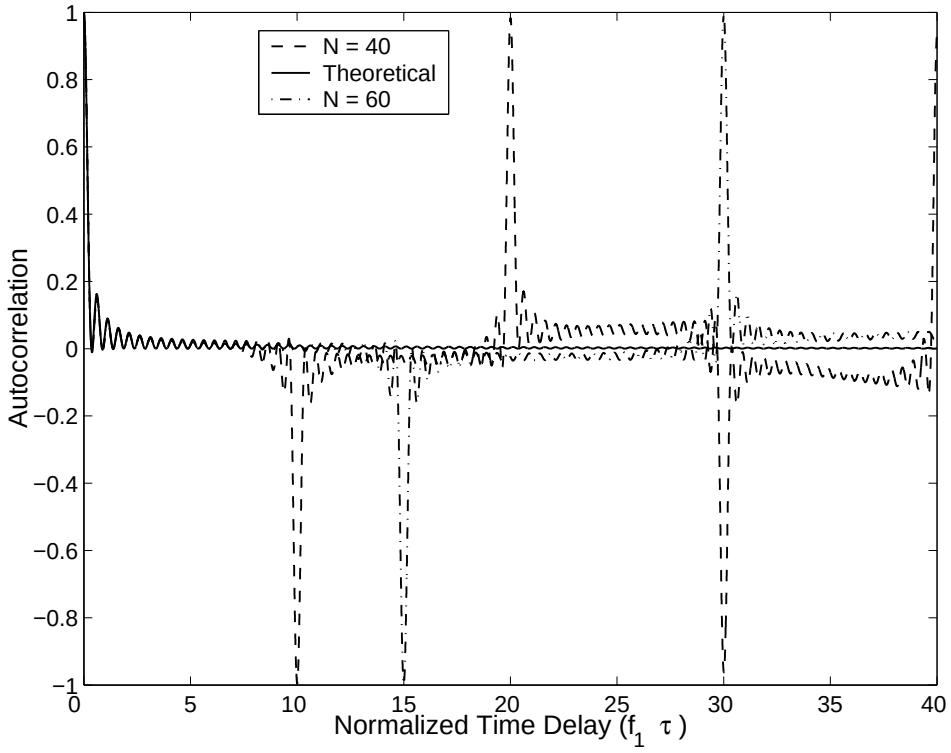

Figure 18: Auto-correlation of the complex envelope simulated by the discrete line spectrum method

example, the auto-correlation attains very high values for time delay τ approximately equal to integral multiples of $(N)/(2f_1[1+a])$. As a result, the stochastic process itself shows periodicity. For longer waveform durations, such behavior is undesirable. To remedy the situation the number of paths N may be increased. The auto-correlation using $N = 60$ is also shown in Figure 18. Though the waveform period increases, the model complexity has also increased due to increase in N. In general, if T_s denotes the sampling period and N_s the number of samples to be simulated, the required $N = 2(1+a)(f_1T_s)N_s$. For example, with $f_1T_s = 0.001$, $a = 1$, and $N_s = 10^5$, $N = 400$ sinusoids will be required, which is often not practical in terms of complexity.

The foregoing analysis clearly reveals the drawbacks of Wang and Cox's model. Moreover, the numerical integrations required to obtain the model parameters make the implementation complex and not easily reconfigurable for different Doppler frequencies or the Doppler frequency ratio a. Hence, we propose alternate simulation models in the next section.

4.4 New Simulation Models

In this section, we present SoS statistical and deterministic models to simulate mobile-to-mobile channels. First, we introduce a "double ring" scattering environment for mobile-to-mobile channels. Using this "double ring" model, we provide our simulation models and verify their properties. The statistical SoS model presented here extends the model proposed by Zheng and Xiao [85] for cellular channels to the more general case of mobile-to-mobile channels while the deterministic model extends the MEDS model [56].

An important distinction between cellular channels and mobile-to-mobile channels arises due to the difference in the Tx and the Rx antenna elevations for these channels. In contrast to cellular channels, it is natural for both the Tx and the Rx antenna to have low elevations in mobile-to-mobile channels. This results in local scattering

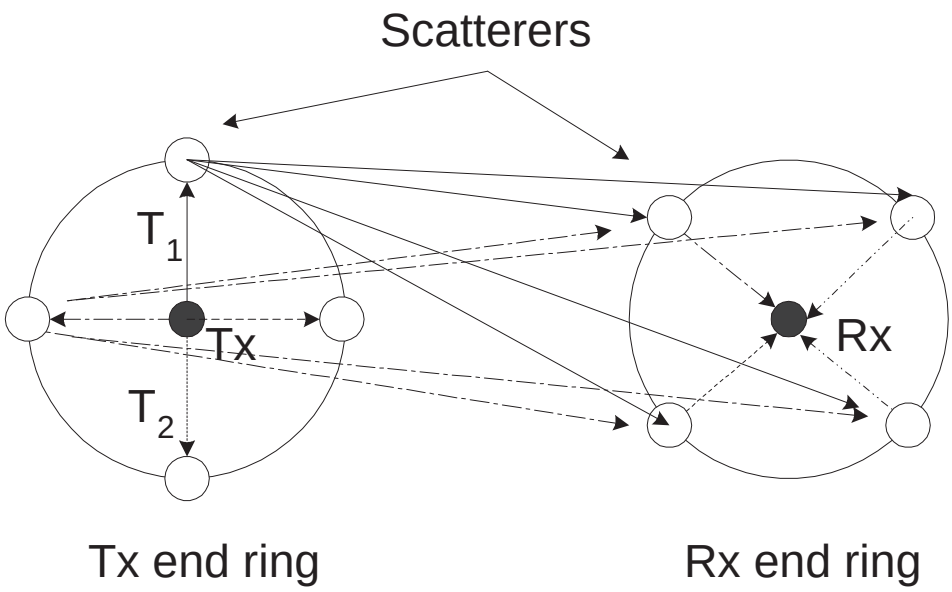

Figure 19: Double ring model for mobile-to-mobile scattering environment.

around the Tx and the Rx which led to the 2-D isotropic scattering assumption in Akki and Haber's original model. To simulate such local scattering, we propose an extension to the "single ring" model of cellular channels [42], which defines scatterers as lying uniformly on a ring around the MS, to a "double ring" model. It should be emphasized here that the "double ring" model has been proposed previously in various forms, for example in [16] and the references therein, for the study and simulation of spatial correlations and capacity in MIMO systems. But, to the best of our knowledge, this is its first application where mobility has been incorporated at both ends of the communication link to simulate a complete mobile-to-mobile channel. The "double ring" model defines a ring of uniformly spaced scatterers around both the Tx and the Rx, thus giving rise to isotropic local scattering, as illustrated in Figure 19. Assuming omni-directional antennas at both ends, the waves from the Tx antenna arrive at each of the scatterer located on the Tx end ring, for example paths T_1 and T_2. Considering these scatterers as "virtual base-stations," we model the communication link from each of these scatterers to the Rx as a conventional cellular BS to MS link. Hence,

each "virtual base-station" transmits a signal that arrives at the Rx uniformly from all directions in the horizontal plane due to isotropic scatterers located on the Rx end ring. We can then model the received signal as

$$g(t) = \sqrt{\frac{2}{NM}} \sum_{n=1}^{N} \sum_{m=1}^{M} \exp\left[j\{2\pi f_1 \cos(\alpha_n)t + 2\pi f_2 \cos(\beta_m)t + \theta_{nm}\}\right], \quad (124)$$

where the index 'n' refers to the paths traveling from the Tx to the N scatterers located on the Tx end ring, the index 'm' refers to the paths traveling from the M scatterers on the Rx end ring to the Rx, and the phases $\phi_{nm} \sim U[-\pi, \pi)$ are independent for all n, m pairs. Note that the single summation in the Akki and Haber's model is now replaced by a double summation because of the double reflection incorporated by the "double ring" model. Nevertheless, the channel essentially remains the same, since each path will undergo a Doppler shift due to the motion of the Tx and the Rx.

The reasons behind employing this model are manifold. First and foremost, it is a mathematically convenient model that enables simulation of the reference model. Second, considering the lack of a detailed and standardized mobile-to-mobile channel model, the model provides a generic scenario with isotropic scattering at both ends of the communication link. Finally, Doppler spectrum measurements in urban and highway environments [8] somewhat match those predicted by the isotropic scattering assumption, thus providing an approximate heuristic verification of the model. A rigorous verification should be explored in future research work.

Using this general model, we now proceed to describe our simulation models.

4.4.1 Statistical simulation model

Definition: The narrowband complex envelope of mobile-to-mobile channel can be simulated as

$$g(t) = g_i(t) + jg_q(t) \quad (125)$$

$$g_i(t) = \sqrt{\frac{2}{NM}} \sum_{n,m=1}^{N,M} \cos\{2\pi f_1 \cos(\alpha_n)t + 2\pi f_2 \cos(\beta_m)t + \phi_{nm}^i\} \quad (126)$$

$$g_q(t) = \sqrt{\frac{2}{NM}} \sum_{n,m=1}^{N,M} \cos\{2\pi f_1 \sin(\alpha_n)t + 2\pi f_2 \cos(\beta_m)t + \phi_{nm}^q\} \quad (127)$$

$$\alpha_n = \frac{2\pi n - \pi + \theta}{4N} \qquad n = 1, 2, ..., N \quad (128)$$

$$\beta_m = 2\left(\frac{2\pi m - \pi + \psi}{4M}\right) \qquad m = 1, 2, ..., M, \quad (129)$$

where $\theta \sim U[-\pi, \pi)$ and $\psi \sim U[-\pi, \pi)$ are mutually independent. Also, the random phases $\phi_{nm} \sim U[-\pi, \pi)$ are mutually independent for all n, m, and the I and Q components. The motivation behind this model originates in Zheng and Xiao's Model II discussed in the earlier chapter in the context of cellular channels. We adapt the parameters of this model appropriately for mobile-to-mobile channels.

It can be shown that the statistical properties of this model match those of the reference model in (106)-(109). The proof of the derivation of the auto-correlation of the I component is provided in Appendix 4.1. Other properties can be derived analogously. The Central Limit Theorem ensures the Gaussian nature of the quadrature components when sufficiently large number of sinusoids are added. Thus, the properties of the proposed model statistically match those of the reference model. It is worth noting that α_ns in (128) are identical to the ones used in Zheng and Xiao's Model II (eqn. 66). But, β_ms in (129) are adapted to provide desired statistical correlations for mobile-to-mobile channels, which can be noticed from the derivation in Appendix 4.1. Also, the angle of departures and arrivals in (125) can be chosen in numerous ways to obtain the same statistical properties, as demonstrated in [85] and [83] for the case of cellular channels. However, our analysis of cellular channels revealed that the parameters of Model II are best suited for simulation. Therefore, using this intuition, the above parameters were selected for mobile-to-mobile channels to obtain the best performance.

The time-average correlations can be derived as:

$$\hat{R}_{g_i g_i}(\tau) = \frac{1}{NM} \sum_{n,m=1}^{N,M} \cos\{2\pi f_1 \cos(\alpha_n)\tau + 2\pi f_2 \cos(\beta_m)\tau\} \quad (130)$$

$$\hat{R}_{g_q g_q}(\tau) = \frac{1}{NM} \sum_{n,m=1}^{N,M} \cos\{2\pi f_1 \sin(\alpha_n)\tau + 2\pi f_2 \cos(\beta_m)\tau\} \quad (131)$$

$$\hat{R}_{g_i g_q}(\tau) = \hat{R}_{g_q g_i}(\tau) = 0 \quad (132)$$

$$\hat{R}_{gg}(\tau) = \frac{1}{NM} \sum_{n,m=1}^{N,M} [\cos\{2\pi f_1 \cos(\alpha_n)\tau + 2\pi f_2 \cos(\beta_m)\tau\} + \cos\{2\pi f_1 \sin(\alpha_n)\tau + 2\pi f_2 \cos(\beta_m)\tau\}]. \quad (133)$$

Being a statistical model, its time-average correlations are random and depend on the random Doppler frequencies. However, the model performs better than the Akki and Haber's simulation model in terms of the variance of these correlations, a fact verified in the next section. Note that expressions for variances of the correlation functions for the proposed statistical model are not provided because they cannot be obtained in a closed form.

4.4.2 Deterministic simulation model

As noted earlier, the model described above may require several simulation trials to achieve desired convergence in its properties. A low complexity alternative is proposed in this section by adapting the MEDS discussed in Section 3.4.4 in the context of cellular channels [56]. We call this model the modified MEDS model.

Definition: The modified MEDS generates the complex as

$$g(t) = g_i(t) + j g_q(t) \quad (134)$$

$$g_i(t) = \sqrt{\frac{2}{N_i M_i}} \sum_{n,m=1}^{N_i,M_i} \cos\{2\pi f_{1,n}^i t + 2\pi f_{2,m}^i t + \phi_{nm}^i\} \quad (135)$$

$$g_q(t) = \sqrt{\frac{2}{N_q M_q}} \sum_{n,m=1}^{N_q,M_q} \cos\{2\pi f_{1,n}^q t + 2\pi f_{2,m}^q t + \phi_{nm}^q\} \quad (136)$$

$$f_{1,n}^{i/q} = f_1 \cos\left(\frac{\pi(n-1/2)}{2N_{i/q}}\right) \qquad n = 1, 2, ..., N_{i/q} \quad (137)$$

$$f_{2,m}^{i/q} = f_2 \cos\left(\frac{\pi(m-1/2)}{M_{i/q}}\right) \qquad m = 1, 2, ..., M_{i/q}, \quad (138)$$

where the phases $\phi_{nm} \sim U[-\pi, \pi)$ and are independent for all n, m, and the I and Q components.

A few remarks are made below in order to fully describe this model:

Remark 1: The Doppler frequencies in (137) are essentially the same as the original MEDS model. The Doppler frequencies in (138) are chosen to reproduce desired properties for mobile-to-mobile channels.

Remark 2: To make the time average correlations deterministic and independent of the random phases ϕ_{nm}'s, not only all the frequencies, $f_{1,n}^i + f_{2,m}^i$ in I and $f_{1,k}^q + f_{2,l}^q$ in Q components must be distinct, but they must also be distinct among themselves for all pairs of (n, m) and (k, l)s. Though it is difficult to establish a general rule to meet this criterion, we found from simulations that with $N_i = M_i = N_I$ and $N_q = M_q = N_I + 1$, the Doppler frequencies are indeed distinct for practical ranges of N_I varying from 5 to 60 and for different Doppler frequency ratios, i.e., as. This rule is similar to the one used in the original MEDS model. Under these assumptions, it can be shown that the time average correlations, which are equal to the statistical correlations, are

$$\hat{R}_{g_i g_i}(\tau) = \frac{1}{N_I^2} \sum_{n,m=1}^{N_I,N_I} \cos\{2\pi f_{1,n}^i \tau + 2\pi f_{2,m}^i \tau\} \tag{139}$$

$$\hat{R}_{g_q g_q}(\tau) = \frac{1}{(N_I+1)^2} \sum_{n,m=1}^{(N_I+1),(N_I+1)} \cos\{2\pi f_{1,n}^q \tau + 2\pi f_{2,m}^q \tau\} \tag{140}$$

$$\hat{R}_{g_i g_q}(\tau) = \hat{R}_{g_q g_i}(\tau) = 0. \tag{141}$$

Remark 3: Since nothing concrete can be said about the distinctness of the Doppler frequencies for arbitrary $N_{i/q}$ and $M_{i/q}$'s, it is difficult to obtain the asymptotic properties, i.e., for $N_{i/q} \to \infty$ and $M_{i/q} \to \infty$, of the model. This may be of interest for future research.

Remark 4: Finally, it is worth noting that the modified MEDS model retains the property of exactly reproducing the Doppler spread in the simulation model. A brief outline of the proof for this property is provided in Appendix 4.2.

4.5 Simulation Results

Having provided the simulation models, we now compare their performance in this section. Unless stated otherwise, all the simulation results presented here are obtained using $a = 1$, $f_1 = 100$ Hz, $N = M = N_I = 8$, and a sampling period T_s of 10^{-5} s.

Figure 20 shows the auto-correlation of the simulated complex envelope. The figure also plots the time averaged auto-correlation for the statistical model averaged over 5 and 10 trials. For the normalized time delay range $0 \leq f_1 T_s \leq 3$, which is typically of interest for most communication systems, the modified MEDS and the statistical model provide a good approximation to the desired auto-correlation. Also, periodicity encountered in Wang and Cox's model is not observed here. It is also evident that by averaging over more trials, the performance of statistical model improves and is better compared to the modified MEDS model.

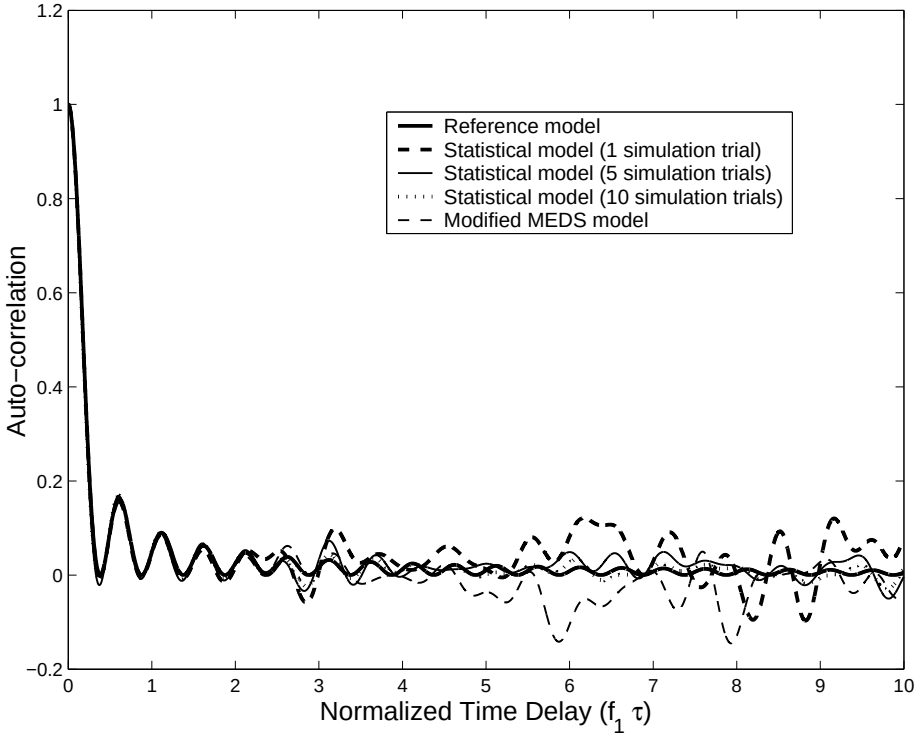

Figure 20: Auto-correlation of the complex envelope.

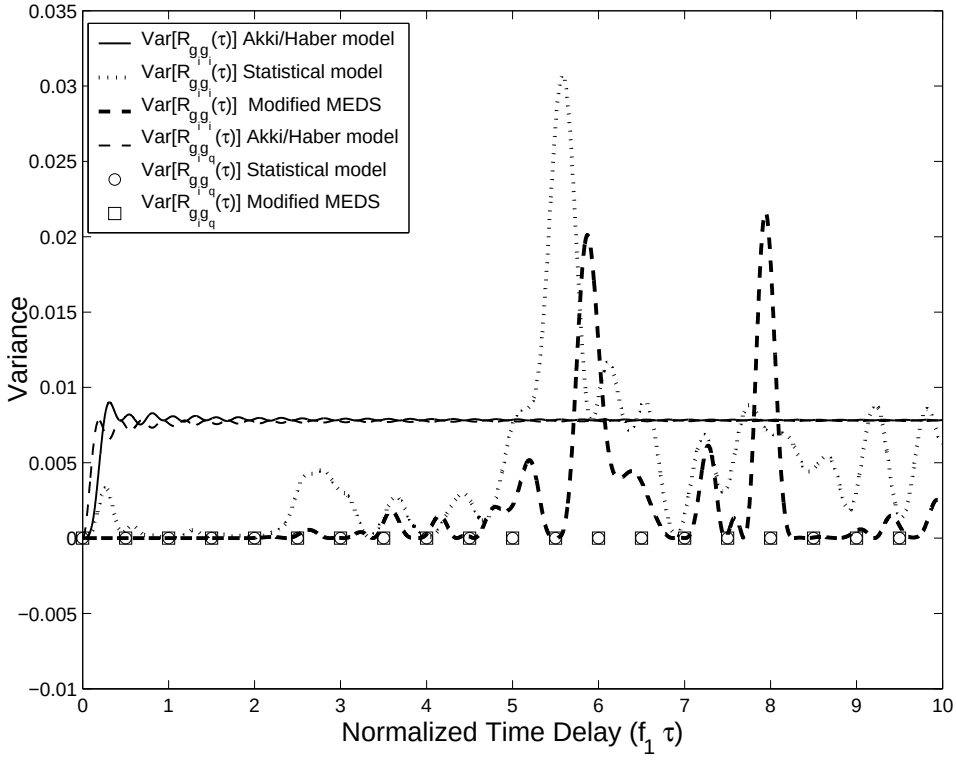

Figure 21: Variance of the auto-correlation and cross-correlations.

Figure 21 compares the variance in auto-correlation and cross-correlation of the quadrature components for different models. The results for the statistical model are obtained by averaging the squared error in correlations over 10^4 trials. For the modified MEDS model, the equivalent quantity is the squared error $|\hat{R}(\cdot) - R(\cdot)|^2$ which is also plotted in Figure 21. The variances for Akki and Haber's model are obtained using (111) and (112). For a fair comparison, we use $N = 64$ sinusoids in Akki and Haber's model (which is equal to Nx$M = 64$ sinusoids used for the proposed models). From the Figure 21, we see that the variances of the proposed models are considerably lower than those of Akki and Haber's model for time delay ranges of interest. Also, the modified MEDS model performs better compared to the statistical model for a single simulation trial. Future work should investigate performance improvements in the statistical model by employing techniques described in [34] to make it more efficient.

Finally, the performance in terms of level crossing rates is verified in Figure 22, thereby further strengthening the validity of these models.

4.6 Summary

In this chapter, we presented new statistical and deterministic SoS models based upon a "double ring" local scattering environment for simulating Rayleigh faded mobile-to-mobile radio channels. The statistical model can be used for obtaining good performance while the deterministic model can be used when simulation complexity is to be minimized. The performance of the proposed models has been verified in terms of the probability distribution function, the auto-correlation, the cross-correlation, and the level crossing rate of the channel waveform through theoretical and simulation results. Our analysis reveals that the proposed models perform better than the existing models. Thus, our models can be useful in designing mobile-to-mobile communication systems.

Appendix 4.1: Derivation of the auto-correlation of the in-phase component of the statistical simulation model

Consider the in-phase component of the received signal given in (126). The auto-correlation function of $g_I(t)$ is

$$\begin{aligned} R_{g_i g_i}(\tau) &= E[g_i(t+\tau)g_i(t)] \\ &= \frac{2}{NM}\sum_{n,m=1}^{N,M}\sum_{p,k=1}^{N,M} E\Big[\cos\{2\pi f_1\cos(\alpha_n)(t+\tau)+2\pi f_2\cos(\beta_m)(t+\tau)+\phi^i_{nm}\} \\ &\quad \cos\{2\pi f_1\cos(\alpha_p)t+2\pi f_2\cos(\beta_k)t+\phi^i_{pk}\}\Big] \\ &= \frac{1}{NM}\sum_{n,m=1}^{N,M} E\left[\cos\{2\pi f_1\cos(\alpha_n)\tau+2\pi f_2\cos(\beta_m)\tau\}\right], \end{aligned} \tag{142}$$

where we use, for simplification, the fact that ϕ_{nm} are independent for all $(n,\ m)$'s. Since θ in the angle of departure α and ψ in the angle of arrival β [refer to (128, 129)]

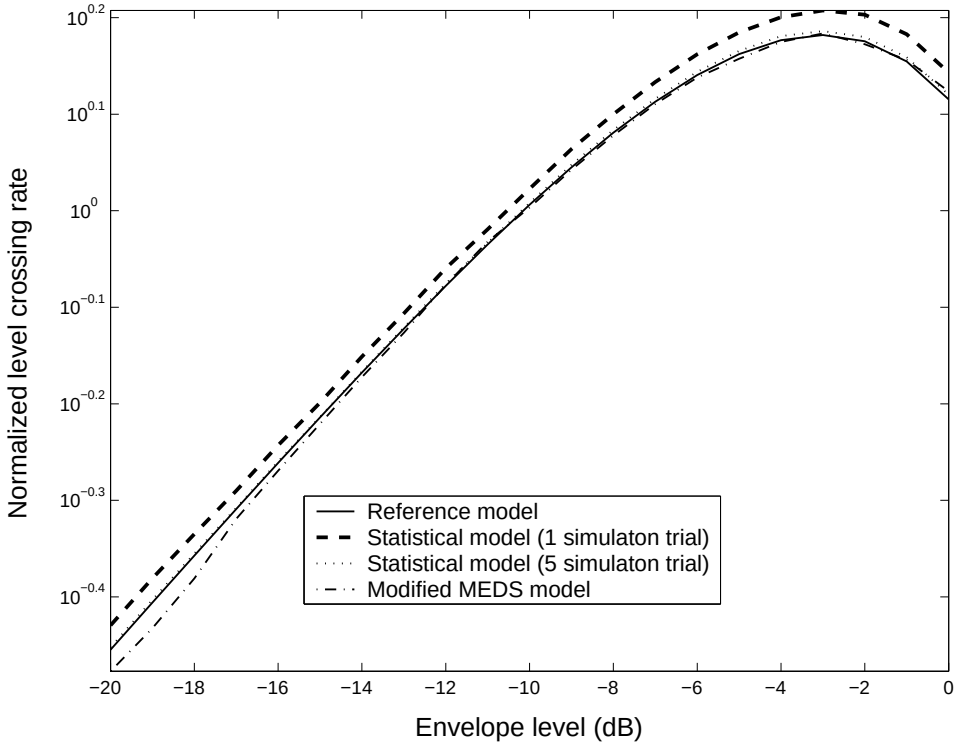

Figure 22: Normalized level crossing rate.

are independent, (142) can be further simplified, using [28, pp. 414 (13), pp. 415 (18), (19)], as

$$\begin{aligned} R_{g_i g_i}(\tau) &= \frac{1}{NM} E\left[\sum_{n=1}^{N} \cos\{2\pi f_1 \cos(\alpha_n)\tau\} \sum_{m=1}^{M} \cos\{2\pi f_2 \cos(\beta_m)\tau\}\right. \\ &\quad \left. - \sum_{n=1}^{N} \sin\{2\pi f_1 \cos(\alpha_n)\tau\} \sum_{m=1}^{M} \sin\{2\pi f_2 \cos(\beta_m)\tau\}\right] \\ &= \frac{2}{\pi}\int_0^{\frac{\pi}{2}} \cos\{2\pi f_1 \cos(\alpha)\tau\} d\alpha \frac{1}{\pi}\int_0^{\pi} \cos\{2\pi f_2 \cos(\beta)\tau\} d\beta \\ &\quad - \frac{2}{\pi}\int_0^{\frac{\pi}{2}} \sin\{2\pi f_1 \cos(\alpha)\tau\} d\alpha \frac{1}{\pi}\int_0^{\pi} \sin\{2\pi f_2 \cos(\beta)\tau\} d\beta \\ &= J_o(2\pi f_1 \tau) J_o(2\pi f_2 \tau) - 0 \\ &= J_o(2\pi f_1 \tau) J_o(2\pi f_2 \tau), \end{aligned} \tag{143}$$

which is the desired expression.

Appendix 4.2: Proof of the exactness of MEDS model's Doppler Spread

As discussed in Chapter II, the Doppler spread provides a measure of how fast the channel varies in time. Therefore, the Doppler spread is a parameter of interest. Here, we prove that the modified MEDS model exactly reproduces the channel Doppler spread in simulations. The Doppler spread of a channel $g(t)$ with auto-correlation $R_{gg}(\tau)$ is defined as [56]

$$B_d = \frac{1}{2\pi}\sqrt{\left[\left(\frac{\dot{R}_{gg}(\tau)}{R_{gg}(0)}\right)^2 - \frac{\ddot{R}_{gg}(\tau)}{R_{gg}(0)}\right]_{\tau=0}}, \tag{144}$$

where $\dot{X}$ represents the differentiation of X with respect to τ. It can be shown that the first term in the above equation is zero. Therefore, the Doppler spread of the I and Q components of the reference model can be written as

$$\begin{aligned} B^i_{d,ref} &= B^q_{d,ref} = \left[\frac{1}{2\pi}\sqrt{-\frac{d^2 J_0(2\pi f_1\tau)J_0(2\pi f_2\tau)}{d\tau^2}}\right]_{\tau=0} \\ &= \sqrt{\frac{f_1^2+f_2^2}{2}}. \end{aligned} \tag{145}$$

For the I component of the modified MEDS model, after differentiating the auto-correlation in (139) twice w.r.t. τ and evaluating it at $\tau = 0$, the Doppler spread is

$$B^i_{d,MEDS} = \frac{1}{2\pi}\sqrt{\frac{1}{N_I^2}\sum_{n,m=1}^{N_I,N_I}(2\pi f^i_{1,n} + 2\pi f^q_{1,m})^2} = \sqrt{T_1+T_2+T_3}, \tag{146}$$

with

$$\begin{aligned} T_1 &= \frac{f_1^2}{N_I}\sum_{n=1}^{N_I}\cos^2\left(\frac{\pi(n-1/2)}{2N_I}\right), \quad T_2 = \frac{f_2^2}{N_I}\sum_{m=1}^{N_I}\cos^2\left(\frac{\pi(m-1/2)}{N_I}\right), \text{and} \\ T_3 &= \frac{f_1^2 f_2^2}{N_I^2}\left[\sum_{n=1}^{N_I}\cos\left(\frac{\pi(n-1/2)}{2N_I}\right)\right]\left[\sum_{m=1}^{N_I}\cos\left(\frac{\pi(m-1/2)}{N_I}\right)\right]. \end{aligned} \tag{147}$$

By applying the identities

$$\sum_{n=1}^{N_I}\cos^2\left(\frac{\pi(n-1/2)}{N_I}\right) = \sum_{n=1}^{N_I}\cos^2\left(\frac{\pi(n-1/2)}{2N_I}\right) = \frac{N_I}{2}, \tag{148}$$

$$\sum_{n=1}^{N_I} \cos\left(\frac{\pi(n-1/2)}{N_I}\right) = 0, \tag{149}$$

to simplify T_1, T_2, and T_3 terms, we get

$$B^i_{d,MEDS} = \sqrt{\frac{f_1^2 + f_2^2}{2}}, \tag{150}$$

which matches that of the reference model. Similarly, we can prove that the Doppler spread of the Q-phase component is also equal to that of the reference model. Thus, the modified MEDS model produces exact Doppler spread in the simulations of mobile-of-mobile channels.

CHAPTER V

PROPERTIES OF AMPLIFY AND FORWARD RELAY CHANNELS

5.1 Overview

To make practical deployment of cooperation diversity schemes, it is necessary to study the underlying channel model and system performance in the presence of channel impairments. With this goal in mind, we present statistical properties of amplify and forward (AF) relay channels in this chapter.

We discussed in Chapter II that AF relays are preferred over decode and forward (DF) relays because of their low complexity. At the same time, such AF relays change the nature of the effective channel from the Tx to the Rx. Fading relay channels are often modeled as a double Gaussian channel, i.e., a product of two complex Gaussian channels [20]. Relay channels are statistically identical to the "pinhole" channels encountered in certain MIMO channel environments [18, 26]. Therefore, their first order properties like the envelope distribution are known. Several authors have provided performance analysis of AF systems in terms of their BER and outage probability under different assumptions on the amplifier gain [13, 15, 37, 32, 88]. However, these performance metrics do not completely reflect the dynamic, time varying nature of a fading relay channel resulting from the mobility of the relay as well as the MS. Since very little is known about their properties such as the auto-correlation, level crossing rate, etc., we present an analysis of these statistical properties of fading relay channels.

Our study of relay channels combines the earlier work on fixed-to-mobile and mobile-to-mobile channels. Different types of relays - fixed gain relays and variable gain relays are considered while obtaining the overall channel model. Often closed

form expressions of the desired properties seem intractable. In such cases, integral expressions are provided that can be evaluated numerically. Our results are verified by using the simulation models developed in earlier chapters.

Notation. Throughout the chapter, following notations are applied. $\mathcal{N}(\mu,\sigma^2)$ denotes normal distribution with mean μ and variance σ^2. $j = \sqrt{-1}$ is the imaginary unit value. $\mathbf{E}[\ \cdot\ ]$ is the statistical expectation operation. $|Z|$ and Z^* are the absolute value and the conjugate of the complex Z, respectively.

5.2 Relay Channel Model

Referring to the amplify and forward relay system model provided in Section 2.3.2, we are interested in analyzing the properties of the overall relay channel $h(t)$. We showed that for the BS-relay-MS link, the overall channel is

$$h(t) = A(t)h_1(t)h_2(t). \tag{151}$$

Here, $A(t)$ is the gain of the AF relay, $h_1(t)$ is the BS-relay fading channel modeled as a zero mean complex Gaussian (ZMCG) process with power σ_1^2, and $h_2(t)$ is the relay-MS fading channel modeled as a ZMCG process with power σ_2^2. In the subsequent discussion, we drop the time index t for convenience while remembering that all the random processes involved are wide-sense stationary. Several different choices of the amplification factor A have been proposed in the literature such as

$$A_1 = \sqrt{\frac{E_2}{\mathbf{E}[|r_1|^2]}} = \sqrt{\frac{E_2}{E_1\sigma_1^2 + \sigma_n^2}} \quad \text{and} \tag{152}$$

$$A_2 = \sqrt{\frac{E_2}{E_2|h_1|^2 + \sigma_n^2}} \tag{153}$$

in [47] and [40], respectively. Here, E_2 denotes the average power transmitted by the relay. The gain A_1 in (152) requires the knowledge of the average power received by the relay while the gain A_2 in (153) requires the relay to have instantaneous channel knowledge h_1. The relays with gain A_1, which is constant or fixed, are called fixed

gain relays while relays using gain A_2 are called variable gain relays because they continuously adjust their gain depending on the instantaneous channel [32]. Since fixed gain relays are simpler, our subsequent analysis largely assumes fixed gain relays.

5.3 Statistical Properties of the Fixed Gain Relay Channel

Statistical properties such as the pdf of the real and the imaginary components, their joint pdf, and the envelope pdf are known. Consider the the fixed gain relay channel $h = h_1 h_2$. Note that the gain A_1 is omitted from the overall channel because being a constant it can be absorbed into the variance of h_2.

Let $h_1 = x_1 + jy_1$ and $h_2 = x_2 + jy_2$, where x_i, y_i, i =1,2 are i.i.d. random variables with pdf $\mathcal{N}(0,\sigma_i^2/2)$. Then, $h = x + jy$, where $x = x_1x_2$ - y_1y_2 and $y = x_1y_2 + x_2y_1$.

5.3.1 Distributions of the quadrature components and the channel envelope

The following properties can be readily obtained from [38] and [71].

1. The real and imaginary parts of h are identically distributed Laplacian random variables with pdfs

$$f_X(x) = \frac{1}{2b}\exp(-|x|/b), \quad f_Y(y) = \frac{1}{2b}\exp(-|y|/b), \tag{154}$$

   where $b = (\sigma_1\sigma_2)/2$.

2. The real and imaginary parts of h are uncorrelated and their joint pdf is

$$f_{X,Y}(x,y) = \frac{2}{\pi\sigma_1^2\sigma_2^2} K_0\left(2\sqrt{\frac{x^2+y^2}{\sigma_1^2\sigma_2^2}}\right), \tag{155}$$

   where $K_0(x)$ is the zeroth order modified Bessel function of the second kind.

3. The pdf of the envelope $\alpha = |h|$ is

$$f_\alpha(\alpha) = \frac{4\alpha}{\sigma_1^2\sigma_2^2} K_0\left(2\sqrt{\frac{\alpha^2}{\sigma_1^2\sigma_2^2}}\right). \tag{156}$$

We now go onto our novel work, including the time-correlation characteristics of relay channels, which should also apply to key-hole channels.

5.3.2 Time-domain correlations

Most of our results continue under the assumption of omni-directional antennas operating in a 2-D isotropic scattering environment, corresponding to NLOS conditions at the relay and mobile station, an assumption justified by the low elevation of mobile relay and destination terminals. The local area around the BS is assumed to be scatterer free owing to its high elevation.

The auto-correlations of $x(t)$, $y(t)$, and $h(t)$ are

$$\begin{aligned} R_{xx}(\tau) &= R_{yy}(\tau) = \mathbf{E}[x(t+\tau)x(t)] \\ &= \frac{\sigma_1^2\sigma_2^2}{2} J_0(2\pi f_1\tau) J_0(2\pi \hat{f}_1\tau) J_0(2\pi f_2\tau), \qquad (157) \\ R_{hh}(\tau) &= \frac{1}{2}\mathbf{E}[h(t+\tau)h^*(t)] = \frac{\sigma_1^2\sigma_2^2}{2} J_0(2\pi f_1\tau) J_0(2\pi \hat{f}_1\tau) J_0(2\pi f_2\tau) \qquad (158) \\ f_1 &= \frac{v_1}{\lambda_1},\ \hat{f}_1 = \frac{v_1}{\lambda_2},\ f_2 = \frac{v_2}{\lambda_2}, \qquad (159) \end{aligned}$$

where $J_0(x)$ is the zeroth order Bessel function of the first kind, f_1 is the maximum Doppler shift induced by the motion of the relay with speed v_1 in the BS-relay link having a carrier wavelength of λ_1, $\hat{f}_1$ and f_2 are the maximum Doppler shift induced by the motion of the relay and the destination MS, respectively, in the relay-destination MS link (carrier wavelength of λ_2).

The auto-correlation can be derived as shown below:

$$\begin{aligned} R_{hh}(\tau) &= \frac{1}{2}\mathbf{E}[h_1(t+\tau)h_2(t+\tau)h_1^*(t)h_2^*(t)] \\ &= \frac{1}{2}\mathbf{E}[h_1(t+\tau)h_1^*(t)]\mathbf{E}[h_2(t+\tau)h_2^*(t)] \\ &= 2R_{h_1h_1}(\tau)R_{h_2h_2}(\tau) \\ &= 2\left\{\frac{\sigma_1^2}{2}J_0(2\pi f_1\tau)\right\}\left\{\frac{\sigma_2^2}{2}J_0(2\pi \hat{f}_1\tau)J_0(2\pi f_2\tau)\right\} \\ &= \frac{\sigma_1^2\sigma_2^2}{2} J_0(2\pi f_1\tau) J_0(2\pi \hat{f}_1\tau) J_0(2\pi f_2\tau), \end{aligned}$$

where in the second line we use the independence of h_1 and h_2; in the fourth line we substitute the auto-correlation value of h_1 for fixed-to-mobile channels [36] and that of h_2 using Akki and Haber's mobile-to-mobile channel model [10].

The carrier frequencies used in the BS-relay link and the relay-destination MS link may be the same or be different. When TDMA based multi-access protocol is used such that the BS-relay transmissions occur in one time slot and the relay-MS transmissions occur in the next slot, same carrier frequency can be used in both the time slots [47], i.e., $f_1 = \hat{f}_1$. The assumption $f_1 = \hat{f}_1$ yields the simplified auto-correlation function

$$\begin{aligned} R_{hh}(\tau) &= \frac{\sigma_1^2\sigma_2^2}{2} J_0(2\pi f_1\tau)^2 J_0(2\pi f_2\tau) \\ &= \frac{\sigma_1^2\sigma_2^2}{2} J_0(2\pi f_1\tau)^2 J_0(2\pi a f_1\tau), \end{aligned} \tag{160}$$

where a is the ratio of the Doppler two shifts (or MS and relay speeds), $a = f_2/f_1$. While the auto-correlation for cellular channels consists of a single Bessel function $[(\sigma_1^2/2)J_0(2\pi f_1\tau)]$ [36], the auto-correlation of relay channels is a product of three Bessel functions. Figure 23 compares the auto-correlation of the fixed gain relay channel h with a cellular channel for the same f_1. We find that the relay channel has a more rapid envelope de-correlation that can work to our advantage.

Doppler Spectrum: Often wireless channels are characterized by their Doppler spectrum, which is the Fourier Transform of the auto-correlation function. The U-shaped spectrum of cellular channels is well-known. Since a closed form expression for the Doppler spectrum seems intractable (except for the case $a = 0$), Figure 24 plots several Doppler spectra obtained by numerical analysis. The Doppler spectra are a function of the maximum Doppler frequency f_1 and the Doppler ratio a. Therefore, for fixed f_1, different spectra are obtained by varying the Doppler ratio a. The maximum Doppler frequency in relay channels is $f_{max} = f_1 + \hat{f}_1 + f_2$. Though the Doppler spectra have singularities at some points, they are not revealed in the plots since

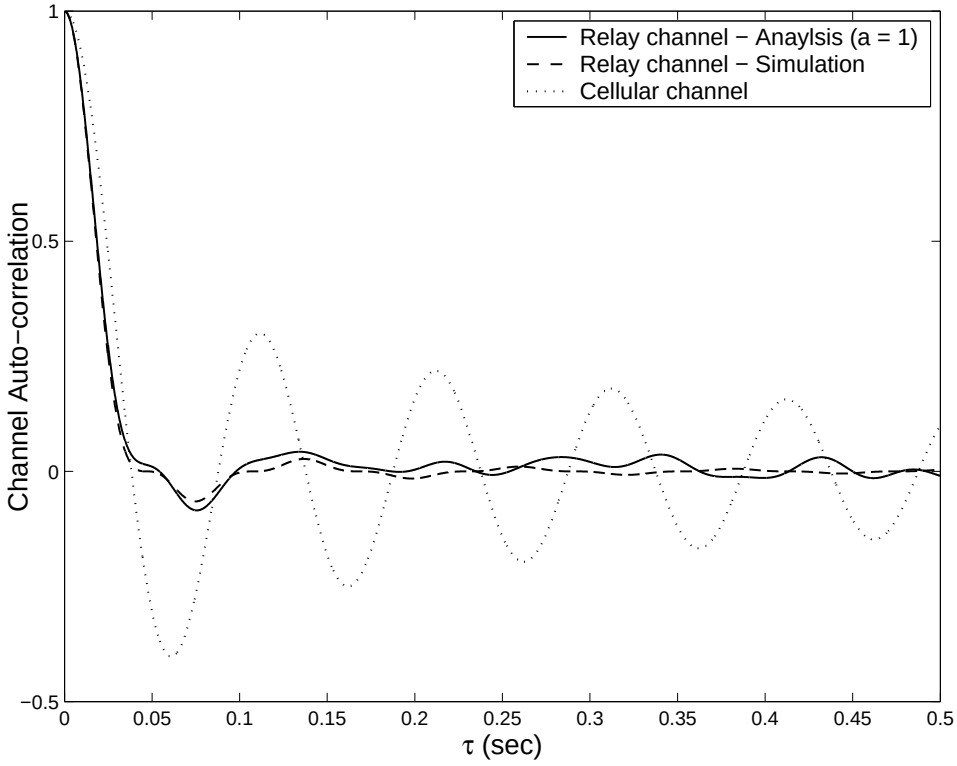

Figure 23: Comparison between the auto-correlation of relay channels vs. cellular channels.

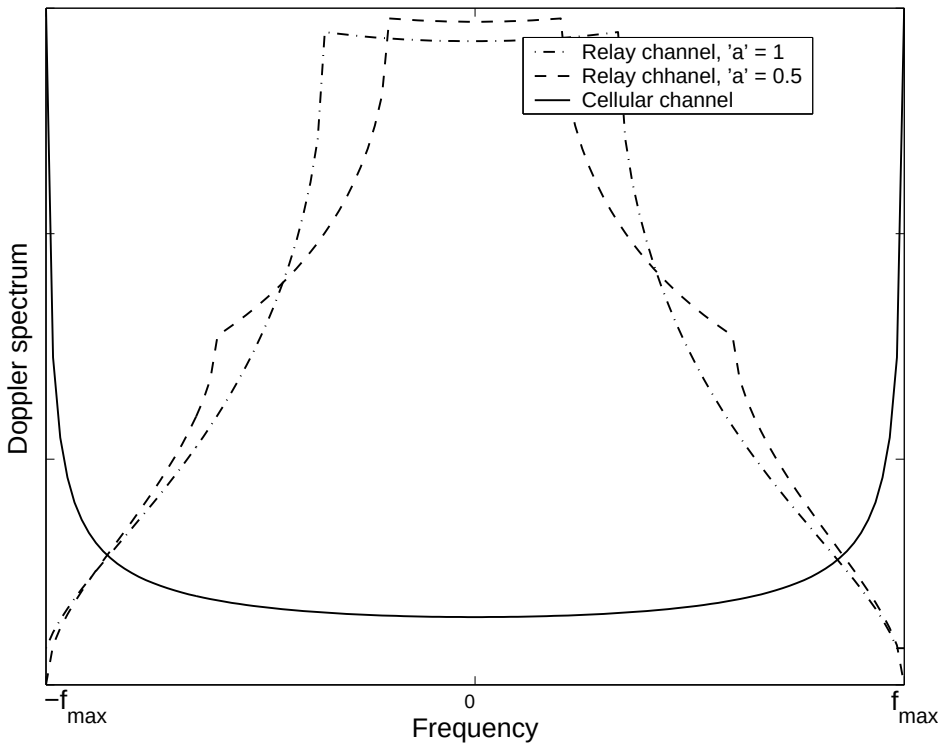

Figure 24: Comparison between Doppler spectra of relay channels vs. cellular channels.

numerical integration was used to obtain the plots. Further, it is evident from the Figure 24 that the Doppler spectra are very different from the U-shaped spectrum of cellular channels. Important thing to note here is that the Doppler spectra are more concentrated near zero frequencies. This is due to the mobile-to-mobile link presence, where more frequencies will be at or near zero value when the two stations move with identical speeds.

Doppler spread: As we mentioned earlier in Chapter II, the Doppler spread is an important parameter because it measures the rate of fading in a radio channel. Using the definition of Doppler spread provided in (144) of Appendix 4.2 along with the knowledge of channel auto-correlations discussed previously, we compare the Doppler spread of different channels below

$$\text{Cellular channel}: B_d = \sqrt{\frac{f_1^2}{2}} \tag{161}$$

$$\text{Mobile} - \text{to} - \text{Mobile channel}: B_d = \sqrt{\frac{f_1^2 + f_2^2}{2}} \tag{162}$$

$$\text{Relay channel}: B_d = \sqrt{f_1^2 + \frac{f_2^2}{2}}. \tag{163}$$

As expected, the relay fading channels have a higher Doppler spread when compared to cellular channels and mobile-to-mobile channels. For example, with $f_1 = f_2$ the Doppler spread for relay channels is approximately 70% and 25% higher than cellular channels and mobile-to-mobile channels, respectively (assuming f_1 is the same in all cases).

Level crossing rate:

The LCR of the envelope α at level R for a relay fading channel h can be quantified as

$$L_R(\alpha = R) = \frac{4\sqrt{\pi}R}{\sqrt{2}\sigma_1^2\sigma_2^2} \int_0^\infty \frac{1}{y^2} \exp\left(-\frac{\sigma_2^2 R^2 + \sigma_1^2 y^4}{\sigma_1^2\sigma_2^2 y^2}\right) \sqrt{\sigma_1^2 f_1^2 y^4 + \sigma_2^2(f_1^2 + f_2^2)R^2}\mathrm{d}y. \tag{164}$$

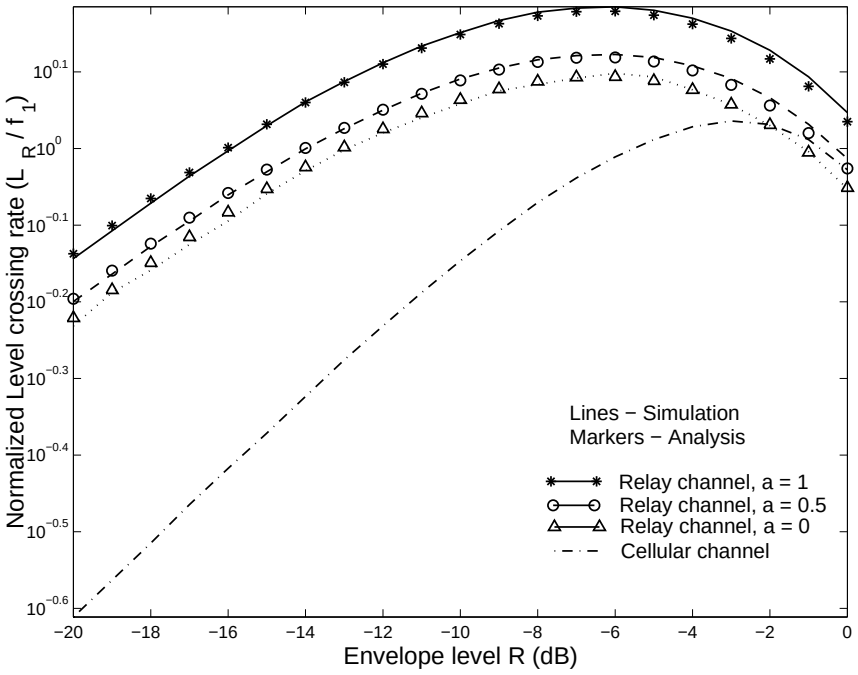

Figure 25: Normalized level crossing rate of relay channels.

The proof of the above equation is given in Appendix 5.1. It should be noted that a closed form expression of the LCR cannot be obtained. Approximations are possible but not pursued. The form of the above integral is one that can be easily and quickly computed using tools like Mathematica.

The LCRs of relay fading channels are plotted in Figure 25 for various speed ratios a and assuming $\sigma_1^2 = \sigma_2^2 = 1$. As a increases, the LCR increases due to increased mobility in the channel. Further, the LCRs of relay channels are higher than cellular channels for a given envelope level R. The average fade durations (AFD) can be calculated using this LCR expression and the cdf of the envelope.

5.3.3 Signal-to-Noise Ratio (SNR)

The SNR is a parameter of interest because it determines the end-to-end link performance. From the AF relay system model provided in Section 2.3.2, the signal received by the MS is given by

$$r = Ah_1h_2s + Ah_2n_1 + n_2. \tag{165}$$

Note that we have dropped the time index from the above equation for convenience as done earlier in the chapter. Here, n_1 and n_2 are the additive white Gaussian noise of the relay and the MS, respectively, each having zero mean and variance σ_n^2. Using the above equation along with gain $A = A_1$ for fixed gain relays, the instantaneous SNR conditioned upon h_1 and h_2 is given by

$$\begin{aligned} \gamma &= \frac{A^2|h_1|^2|h_2|^2E_1}{A^2|h_2|^2\sigma_n^2 + \sigma_n^2}, \\ &= \frac{\gamma_1\gamma_2}{\gamma_2 + C}, \qquad (166) \\ C &= 1 + \bar{\gamma}_1, \qquad (167) \end{aligned}$$

where $\gamma_i = E_i|h_i|^2/\sigma_n^2$ is the instantaneous SNR of the i^{th} individual channel (or i^{th} hop) with an average SNR value $\bar{\gamma}_i = E_i\sigma_i^2/\sigma_n^2$. The authors in [32] presented the BER and outage probability analysis based upon this SNR. We are interested in obtaining statistics such as the frequency of outage (FoO) and the average outage duration (AOD), which include the effect of time varying nature of the channel. A system is said to be in outage if the instantaneous SNR γ falls below a specified threshold γ_{th}. As the names suggest, FoO measures how frequently outages occur while AOD measures the average duration of such outages. In other words, FoO and AOD are the LCR and AFD of the SNR, respectively.

Before proceeding, it is interesting to note that for AF systems knowledge of the LCR or the AFD of the channel h is not sufficient. For fixed BS channels, the SNR with slow flat fading is $\gamma = |h|^2E_s/\sigma_n^2$. Hence, knowledge of the LCR and the AFD of the channel envelope $|h|$ is sufficient to calculate the FoO and AOD. However, for relay channels the form of the SNR is quite different, requiring separate evaluation of the LCR and AFD of the SNR to obtain the quantities of interest.

It is unknown if a closed form expression for the LCR of the SNR exists, but it is very unlikely. However, the LCR can be represented by the following integral

expression:

$$L_\gamma(\gamma) = \frac{2\sqrt{2\pi\gamma}}{\bar{\gamma}_1\bar{\gamma}_2}\exp\left(-\frac{\gamma}{\bar{\gamma}_1}\right) I \tag{168}$$

$$I = \int_0^\infty \frac{\sqrt{f_1^2\bar{\gamma}_1 y^4(y^2+C)+C^2(f_1^2+f_2^2)\bar{\gamma}_2\gamma}}{y^2}\exp\left(-\frac{\bar{\gamma}_1 y^4+C\bar{\gamma}_2\gamma}{\bar{\gamma}_1\bar{\gamma}_2}\right)\mathrm{d}y.$$

A brief outline for obtaining this integral is provided in Appendix 5.2. Using the above LCR expression along with the outage probability expression provided in [32], the average outage duration is obtained as

$$T_{AOD}(\gamma_{th}) = \frac{P_{out}(\gamma_{th})}{L_\gamma(\gamma_{th})} \tag{169}$$

We later use (168) and (169) to compare the FoO and AOD of systems using fixed vs. variable gain relays.

5.3.4 Comparisons with the variable gain relay channel

Our analysis in the earlier subsections dealt with fixed gain relays. It is possible at this point to consider the effect of variable gain relays on the channel- and system-level performance. For a relay with variable gain A_2 in (153), the overall relay channel is given by

$$h^v = \frac{\sqrt{E_2}h_1h_2}{\sqrt{E_1|h_1|^2+\sigma_n^2}}, \tag{170}$$

with squared envelope

$${\alpha_v}^2 = \frac{E_2|h_1|^2|h_2|^2}{E_1|h_1|^2+\sigma_n^2}. \tag{171}$$

Interestingly, the squared envelope has a form identical to the SNR of the channel with fixed gain relays, as evident from (166). Therefore, by applying the properties of SNR provided in [32] along with a simple transformation of variables, the envelope pdf of the variable gain relay channel is

$$f_{\alpha_v}(\alpha_v) = \frac{4\alpha_v E_1\exp\left(-\frac{E_1\alpha_v^2}{E_2\sigma_2^2}\right)}{E_2\sigma_2^2}\left(\sqrt{\frac{\sigma_n^2\alpha_v^2}{E_2\sigma_1^2\sigma_2^2}}K_1\left[2\sqrt{\frac{\sigma_n^2\alpha_v^2}{E_2\sigma_1^2\sigma_2^2}}\right]+\frac{\sigma_n^2}{E_1\sigma_1^2}K_0\left[2\sqrt{\frac{\sigma_n^2\alpha_v^2}{E_2\sigma_1^2\sigma_2^2}}\right]\right), \tag{172}$$

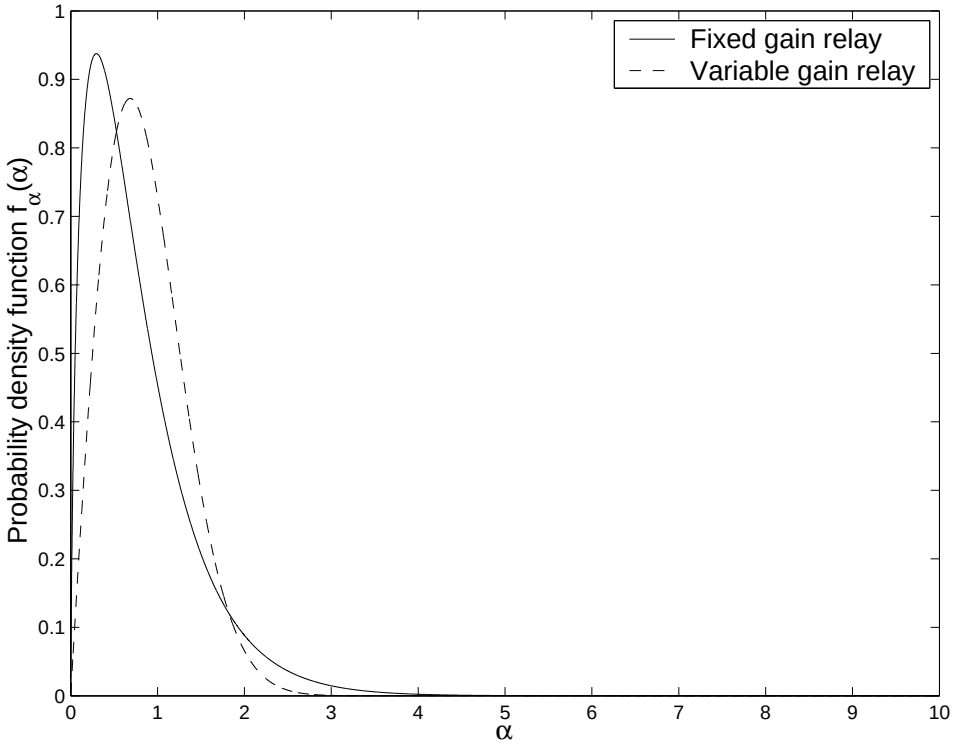

Figure 26: Comparison between the envelope pdf of fixed gain vs. variable gain relay channels

where $K_1[\cdot]$ is the first order modified Bessel function of the second kind. In the above envelope pdf equation, the noise variance σ_n^2 term explicitly shows the noise propagation from the relay. Figure 26 compares the pdfs of the envelopes of fixed gain channel $h = A_1 h_1 h_2$ and the variable gain channel h^v.

For comparison purposes, we assume $\bar{\gamma}_1 = \bar{\gamma}_2 = 20$ dB with E_1, E_2, σ_1^2, and σ_2^2 normalized to unity. Observe that the envelope pdf for the fixed gain channel is more concentrated at lower values of the envelope. This suggests harsher fading with fixed gain relays as compared to the variable gain relays.

A closed form expression for the channel auto-correlation in this case is hard to come by. However, consider the asymptotic, i.e., high SNR, behavior of the channel in (170) by neglecting the noise variance term in the denominator, yielding the

approximation

$$h^v(t) \approx \frac{\sqrt{E_2}h_1(t)h_2(t)}{\sqrt{E_1|h_1(t)|^2}} = \frac{\sqrt{E_2}\alpha_1(t)\exp[j\theta_1(t)]h_2(t)}{\sqrt{E_1}\alpha_1(t)} \quad (173)$$

$$= \sqrt{\frac{E_2}{E_1}}\exp[j\theta_1(t)]h_2(t), \quad (174)$$

where $\theta_1(t)$ is the time varying random phase of the channel h_1. Then, the approximate channel auto-correlation is

$$R_{h_vh_v}(\tau) \approx \frac{E_2}{E_1}\mathbf{E}[\exp\{j\theta_1(t+\tau)\}\exp\{-j\theta_1(t)\}]R_{h_2h_2}(\tau). \quad (175)$$

Using the properties of the random phase of the channel [36] and applying some calculus, we simplify (175) to

$$R_{h_vh_v}(\tau \neq 0) \approx \frac{\zeta E_2\pi J_0(2\pi f_1\tau)[1-J_0(2\pi f_1\tau)^2]}{4E_1}\,{}_2F_1\left(\frac{3}{2},\frac{3}{2},2,J_0(2\pi f_1\tau)^2\right)R_{h_2h_2}(\tau)$$

$$= \frac{\zeta E_2\sigma_2^2}{2E_1}, \qquad \tau = 0 \quad (176)$$

$$\zeta = \left(1-\frac{\exp(\sigma_n^2/\sigma_1^2)\mathrm{E}_1(\sigma_n^2/\sigma_1^2)}{\sigma_n^2/\sigma_1^2}\right), \quad (177)$$

where $2F_1(\cdot,\cdot,\cdot;\cdot)$ is the hypergeometric function and $\mathrm{E}_1(\cdot)$ is the exponential integral function [28]. The validity of the above asymptotic auto-correlation function is verified in the next section. This approximation is useful for designing channel estimators for variable gain relay systems in the next Chapter. Other statistical properties of the SNR such as the LCR and the AFD are not discussed because good approximations are difficult to find.

We compare the system-level performance of fixed vs. variable gain relays in terms of their respective FoOs and AODs. Such results are useful when developing QoS models for pedestrian environments. Others have made BER comparisons [32] that are useful when developing QOS models for vehicular traffic channels. Our results for the variable gain case are later obtained using the SNR expression [32, 88]

$$\gamma^v = \frac{\gamma_1\gamma_2}{\gamma_1+\gamma_2+1}. \quad (178)$$

5.3.5 Uplink and Downlink asymmetries and similarties

Until now we have only considered the downlink channel from the BS to the relay to the MS. Since the BS-relay (h_1) and relay-MS (h_2) links are not completely identical, the uplink channel from the MS to the BS will be different in several ways. We briefly point out these differences here.

For the fixed gain relays, the overall channel $h = h_1 h_2$ is symmetric in h_1 and h_2. Therefore, the channel properties in the uplink remain the same. However, the SNR given in (166) is not symmetric w.r.t. these two individual channels. The γ_2 term in the denominator is now replaced by γ_1. The BER in the uplink will remain same assuming identical distributions for γ_1 and γ_2 terms. However, properties such as the FoO and AODs will be different for the uplink because the dynamical properties of the channels h_1 and h_2 are completely different.

Likewise, for variable gain relays, the overall channel h^v in (170) is asymmetric w.r.t h_1 and h_2. Therefore, the channel properties will be different for the uplink. The channel auto-correlation for this case may be derived following the analysis given earlier. It is interesting that the SNR for variable gain relays in (178) is symmetric w.r.t. individual link SNRs γ_1 and γ_2. Therefore, the FoO and AODs will be identical for the uplink and the downlink.

5.4 Results

We now verify our theoretical analysis by means of simulations. To simulate a relay channel, we need to simulate the BS-relay channel h_1 and the relay-MS channel h_2. We utilize Zheng and Xiao's Model II discussed in Chapter III to simulate h_1 because h_1 is similar to traditional fixed-to-mobile cellular channels. For channel h_2, which is a mobile-to-mobile channel, we employ the statistical model proposed in Chapter IV. We simulate relay channels with fixed and variable gain relays to verify our theoretical

analysis assuming $f_1 = f_2 = 100$ Hz (i.e., $a = 1$), and a sampling time of 10^{-4} s. Unless specified otherwise, all simulation results assume E_1, E_2, σ_1^2, and σ_2^2 normalized to unity.

Figure 23 (p.86) compares the simulated auto-correlation (time averaged over 2×10^5 samples) with the theoretical one for the fixed gain relay channel. They are approximately equal, thus validating our theoretical auto-correlation. The theoretical LCR expression is verified by the simulation plots shown in Figure 25 (p.88).

Figure 27 validates the approximate auto-correlation for the variable gain case by comparing the simulated auto-correlation with the approximation provided in (175). Also, comparing the auto-correlation plots in Figure 23 and Figure 27 after proper power normalization, we find that the correlations are almost identical for variable and fixed gain relay cases.

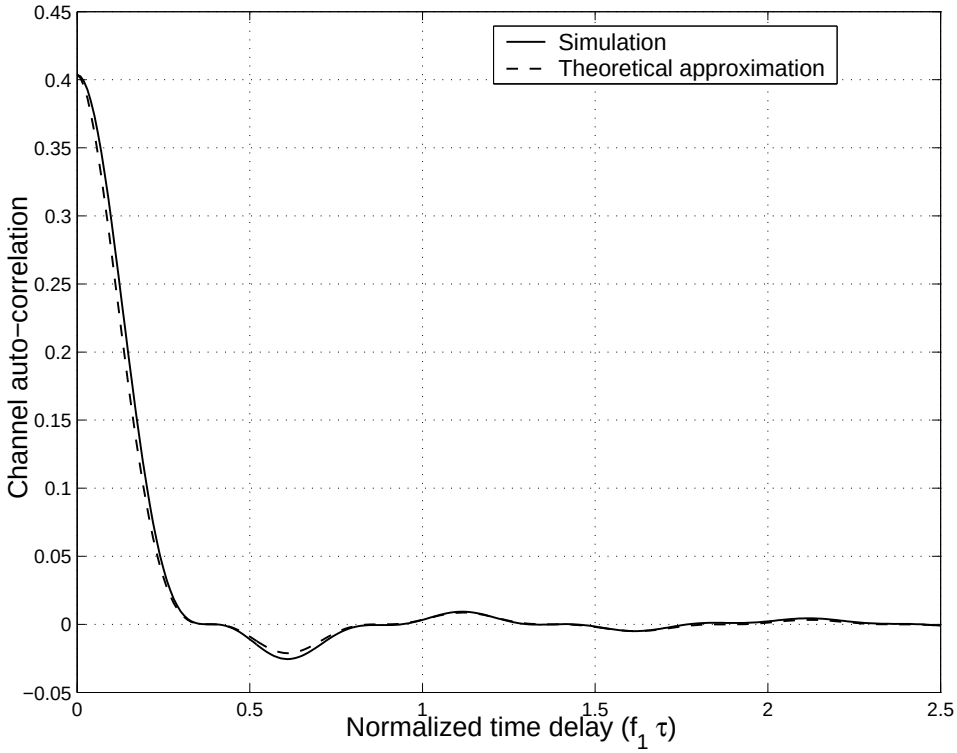

Figure 27: Auto-correlation of variable gain relay channels.

Figure 28 and Figure 29 provide FoO vs. SNR and AOD vs. SNR per hop $\bar{\gamma}_i$ ($\bar{\gamma}_1 = \bar{\gamma}_2$) plots, respectively, for threshold SNR values of $\gamma_{th} = 0$ dB and 5 dB. We observe that for moderate to high SNR per hop values, the variables gain systems have infrequent and shorter outages compared to the fixed gain system. However, at low SNR per hop values, the variable gain system has infrequent outages but with longer durations compared to the fixed gain system suggesting that their outage probability is relatively higher. This effect has also been observed in [32] in terms of outage probability events in the two systems while using a different fixed gain relay. A low SNR value $\bar{\gamma}_1$ implies frequently occuring smaller instantaneous $|h_1|^2$ values, thereby, limiting the gain of variable gain relays, which leads to longer outage durations at low SNR. On the other hand, at higher SNR, the fading compensation provided by the variable gain relays leads to better performance. We also show the FoO and AOD plots for the uplink with fixed gain relays in Figure 28 and Figure 29, respectively. As mentioned earlier, we observe some difference between the uplink and downlink characteristics. Though not shown in these figures, we found that this difference becomes more pronounced when the Doppler frequencies f_1 and f_2 differ considerably, an effect caused by the higher asymmetry in the channels h_1 and h_2.

5.5 Summary

In this chapter, we presented a comprehensive analysis of the statistical properties of amplify and forward relay channels. Several properties such as the auto-correlation, level crossing rates, and average outage durations were studied and verified by means of simulation models. These results will be useful for designing AF relay systems to improve network coverage and reliability.

Finally, it should be noted that all our results have only considered the range extended link from the BS to the MS via the relay. Both links assumed a NLOS mobile radio channel. Other operating environments may include the direct (LoS

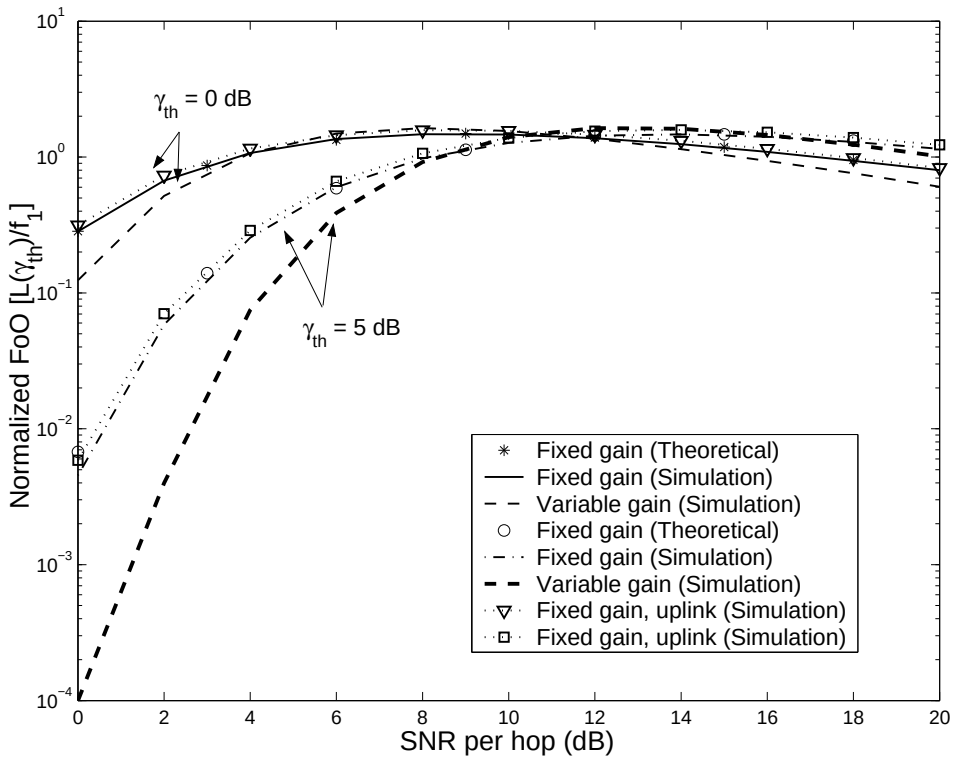

Figure 28: Frequency of outages in relay channels.

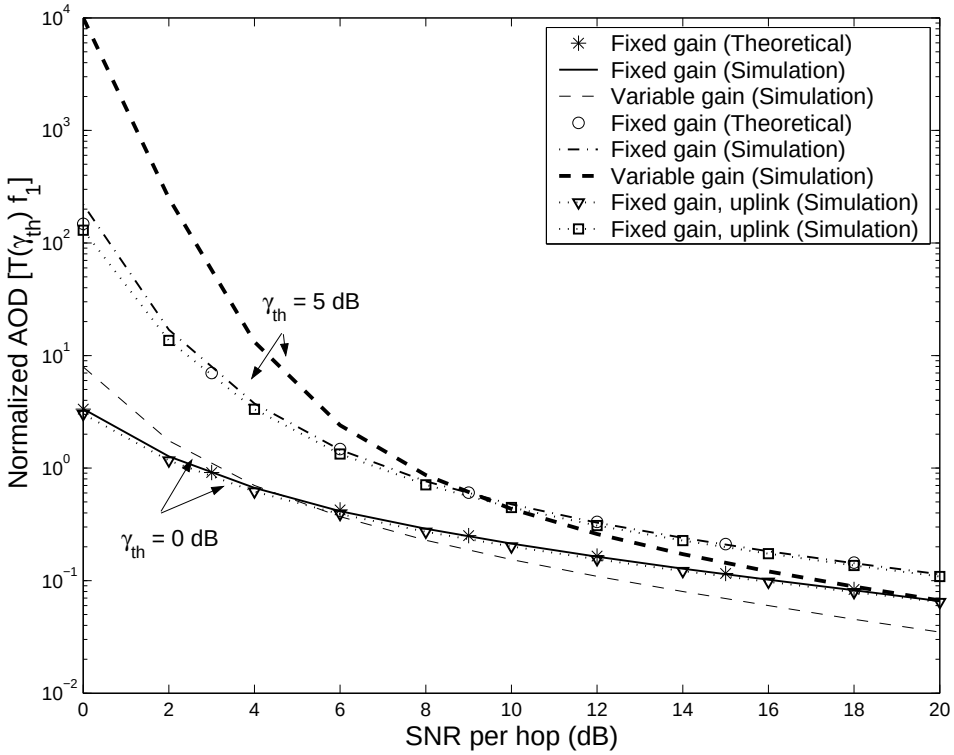

Figure 29: Average outage durations in relay channels.

or NLoS) link from BS to MS. Generally speaking, the presence of the direct-link component provides additional diversity that should improve performance compared to the performance of our range extended link.

Appendix 5.1: Proof of (164)

Here, we provide a brief outline for the derivation of the LCR expression given in (164). The LCR of a stationary random process $\alpha(t)$ at a level R is given as [74]

$$L_R(\alpha = R) = \int_0^\infty \dot{\alpha} f_{\alpha,\dot{\alpha}}(R, \dot{\alpha}) \mathrm{d}\dot{\alpha}. \tag{179}$$

With $\alpha = |h| = |h_1 h_2| = \alpha_1 \alpha_2$, from [56]

$$\begin{aligned} f_{\alpha,\dot{\alpha}}(\alpha, \dot{\alpha}) &= \int_0^\infty \int_{-\infty}^\infty \frac{1}{y^2} f_{\alpha_1,\dot{\alpha}_1}\left(\frac{\alpha}{y}, \frac{\dot{\alpha}}{y} - \frac{\alpha \dot{y}}{y^2}\right) f_{\alpha_2,\dot{\alpha}_2}(y, \dot{y}) \mathrm{d}\dot{y} \mathrm{d}y \\ &= \int_0^\infty \frac{1}{y^2} f_{\alpha_1}\left(\frac{\alpha}{y}\right) f_{\alpha_2}(y) \left(\int_{-\infty}^\infty f_{\dot{\alpha}_1}\left(\frac{\dot{\alpha}}{y} - \frac{\alpha \dot{y}}{y^2}\right) f_{\dot{\alpha}_2}(\dot{y}) \mathrm{d}\dot{y}\right) \mathrm{d}y, \end{aligned} \tag{180}$$

where we used the fact that the envelope α_i is independent of its time derivative $\dot{\alpha}_i$ for $i = 1{,}2$ [74]. For Rayleigh faded envelopes α_1 and α_2, it is known that [10, 74]

$$f_{\dot{\alpha}_1} = \frac{1}{\sqrt{2\pi b_2^1}} \exp\left(-\frac{\dot{\alpha_1}^2}{2b_2^1}\right), \; f_{\dot{\alpha}_2} = \frac{1}{\sqrt{2\pi b_2^2}} \exp\left(-\frac{\dot{\alpha_2}^2}{2b_2^2}\right), \tag{181}$$

where b_2^1 and b_2^2 are the second moments of the spectrum of the channels h_1 and h_2, respectively. From the results in [10] and [36], for the assumed auto-correlation functions of the channels h_1 and h_2, it can be verified that

$$b_2^1 = \pi^2 \sigma_1^2 f_1^2, \;\; b_2^2 = \pi^2 \sigma_2^2 (f_1^2 + f_2^2). \tag{182}$$

Then, after evaluating the inner integral in (180) and some algebraic manipulations,

$$f_{\alpha,\dot{\alpha}}(\alpha, \dot{\alpha}) = \frac{1}{\sqrt{2\pi}} \int_0^\infty f_{\alpha_1}\left(\frac{\alpha}{y}\right) f_{\alpha_2}(y) \frac{1}{\sqrt{b_2^1 y^4 + b_2^2 \alpha^2}} \exp\left(-\frac{y^2 \dot{\alpha}^2}{2(b_2^1 y^4 + b_2^2 \alpha^2)}\right) \mathrm{d}y. \tag{183}$$

Substituting (183) in (179) and changing the order of integration,

$$\begin{aligned} L_R(\alpha = R) &= \frac{1}{\sqrt{2\pi}} \int_0^\infty \frac{f_{\alpha_1}(\alpha/y) f_{\alpha_2}(y)}{\sqrt{b_2^1 y^4 + b_2^2 \alpha^2}} \left(\int_0^\infty \dot{\alpha} \exp\left(-\frac{y^2 \dot{\alpha}^2}{2(b_2^1 y^4 + b_2^2 \alpha^2)} \right) \mathrm{d}\dot{\alpha} \right) \mathrm{d}y \\ &= \frac{1}{\sqrt{2\pi}} \int_0^\infty f_{\alpha_1}(\alpha/y) f_{\alpha_2}(y) \frac{\sqrt{b_2^1 y^4 + b_2^2 \alpha^2}}{y^2} \mathrm{d}y \end{aligned} \tag{184}$$

Finally, after substituting all the relevant quantities in (184) and making some simplifications, we obtain the required integral expression (164).

Appendix 5.2: Proof of (168)

Here, an outline for deriving the LCR of the SNR given in (168) is provided. Some of the notations used in Appendix 5.1 are also used here. First, consider the random variable

$$z = \sqrt{\gamma} = \frac{\alpha_1}{\sqrt{1 + C/\alpha_2^2}} = \frac{\alpha_1}{w}, \tag{185}$$

where $w = \sqrt{1 + C/\alpha_2^2}$. Note that here $\mathbf{E}[\alpha_i^2] = \bar{\gamma}_i$ since we are dealing with SNR. To obtain LCR of z by generalizing (179), we require the joint pdf of z and its time derivative $\dot{z}$. This joint pdf can be obtained as

$$f_{z,\dot{z}}(z, \dot{z}) = \int_0^\infty \int_{-\infty}^\infty f_{z,\dot{z}}(z, \dot{z} | \alpha_2, \dot{\alpha}_2) f_{\alpha_2, \dot{\alpha}_2}(\alpha_2, \dot{\alpha}_2) \mathrm{d}\dot{\alpha}_2 \mathrm{d}\alpha_2. \tag{186}$$

Given $\dot{\alpha}_2$ and α_2, z and $\dot{z}$ are two functions of two random variables $\dot{\alpha}_1$ and α_1. Therefore, by using [49] and the fact that $\dot{\alpha}_1$ and α_1 are independent, we obtain

$$f_{z,\dot{z}}(z, \dot{z} | \alpha_2, \dot{\alpha}_2) = w^2 f_{\alpha_1}(wz) f_{\dot{\alpha}_1}(w\dot{z} + z\dot{w}). \tag{187}$$

Then, substituting (187) and (186) along with the appropriate pdfs of the envelopes and their time derivatives into the LCR equation

$$L_z(z) = \int_0^\infty \dot{z} f_{z,\dot{z}\alpha}(z, \dot{z}) \mathrm{d}\dot{z}, \tag{188}$$

we get a triple integral. Evaluating this integral first w.r.t. $\dot{\alpha}_2$, then w.r.t. $\dot{z}$, and substituting $z = \sqrt{\gamma}$, we get the LCR expression given in (168).

CHAPTER VI

CHANNEL ESTIMATION FOR AMPLIFY AND FORWARD RELAY CHANNELS

6.1 Overview

In the previous chapter, we showed that two key factors distinguish an AF wireless link from a conventional cellular link: 1) the non-Gaussian channel nature of the overall channel resulting from a cascading of the BS-relay and the relay-MS links and 2) noise propagation from the relay to the destination. Consequently, the performance of such AF systems is quite different from conventional cellular links. Several authors have analyzed the performance of AF systems in terms of their BER and outage probability, under different assumptions on the amplifier gain [13, 15, 32, 88]. But all of these results assume perfect channel knowledge at the destination and, in some cases, at the relay as well. The authors in [79] briefly discuss the impact of pilot symbol aided channel estimation for cooperation diversity systems. However, because the main focus in [79] is on designing a maximum likelihood sequence estimator, issues such as the channel model and estimator design criteria for different relay mobilities and gains are not discussed in detail. Thus, to the best of our knowledge, the problem of channel estimation for AF relay wireless links has not been satisfactorily addressed. Therefore, we present our results on channel estimation for AF relay systems in this chapter.

Periodic insertion of known symbols called "pilots" along with the transmitted data is widely used for channel estimation [17, 77]. We use this idea to study channel estimation in the AF relay systems. We investigate issues such as 1) the selection of appropriate channel models based upon relay mobility and relay gain, 2) the impact of the underlying channel on the pilot insertion strategy and estimator design, and

3) approximation of the BER by taking into account channel estimation errors.

The AF relay channel from the BS to the MS via the relay is a cascade of two links: the BS-relay link and the relay-MS link. Optimal channel estimation of each individual channel is possible by applying the Minimum Mean Square Error (MMSE) estimation theory [33, 68]. However, optimal estimation of the cascaded links in the relay channel is non-trivial. Further, we know that depending upon the mobility of the relay, the overall channel is either a cascade of fixed-to-fixed and fixed-to-mobile or fixed-to-mobile and mobile-to-mobile links. Therefore, the estimator must be designed appropriately to yield acceptable performance under these fast fading conditions. We found that optimal channel estimation using MMSE is perhaps not possible due to mathematical intractability of the derivation of the MMSE estimator. Therefore, we resort to sub-optimal linear minimum mean square error (LMMSE) estimator design. The LMMSE estimates the channel as a linear function of the received signal in contrast to the MMSE, which can yield a non-linear function. Therefore, LMMSE estimator is simple but sub-optimal. We exploit the knowledge of underlying channel statistics to obtain satisfactory performance by using the LMMSE estimator. Our work demonstrates the usefulness of the LMMSE and other sub-optimal estimators for channel estimation in AF relay systems. A recursive estimation scheme using the extended Kalman filter (EKF) was also studied. However, the EKF estimator does not perform well compared to the LMMSE estimator. Therefore, results on the EKF are relegated to Appendix 6.1. We begin our discussion by describing the AF system model. A discrete time system model is presented here for the ease of analysis.

6.2 System Model

Consider the downlink relay channel from a fixed BS transmitter to a MS receiver via a relay in a cellular network arrangement. We assume time division multiplexing (TDM) multi-access so that the BS-relay and the relay-MS transmissions occur

in different time slots on the same carrier frequency. To achieve this TDM operation, the relays store the received signal by using an analog or a digital delay circuit. Delays in digital domain can be efficiently implemented by implementing bandpass sampling using an analog-to-digital (ADC) converter and storing the digital samples. The bandpass signal can be reconstructed using a digital-to-analog (DAC) converter. Note that baseband processing including front end processing, demodulation, and decoding are not required after the ADC in AF relays, which makes them potentially less complex than DF relays. Alternatively, a frequency division multiplexing (FDM) mode is also possible if the relays convert the received signal to a different carrier frequency and forward it to the MS. However, to illustrate channel estimation concepts for AF relay links, the mode of operation is not important. Therefore, in our subsequent discussion we assume the TDM mode of operation.

We consider a discrete time description, where all the samples have been obtained using a sampling period equal to the symbol duration T_s and assume that perfect time synchronization has been achieved at the relay and the receiver. Assuming frequency flat-fading, the signal received by the relay at discrete time k is

$$r_1(k) = h_1(k)s(k) + n_1(k), \tag{189}$$

where $s(k)$ is the modulated, complex data symbol with energy E_1, $h_1(k)$ is the BS-relay channel, and $n_1(k)$ is the relay AWGN. The relay amplifies $r_1(k)$ and retransmits it to the destination MS, which receives

$$\begin{aligned} r_2(k) &= A(k)h_2(k)r_1(k) + n_2(k) \\ &= A(k)h_2(k)h_1(k)s(k) + A(k)h_2(k)n_1(k) + n_2(k) \\ &= h(k)s(k) + A(k)h_2(k)n_1(k) + n_2(k), \end{aligned} \tag{190}$$

where $A(k)$ is the relay amplification factor, $h_2(k)$ is the relay-destination MS channel, and $n_2(k)$ is the receiver AWGN. The assumptions on the channel and noise properties are identical to those in the continuous time system model provided in Section 2.3.2.

Following our discussion on the types of AF relays in Section 5.2, $A(k)$ can be either

$$A_1(k) = \sqrt{\frac{E_2}{\mathbf{E}[|r_1(k)|^2]}} = \sqrt{\frac{E_2}{E_1\sigma_1^2 + \sigma_n^2}} \quad \text{or} \tag{191}$$

$$A_2(k) = \sqrt{\frac{E_2}{E_1|h_1(k)|^2 + \sigma_n^2}}. \tag{192}$$

The gain in (191) is fixed, non-time varying while the gain in (192) is time varying determined by the BS-relay channel $h_1(k)$. Such variable gain relays require channel estimation at the relay also to determine their amplification factor. It must be pointed out here that throughout the chapter the term "fixed relay" implies a relay which is not moving and should not be confused with the type of the relay gain. The nature of the relay gain - fixed or variable will be explicitly mentioned when necessary to avoid ambiguity.

For coherent demodulation, the MS tries to estimate and track the overall fading channel $h(k)$. In addition, variable gain relays track $h_1(k)$ for appropriate power scaling. Before discussing how the estimation is done, we briefly summarize the assumptions made on the channel models. We assume omni-directional transmit and receiver antennas at all the terminals and NLOS propagation with 2-D isotropic scattering around the relay and the MS. The BS is considered free of local scatterers owing to its high elevation antennas. NLOS propagation implies Rayleigh faded channels $h_1(k)$ and $h_2(k)$ with their associated statistical properties such as the time auto-correlation determined by the mobility of the relay and the MS as discussed in Chapter V.

Case I: Fixed relays

When the relay is fixed, the Doppler shift induced in the BS-relay channel is caused by the relative motion of the nearby scattering objects and is very small. The auto-correlation of channels $h_1(k)$ and $h_2(k)$ are [36]

$$R_{h_1h_1}(k') = \mathbf{E}[h_1(k+k')h_1^*(k)] = \sigma_1^2 J_0(2\pi f_1 k') \tag{193}$$

$$R_{h_2h_2}(k^{'}) \quad = \quad \mathbf{E}[h_2(k+k^{'})h_2^*(k)] = \sigma_2^2 J_0(2\pi f_2 k^{'}), \tag{194}$$

where $\mathbf{E}$ is the statistical expectation, $*$ is the complex conjugate operator, $J_0(x)$ is the zeroth order Bessel function of the first kind, and f_1 and f_2 are the maximum Doppler frequencies associated with $h_1(k)$ and $h_2(k)$, respectively. Note that for the BS-relay link, (193) though not completely accurate, can serve our purpose in demonstrating channel estimation by choosing f_1 much smaller than f_2, e.g., $f_1 = f_2/10$. It should be noted that this channel model was applied in [79] for AF systems in a different setting. In our work, we also consider the case of mobile relays.

Case II: Mobile relays

The channel $h_1(k)$ is now a fixed-to-mobile channel, while $h_2(k)$ is a mobile-to-mobile channel. Using the results in [36] and [10], we have

$$R_{h_1h_1}(k^{'}) \quad = \quad \sigma_1^2 J_0(2\pi f_1 k^{'}) \tag{195}$$

$$R_{h_2h_2}(k^{'}) \quad = \quad \sigma_2^2 J_0(2\pi f_1 k^{'}) J_0(2\pi f_2 k^{'}), \tag{196}$$

where f_1 and f_2 are the maximum Doppler frequencies due to the motion of the relay and the MS, respectively.

6.3 Channel Estimator Design

In a cellular channel, pilot symbol based MMSE estimators are often used for optimal channel estimation [77]. However, the MMSE estimator design for the AF relay channels is very complex and perhaps intractable. The reason is that neither the overall channel $h(k)$ nor the effective noise $A(k)h_2(k)n_1(k) + n_2(k)$ in (190) are Gaussian, thereby making the MMSE estimator design difficult. Therefore, we consider sub-optimal LMMSE estimation [68]. Our analysis shows that LMMSE estimators provide satisfactory performance without high complexity.

As illustrated in Figure 30, we consider packetized transmissions where pilot symbols are periodically inserted in each packet with an insertion period of T_p symbols.

The data symbols between two periodic pilots form a sub-packet (SP). The channel estimate at each symbol position in a SP is obtained using N_p pilot symbols.

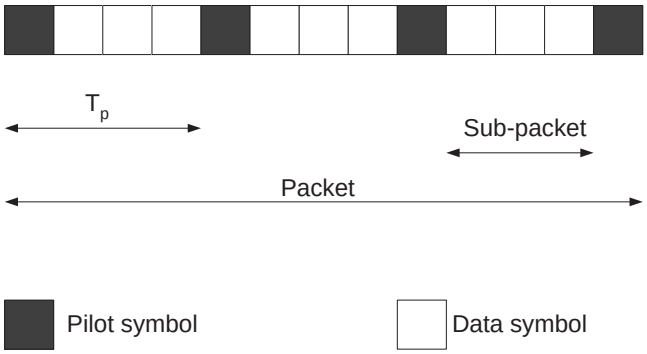

Figure 30: Pilot symbol aided channel estimation.

In our analysis, we assume $N_p = 4$. Thus, each data symbol in a SP uses the two closest pilot symbols from the past and the two closest pilot symbols from the future to estimate the channel. Additional pilot symbols may be used to improve estimation. However, to maintain low complexity, we choose $N_p = 4$. Each symbol position in a SP requires a different estimator. However, the same symbol positions across all SPs in a packet will use identical estimators due to periodic pilot insertion.

Assuming that BPSK modulated unit energy symbols $s(n) = \pm 1$ ($E_1 = 1$) are transmitted as pilot and data symbols, the channel estimate (CE) at a pilot position is obtained using (190) as $\hat{p}(n) = r_2(n)/s(n)$. Let $\hat{\mathbf{p}}$ be the ($N_p \times 1$) vector of pilot symbol CEs used to estimate the channel at time k, $h(k)$, at a data position in a SP. Then the CE obtained by the LMMSE criterion is [68]

$$\hat{h}(k) = \mathbf{a}\hat{\mathbf{p}}. \tag{197}$$

The LMMSE estimator ($1 \times N_p$) vector $\mathbf{a}$ is

$$\mathbf{a} = \mathbf{r}_{h\hat{p}}\mathbf{R}_{\hat{p}\hat{p}}^{-1}, \tag{198}$$

where $\mathbf{r}_{h\hat{p}}$ is the correlation vector between $h(k)$ and $\hat{\mathbf{p}}$ and $\mathbf{R}_{\hat{p}\hat{p}}$ is the auto-correlation matrix of the vector $\hat{\mathbf{p}}$.

Using the system model and channel properties described earlier, we provide the equations necessary to obtain above matrices for fixed and variable gain relays below. Let $p(l)$ denote an element of the vector $\hat{\mathbf{p}}$ corresponding to the pilot CE obtained at time l. Note that the relative time difference (delay) between $h(k)$ and $p(l)$ is $k-l$.

Case I: *Fixed gain relays*

$$\begin{aligned}\mathbf{E}[h(k)p(l)^*] &= \mathbf{E}[A_1h_1(k)h_2(k)\{A_1h_1(l)h_2(l)+A_1h_2(l)n_1(l)/s(l)+n_2(l)/s(l)\}^*] \\ &= \mathbf{E}[A_1h_1(k)h_2(k)\{A_1h_1(l)h_2(l)\}^*] \\ &= A_1^2R_{h_1h_1}(k-l)R_{h_2h_2}(k-l) \qquad (199)\end{aligned}$$

Let $\bar{\gamma}_i = E_i\sigma_i^2/\sigma_n^2$ be the average signal-to-noise ratio (SNR) for the i^{th} hop, with $i=1$ and $i=2$ denoting the BS-relay hop and the relay-MS hop, respectively. Then, (199) can be simplified further by using A_1 from (191) to

$$\mathbf{E}[h(k)p(l)^*] = \frac{E_2}{\sigma_n^2(1+\bar{\gamma}_1)}R_{h_1h_1}(k-l)R_{h_2h_2}(k-l). \qquad (200)$$

Note that the time index has been dropped from the gain A_1 in the above equations because the gain is constant.

$$\begin{aligned}\mathbf{E}[\hat{p}(l_1)\hat{p}(l_2)^*] &= \mathbf{E}\left[\{A_1h_1(l_1)h_2(l_1)+A_1h_2(l_1)n_1(l_1)/s(l_1)+n_2(l_1)/s(l_1)\}\times\right. \\ &\quad \left.\{A_1h_1(l_2)h_2(l_2)+A_1h_2(l_2)n_1(l_2)/s(l_2)+n_2(l_2)/s(l_2)\}^*\right] \\ &= \mathbf{E}[\{A_1h_1(l_1)h_2(l_1)\}\{A_1h_1(l_2)h_2(l_2)\}^*]+ \\ &\quad \mathbf{E}[n_2(l_1)/s(l_1)\{n_2(l_2)/s(l_2)\}^*]+ \\ &\quad \mathbf{E}[\{A_1h_2(l_1)n_1(l_1)/s(l_1)\}\{A_1h_2(l_2)n_1(l_2)/s(l_2)\}^*] \\ &= A_1^2R_{h_1h_1}(l_1-l_2)R_{h_2h_2}(l_1-l_2)+A_1^2\sigma_2^2\sigma_n^2\delta(l_1-l_2)+\sigma_n^2\delta(l_1-l_2) \\ &= \frac{E_2}{\sigma_n^2(1+\bar{\gamma}_1)}R_{h_1h_1}(l_1-l_2)R_{h_2h_2}(l_1-l_2)+ \\ &\quad \frac{\bar{\gamma}_2\sigma_n^2}{1+\bar{\gamma}_1}\delta(l_1-l_2)+\sigma_n^2\delta(l_1-l_2) \qquad (201)\end{aligned}$$

The receiver is assumed to possess the knowledge of channel correlations, average SNRs on the two hops, and the noise variance, which is feasible because these are

long-term properties that can be separately acquired. This issue is important and should be addressed in future work in greater detail. However, in a later section, we evaluate the estimator performance in the absence of precise knowledge of these quantities at the MS. Case II: *Variable gain relays*

The design equations for fixed gain relay case are fairly simple. However, the same is not the case for variable gain relays. We use certain approximations to obtain the correlation functions and to design the estimator.

With variable gain systems, the relay needs to estimate the channel. The LMMSE estimator given above can be modified to estimate the channel h_1. This estimator is also the MMSE estimator because h_1 and the additive noise in the BS-relay link are both Gaussian. Estimator design at the relay is simple and therefore not discussed in detail. The equations used for the estimator at the receiving MS are obtained using the analysis provided in Chapter V as:

$$\begin{aligned}
\mathbf{E}[h(k)p(l)^*] &\approx \zeta R_{h_1h_1}(k-l)R_{h_2h_2}(k-l) && (202)\\
\zeta &= \frac{E_2}{E_1}\left(1-\frac{1}{\bar{\gamma}_1}\exp(1/\bar{\gamma}_1)\mathrm{E}_1^x(1/\bar{\gamma}_1)\right) && (203)\\
\mathbf{E}[\hat{p}(l_1)\hat{p}(l_2)^*] &\approx \zeta R_{h_1h_1}(l_1-l_2)R_{h_2h_2}(l_1-l_2)+ \\
&\quad \frac{\bar{\gamma}_2\sigma_n^2}{\bar{\gamma}_1}\exp(1/\bar{\gamma}_1)\mathrm{E}_1^x(1/\bar{\gamma}_1)\delta(l_1-l_2)+\sigma_n^2\delta(l_1-l_2), && (204)
\end{aligned}$$

where $\mathrm{E}_1^x(y)$ is the exponential integral function. Note that these correlations are approximate.

6.3.1 Pilot insertion period

A small number of pilot symbols must be inserted in the data stream to minimize the loss of power and data rate. However, a certain minimum pilot insertion period is necessary to interpolate the pilot CEs at the data positions. It is well known that in a mobile fading channel, according to the Nyquist sampling theorem, the pilot insertion

Table 3: Pilot insertion period

System	Fixed relays $1/T_p \geq$	Mobile relays $1/T_p \geq$
Fixed gain AF	$2(f_1 + f_2)$	$2(2f_1 + f_2)$
Variable gain AF	$2(f_1 + f_2)$	$2(2f_1 + f_2)$
DF	$2f_2$	$2(f_1 + f_2)$

period T_p must satisfy [66]

$$T_p \leq \frac{1}{2F_{max}T_s}, \tag{205}$$

where F_{max} is the maximum Doppler frequency in the channel. By extending our analysis of the channel properties discussed earlier, the T_ps required under different system configurations - AF or DF, different relay - fixed gain or variable gain, and channel conditions are provided in Table 3.

The insertion period is the same for fixed and variable gain relays, because under both configurations the overall channel has the same maximum Doppler frequency. Naturally, the mobile relay case requires smaller T_p due to faster fading.

We also include comparisons with a DF system in Table 3. In a DF system, the pilot spacing is governed by the link having higher maximum Doppler frequency of the two links $h_1(k)$ and $h_2(k)$. The relay-MS link's Doppler is greater for both cases - fixed and mobile relay. Therefore, with fixed relays, we get $F_{max} = f_2$ while for mobile relays we have $F_{max} = f_1 + f_2$. Clearly, the required number of pilots is less in the DF system compared to the AF system, thereby achieving a higher data rate in the DF system. However, the relay complexity is higher in the DF mode. These trade-offs must be balanced while choosing between DF and AF systems.

Using these design guidelines, we provide a realistic performance evaluation for different systems in Section 6.5 via simulations. However, it is also beneficial to have a theoretical means to quantify the system performance taking into account channel estimation errors. To this end, we provide an approximate BER analysis for fixed gain systems in the next section. The performance of variable gain systems does not

lend itself to simple approximations. Therefore, it is not presented.

6.4 Approximate BER Analysis with Channel Estimation Errors

Consider the case of fixed gain relays. Let the error in estimating the channel $h(k)$ in a SP be $e(k) = h(k) - \hat{h}(k)$ with error variance σ_e^2. The orthogonality principle used in the LMMSE theory suggests [68]

$$\sigma_e^2 = \sigma_h^2 - \mathbf{a}\mathbf{R}_{\hat{\mathbf{p}}\hat{\mathbf{p}}}\mathbf{a}^{\mathrm{H}}, \tag{206}$$

where σ_h^2 is the variance of the overall channel $h(k)$ and H is the Hermitian operator. Then, (190) can be rewritten as

$$r_2(k) = \hat{h}(k)s(k) + w(k) \tag{207}$$

$$w(k) = e(k)s(k) + A_1 h_2(k) n_1(k) + n_2(k), \tag{208}$$

where $w(k)$ can be treated as the total additive noise corrupting the received signal. This noise is not Gaussian due to the presence of the $h_2(k)n_1(k)$ term. Therefore, the usual methods to assess BER performance cannot be applied. Exact BER evaluation is difficult due to the non-Gaussian nature of the noise. However, an upper bound on the BER can be obtained by treating $w(k)$ as Gaussian. The instantaneous symbol SNR conditioned upon $\hat{h}(k)$ is

$$\gamma = \frac{E_1|\hat{h}(k)|^2}{\sigma_w^2} \tag{209}$$

$$\sigma_w^2 = E_1\sigma_e^2 + A_1^2\sigma_2^2\sigma_n^2 + \sigma_n^2. \tag{210}$$

Note that here and in the subsequent analysis, we drop the index k for the ease of notation. It should be remembered that different data positions, i.e., different k, will have different error variances and therefore different γ. The average BER can be obtained by averaging over all the data positions in a SP.

The BER can be evaluated by finding the moment generating function (MGF) of the instantaneous value of γ and applying the analysis provided in [72]. For this, we require the probability distribution function of $|\hat{h}(k)|^2$. Noting the fact that $\hat{h}(k)$ is an estimate of $h(k)$, we approximate the pdf of $|\hat{h}(k)|^2$ as having the same form as the pdf of $|h(k)|^2$. By using the pdf of $|h(k)|$ from (156) in Chapter V, we approximate the MGF of γ as

$$\Phi_\gamma(s) = \frac{1}{\bar{\gamma}s}\exp\left(\frac{1}{\bar{\gamma}s}\right)\mathrm{E}_1^x\left(\frac{1}{\bar{\gamma}s}\right) \quad (211)$$

$$\bar{\gamma} = \mathbf{E}[\gamma] = \frac{E_1^2(\sigma_h^2-\sigma_e^2)}{\sigma_w^2}. \quad (212)$$

Finally, for the BPSK modulated transmission, we obtain the BER

$$P_{BPSK} = \frac{1}{\pi}\int_0^{\pi/2}\Phi_\gamma\left(s\frac{1}{\sin(\theta)^2}\right)\mathrm{d}\theta. \quad (213)$$

The above expression includes the effects of imperfect channel estimation and helps to evaluate the BER without the need for simulations. We verify the accuracy of this approximate BER analysis in the next section. The above MGF can also be utilized to evaluate the BER for other modulation schemes using the analysis in [72].

6.5 Results

In this section, we verify the performance of the proposed LMMSE estimator.We consider transmission of BPSK modulated symbols in the form of packets containing 500 symbols, counting both the data and pilots symbols.. The channels for different packets are generated independently. The Method of Exact Doppler Spread (MEDS) given in [56] is used to simulate the fixed-to-fixed and fixed-to-mobile channels while the modified MEDS model given in Chapter IV is used to simulate the mobile-to-mobile channels. Unless otherwise stated, for fixed relays we use normalized Doppler frequencies $f_1T_s = 0.001$ and $f_2T_s = 0.01$ while for mobile relays we use $f_1T_s = f_2T_s = 0.01$. A pilot insertion period of $T_p = 5$ symbols corresponding to 20% overhead bandwidth

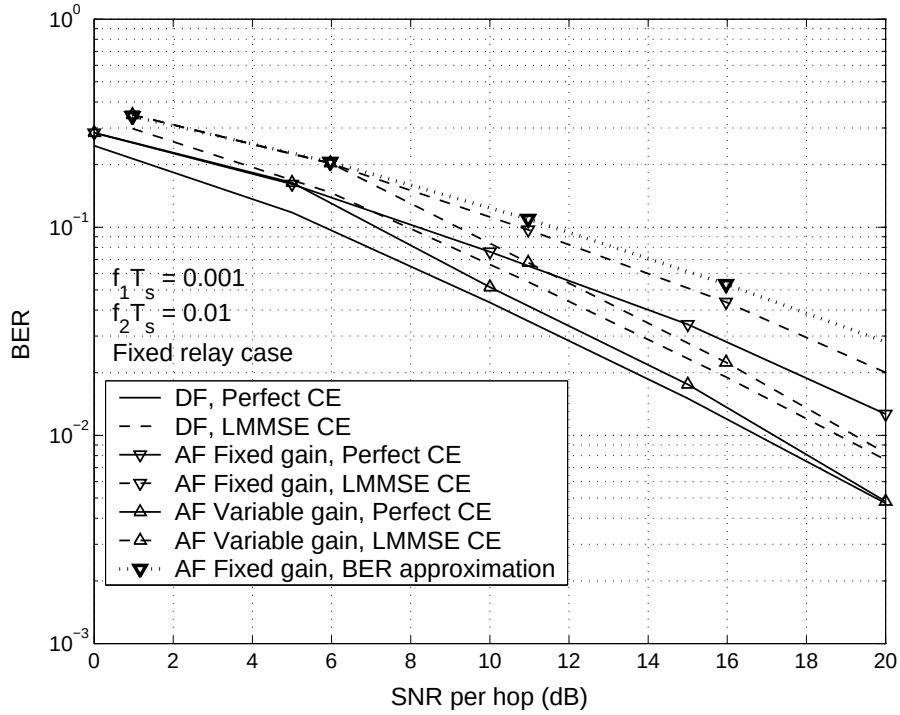

Figure 31: LMMSE estimator performance: BER vs. SNR per hop for fixed relay scenario.

is used in most simulations. The $T_p = 5$ value ensures adequate channel sampling for the Doppler frequencies under consideration. For example, $T_p = 5$ implies three times over-sampling for mobile relays. Note that the power loss resulting from pilots is accounted for in all the BER vs. SNR curves. We also assume equal average SNR on both the hops, i.e., $\bar{\gamma}_1 = \bar{\gamma}_2$.

Results for the DF system are also included for the complete coverage of the topic. The corresponding LMMSE estimators, which for the DF system are the MMSE estimators, used at the relay and the receiver can be designed by easily modifying (199) and (201) by using $A_1 = \sqrt{E_2}$ and neglecting relay noise propagation at the receiver. The effect of the individual channels $h_1(k)$ and $h_2(k)$ alone should be considered at the relay and the receiver for the DF system, respectively.

Figure 31 and Figure 32 illustrate the performance of different systems assuming a fixed relay and a mobile relay, respectively. Plots with perfect CE at the receiver

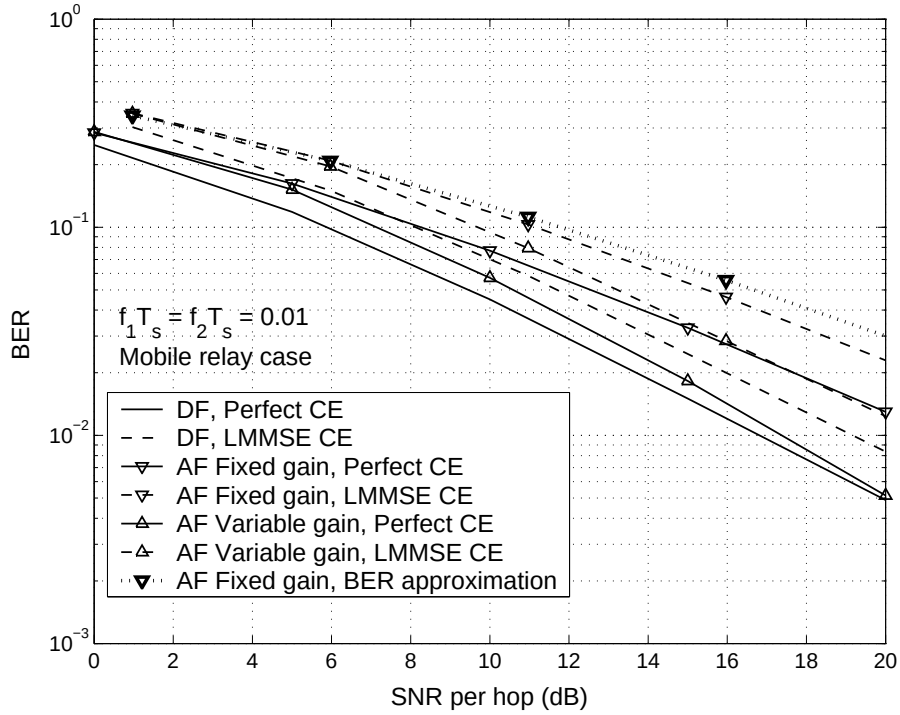

Figure 32: LMMSE estimator performance: BER vs. SNR per hop for mobile relay scenario.

and the relay, wherever applicable, are also provided to serve as benchmarks. The DF system and the AF system with a variable gain relay have comparable performance, in agreement with results in [15], where perfect channel estimation was assumed. Fixed gain relays show poor performance. However, it must be kept in mind that fixed gain relays have the lowest complexity because they do not require channel estimation at the relay.

The results with the LMMSE estimator are within 2.5-3 dB of the perfect channel knowledge curves and therefore the estimator performance can be considered satisfactory. The estimator performance degrades to a certain degree for the mobile relay case as compared to the fixed relay due to faster fading conditions. This is more noticeable at high SNR where the gap between the BER with perfect CE and the BER with LMMSE CE is wider for the mobile relay case in Figure 32 than the fixed relay case in Figure 31. Additional performance improvement in such cases may be

achieved by increasing the number of pilots and developing better estimation schemes. These figures also plot the approximate BER values calculated using our analysis for fixed gain relays. The approximation is particularly good for low-to-moderate SNR. Better approximations should be developed in future work for the high SNR regime.

Having demonstrated that the LMMSE estimator provides good performance, we now study the influence of pilot spacing T_p and other estimation strategies. In most of the results that follow, we restrict our attention to the AF system with fixed gain, mobile relays. The trends are similar for variable gain relays and therefore are not shown.

6.5.1 Influence of pilot spacing

Figure 33 plots the BER vs. SNR per hop for different values of the pilot insertion period T_p: 5, 10, and 20 symbols corresponding to 20%, 10%, and 5% pilot overhead bandwidth, respectively.

We observe that there is an additional loss of approximately 0.5 dB SNR loss at moderate SNR values if $T_p = 10$ is used instead of $T_p = 5$. However, at low SNRs, where the noise is the limiting factor, $T_p = 10$ and T_p =5 perform identically, thereby, suggesting that at low SNRs bandwidth and power should not be expended by inserting more pilots. Further, with $T_p = 20$, the Nyquist sampling condition of (205), which entails a minimum T_p of approximately 16 symbols for the chosen Doppler frequencies, is not satisfied. Therefore, $T_p = 20$ shows significantly worse BER. To further demonstrate the effectiveness of the LMMSE estimator, Figure 33 also plots the BER performance achieved by using differentialdifferentially detected BPSK (DPSK) which does not require channel estimation. We observe that if adequate pilots are inserted, coherent demodulation of the BPSK symbols with the aid of LMMSE estimator performs better than DPSK.

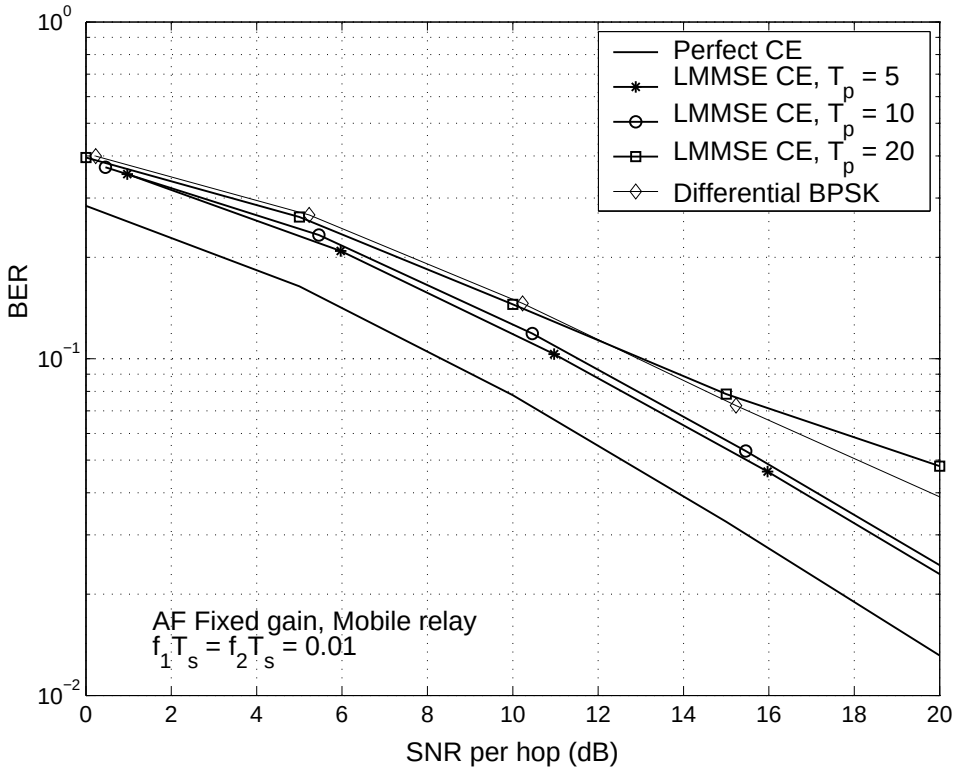

Figure 33: Influence of pilot spacing on the estimator performance.

6.5.2 Influence of the number of pilots, N_p, used in estimation

Though most of the results are obtained using $N_p = 4$ pilots for estimating each channel coefficient, it is also worthwhile to study the performance with different N_p. Fig. 34 compares the results for $N_p = 2$ and $N_p = 6$. For $N_p = 2$, one pilot symbol from the past and future are used while for $N_p = 6$, three pilot symbols from the past and future are used for estimation. Naturally, the use of $N_p = 2$ gives a slightly inferior performance with a loss of approximately 0.5-0.7 dB compared to the $N_p = 4$ case. However, a comparison between $N_p = 4$ and $N_p = 6$ shows that the gain by increasing the number of pilots beyond 4 is insignificant. With $N_p = 6$, the extreme past and future pilot symbols bear low correlation to the current channel values. Therefore, our results suggest that $N_p = 4$ is sufficient to achieve good performance under the assumed mobility conditions.

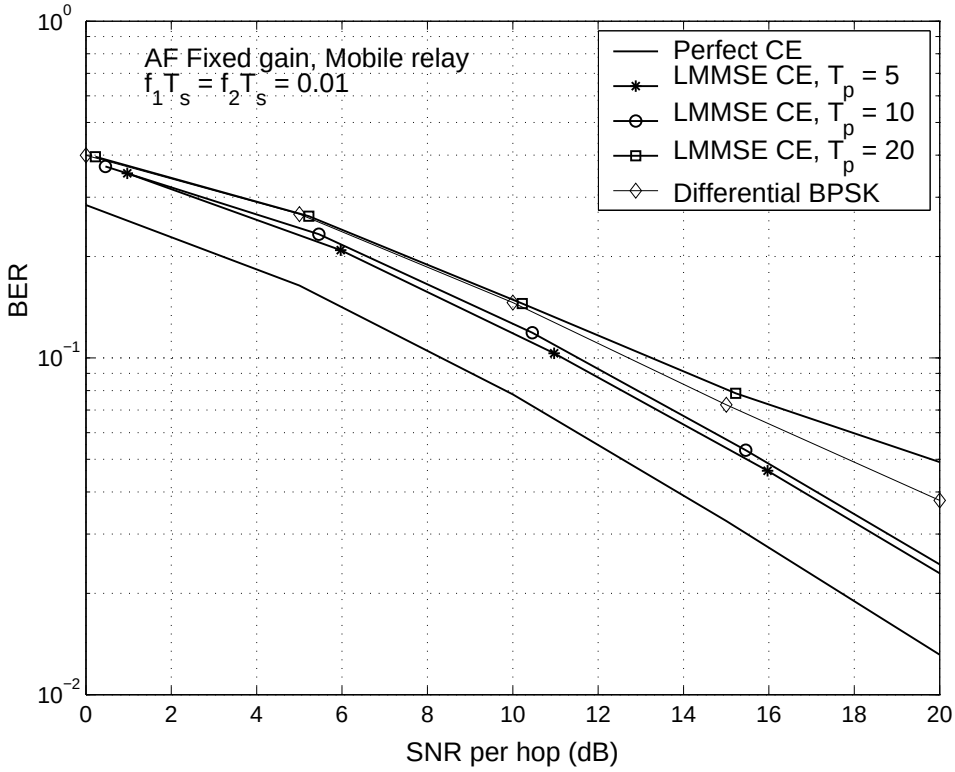

Figure 34: Influence of the number of pilots, N_p, used in estimation

6.5.3 Influence of the Doppler frequencies on the estimator performance

Assuming fixed gain, mobile, relays with $f_1T_s = f_2T_s$, Fig. 35 plots the BER vs. SNR for different values of the normalized Doppler frequency f_1T_s. For very low Doppler frequencies, we observe that the estimator performance is better, but still suffers a loss of 2-2.5 dB compared to perfect channel estimation. This loss arises because of the inherent limitation of the estimator due to AWGN noise, relay propagation noise and the interpolation process itself. For very high Doppler frequencies, the performance loss increases to approximately 4 dB because of increased mobility in the channel.

Finally, it is interesting to compare the DPSK BER curve (obtained using $f_1T_s = f_2T_s = 0.01$) given in Fig. 33 with the high Doppler ($f_1T_s = f_2T_s = 0.02$ or 0.03) BER curves given in Fig. 35. We observe that DPSK is still worse at high SNRs. This suggests the usefulness of the LMMSE estimator for coherent demodulation even under relatively high Doppler frequency conditions.

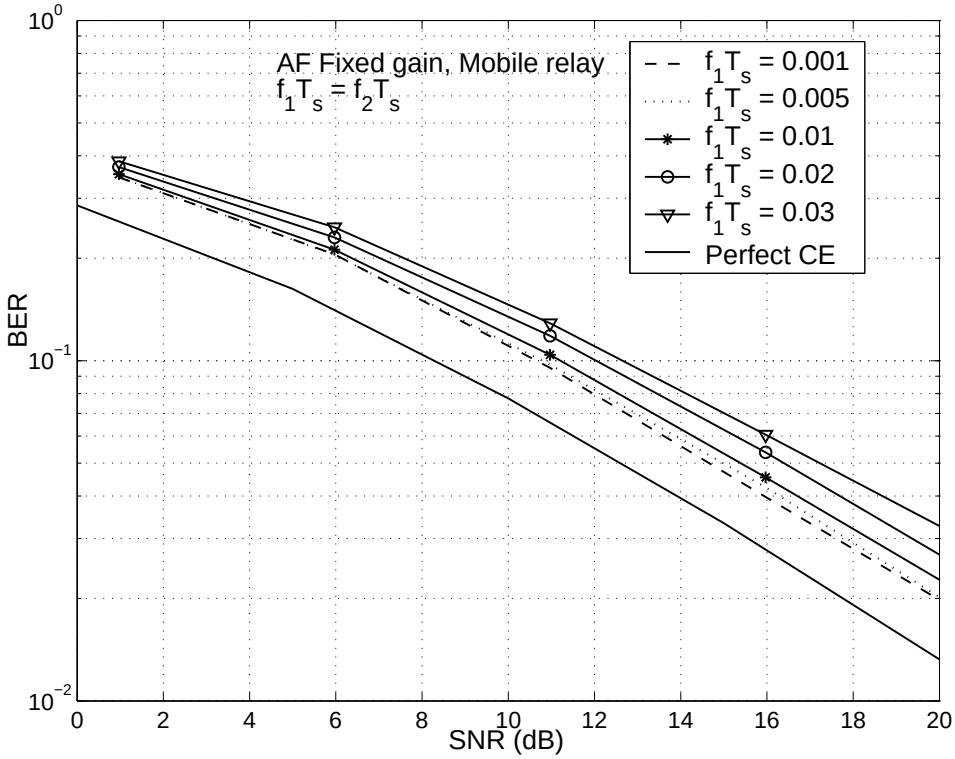

Figure 35: Influence of the Doppler frequencies on the estimator performance

6.5.4 Dependence on the knowledge of channel correlation functions

In all the simulation results discussed so far we assumed perfect knowledge of the channel correlation functions at the destination and at the relay. It is also important to evaluate the performance when perfect knowledge of parameters such as the Doppler frequencies required to design the estimator are not available. Figure 36 plots the BER for different Doppler frequency conditions when the estimator is designed using a fixed set of Doppler values. The "true" values are the actual values used to simulate the channels while the "simulation" values of $f_1T_s = f_2T_s = 0.01$ are the assumed values used to design and simulate the estimator. We observe that when the true Doppler values are smaller than the assumed values, the performance is not significantly affected.

Thus, the estimator can be designed based upon the expected worst case mobility and Doppler frequency conditions in the channel. This is consistent with the general

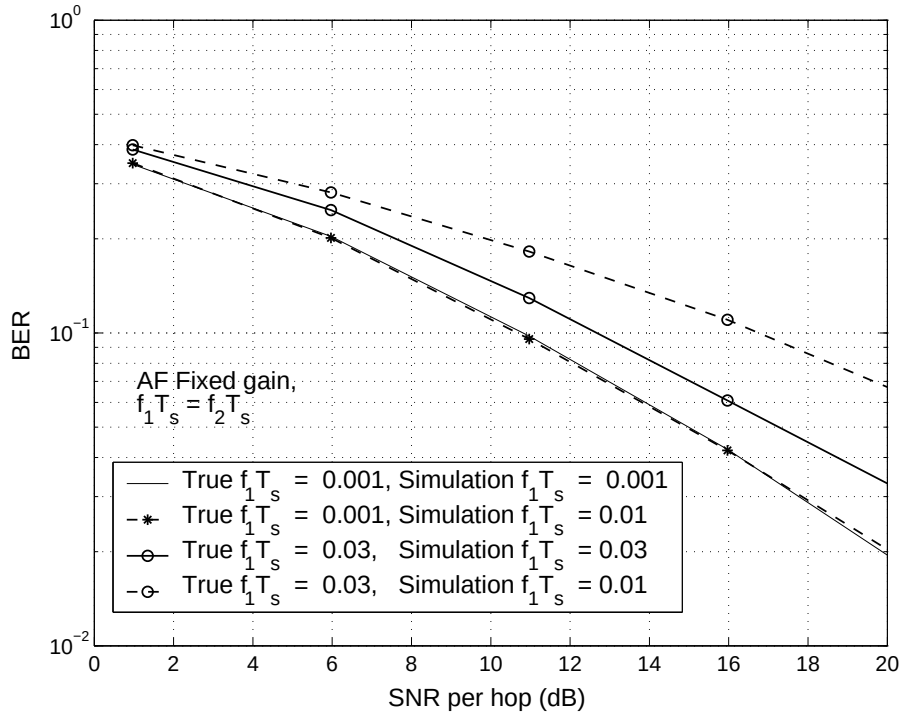

Figure 36: Performance dependence on the knowledge of channel correlation functions.

principle often employed for estimation in traditional cellular channels.

6.5.5 Comparison with alternative estimation schemes

Now, we turn our attention to alternative estimation strategies and compare their performance with the LMMSE scheme. As noted earlier, the LMMSE scheme which obtains the channel estimates at data positions by interpolating the pilot channel estimates is not the optimal scheme for relay channels. Therefore, it is worthwhile to consider other estimation schemes and compare their complexity and performance with the LMMSE scheme. In particular, we consider two schemes, "no-interpolation" and "linear" interpolation schemes, because of their simplicity.

1. *No-interpolation scheme*:

   The pilot at the beginning of a SP is used to obtain the channel estimate at that position and the same estimate is used at all the data positions in a SP.

Thus, there is no interpolation involved in obtaining the channel estimates. The underlying assumption in this scheme is that the channel does not change significantly within a SP. This assumption will not be always true and therefore we expect the performance of this scheme to be inferior to the LMMSE. However, the estimator complexity is considerably less than that of the LMMSE estimator.

2. *Linear interpolation scheme*:

   The pilot channel estimates at the start and the end of a SP are linearly interpolated to obtain the channel estimates at the data positions in the SP. The complexity of this scheme is higher than that of the no interpolation scheme but less than the LMMSE estimator.

Figure 37 compares the BER performance of these schemes with the LMMSE scheme. We observe that the no-interpolation scheme cannot cope up with the fading conditions in the overall channel. The linear interpolation scheme performs approximately 0.5-1 dB worse than the LMMSE scheme. This suggests that if a low complexity solution is required, the linear interpolation may be preferred at the expense of a modest SNR loss.

6.5.6 Performance in the presence of diversity

Returning to our comparisons in Figure 31 and Figure 32, the DF system shows slightly better performance compared to the AF system. However, as noted in [15], AF systems performs better in the presence of diversity such as the presence of a direct BS-MS link in addition to the relay link. Such a link is possible when the MS also receives the BS transmission in the first time slot when the BS transmits to the relay. Channel estimation issues for the direct link have been well studied and therefore are not studied here. However, to complete our comparisons, the BER

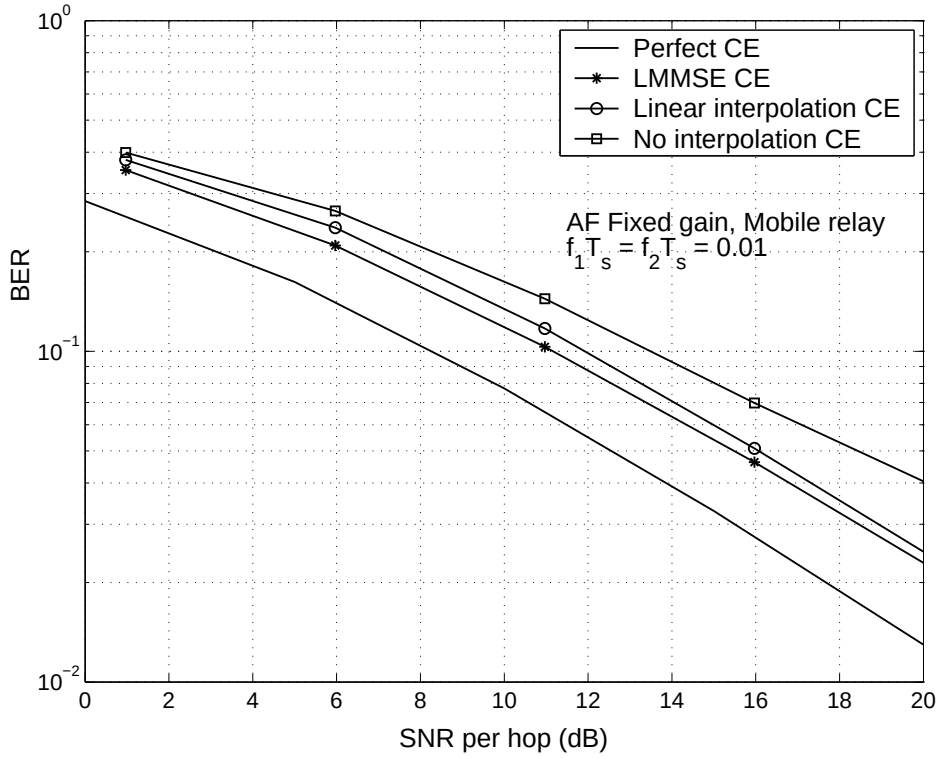

Figure 37: Comparisons with alternative estimation schemes.

results including the direct BS-MS link are shown in Figure 38. The direct link is modeled as a conventional cellular link (similar to $h_1(k)$) with normalized Doppler frequency $f_m T_s = 0.01$. The average SNR on the direct link is assumed 6 dB less than the average SNR on the hops of the indirect link. Estimation is performed using a LMMSE estimator designed for this link. At the MS, maximal ratio combining (MRC) is used to combine the signal received via the direct and indirect relay links.

We observe that the added diversity significantly improves the performance of AF systems, in particular the fixed gain AF system. The improved performance coupled with reduced complexity implementation make AF systems preferable over DF systems when the direct link can be supported.

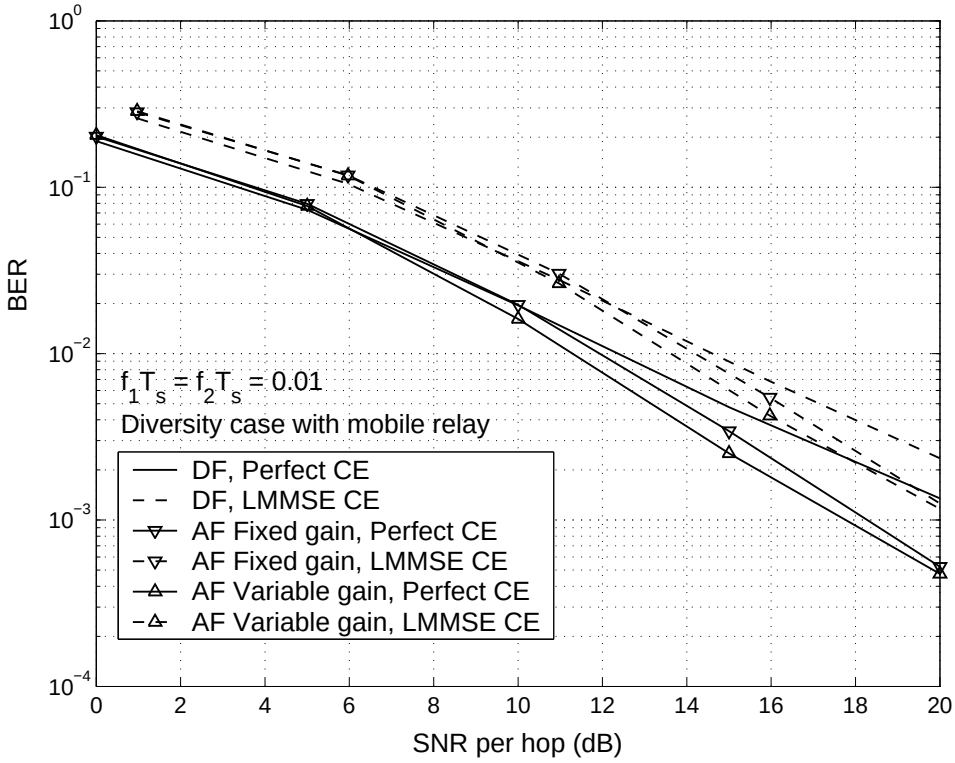

Figure 38: Performance in the presence of diversity from the direct BS-MS link.

6.6 Summary

We provided a realistic evaluation of the performance of cooperation diversity systems by considering the effect of channel estimation. Issues pertaining to channel models and estimator design were addressed for a wide range of scenarios, including different gain and mobility conditions of the relay. The proposed LMMSE estimator was found to provide satisfactory performance. We also provided an approximate analysis for evaluating the BER under imperfect channel estimation for fixed gain relays. This avoids the needs for simulations and also helps to understand the influence of channel estimation errors at different SNRs.

Future research should focus on developing optimal or improved sub-optimal estimation algorithms. Further, the BER analysis for fixed gain relays under imperfect channel estimation should be extended to encompass the case of variable gain relays.

Appendix 6.1: Channel estimation using the Extended Kalman Filter (EKF)

The LMMSE estimator described earlier performs block by block data processing, i.e., in order to utilize pilots from the past and future, the estimator collects a block of data symbols and performs estimation on this block. Often, for real-time channel tracking, a recursive estimation algorithm, where the estimation is done symbol by symbol, is preferred to minimize the delays incurred in block processing. Kalman filter (KF) has been extensively used for recursive channel estimation in cellular applications [21]. In the presence of additive Gaussian noise, the KF is the optimal linear recursive filter [33], thereby giving optimal channel estimates.

The KF filter imposes a state-space model over the channel to be estimated and utilizes the received signal to track the state variable. For example, to track the Rayleigh faded cellular channel $h(k)$ described in Chapter II, the KF filter assumes $h(k)$ to evolve in time as a first-order Gauss-Markov process, i.e.,

$$h(k) = \upsilon h(k-1) + w(k), \tag{214}$$

where υ is determined by the auto-correlation function of $h(k)$ and $w(k)$ is zero mean, white, complex Gaussian noise with variance $\sqrt{1-\upsilon^2}$. As a result, $h(k)$ is zero mean, complex Gaussian with unit variance. By applying the Clarke's model for cellular channels from Chapter II, we have $\upsilon = J_0(2\pi f_d T_s)$, T_s being the sampling period. Further, the KF filter assumes the measured data, say $y(k)$, is a linear function of $x(k)$, i.e.,

$$y(k) = C(k)h(k) + v(k), \tag{215}$$

where $C(k)$ is independent of $h(k)$ and $v(k)$, independent of $w(k)$, is the AWGN in the received signal. The equation shows that the measured data is a linear function of the state-space variable.

However, the KF cannot be directly applied for CE in AF relay channels. For

the AF relay channels, the channel to be estimated, $h(k) = A(k)h_1(k)h_2(k)$, is non-Gaussian due to the product of $h_1(k)$ and $h_2(k)$. Therefore, a state-space model that approximates $h(k)$ as a Gauss-Markov process is not possible. Rather than tracking $h(k)$ directly, we can track $h_1(k)$ and $h_2(k)$ individually by defining a state-space vector consisting of these two variables, i.e.,

$$\begin{aligned}\mathbf{x}(k) &= \begin{pmatrix} x(1,k) \\ x(2,k) \end{pmatrix} = \begin{pmatrix} h_1(k) \\ h_2(k) \end{pmatrix} = \begin{pmatrix} \upsilon_1 & 0 \\ 0 & \upsilon_2 \end{pmatrix} \mathbf{x}(k-1) + \begin{pmatrix} w_1(k) \\ w_2(k) \end{pmatrix} \\ &= \mathbf{B}\mathbf{x}(k-1) + \mathbf{w}(k). \end{aligned} \tag{216}$$

Here, $\mathbf{B}$ is the 2x2 matrix containing the coefficients υ_1 and υ_2, which are determined by the auto-correlation of the BS-relay channel $h_1(k)$ and the relay-MS channel $h_2(k)$, respectively, while $\mathbf{w}(k)$ is the noise vector in the state-space model. Having defined the state-space vector, let us now consider the signal received in an AF relay system. From (190), we can write the received signal as

$$y(k) = A(k)h_1(k)h_2(k) + h_2(k)n_1(k) + n_2(k). \tag{217}$$

Thus, we notice that the received signal is a non-linear function of the state variables $h_1(k)$ and $h_2(k)$, thereby precluding the use of KF. Instead, the extended KF (EKF) can be used to track the state vector in the presence of such non-linearities [33]. Therefore, we apply the EKF algorithm for tracking the individual channels $h_1(k)$ and $h_2(k)$. An apparent problem here is the fact that the received signal $y(k)$ is symmetric in the state variables except for the term $h_2(k)n_1(k)$ due to noise propagation from the relay. Therefore, the individual estimates of $h_1(k)$ and $h_2(k)$ are not likely to be accurate. However, tracking of the overall channel $h(k)$ is still possible.

We discuss channel estimation with fixed gain relays, i.e., the gain $A(n)$ is given by (191). We again assume that pilot symbols are inserted every T_p symbols. When a pilot is available, the EKF updates the state vector using the pilot signal observation while for the non-pilot symbols, the EKF simply predicts the state vector using the state-space model. Using the EKF theory, we summarize EKF equations here:

Initialization: At time $k = 0$, we initialize the state vector and the error covariance matrix P, i.e., the covariance of error between the true state vector and the estimated state vector, as

$$\mathbf{x}(k=0) = [0 \qquad 0]^T \tag{218}$$

$$\mathbf{P} = \begin{pmatrix} 2\sigma_1^2 & 0 \\ 0 & 2\sigma_2^2 \end{pmatrix}. \tag{219}$$

Here, T is the matrix transpose operator and σ_i^2 is the variance of the channel h_i.

Update: For $k \neq 0$, the EKF updates its estimate of the state vector in two phases:

- Measurement update, i.e., update using pilot symbol measurements: For k such that $mod(k, T_p) = 0$, where mod is the modulo operator,

$$\mathbf{P} = \mathbf{BPB}^H + \mathbf{Q_w} \tag{220}$$

$$\nabla_x = [Av_2x(2,k-1) \qquad Av_1v_2x(1,k-1)] \tag{221}$$

$$\mathbf{G} = \frac{\mathbf{P}\nabla_x^H}{(\nabla_x\mathbf{P}\nabla_x^H + \sigma_n^2 + |Av_2x(2,k-1)|^2\sigma_n^2)} \tag{222}$$

$$\mathbf{x}(k) = \mathbf{Bx}(k-1) + \mathbf{G}(y(k) - Av_1v_2x(1,k-1)x(2,k-1)) \tag{223}$$

$$\mathbf{P} = (\mathbf{I}_{2x2} - \mathbf{G}\nabla_x)\mathbf{P} \tag{224}$$

$$\hat{h}(k) = x(1,k-1)x(2,k-1), \tag{225}$$

where $\mathbf{Q_w}$ is the covariance matrix of the vector $\mathbf{w}$, ∇_x computes the gradient of the state vector, $\mathbf{G}$ is the filter gain used for the update, and $\hat{h}(k)$ is the estimate of the channel at time k.

- Prediction, i.e., update in the absence of pilot measurements:
  For k such that $mod(k, T_p) \neq 0$,

$$\mathbf{P} = \mathbf{BPB}^H + \mathbf{Q_w} \tag{226}$$

$$\mathbf{x}(k) = \mathbf{Bx}(k-1) \tag{227}$$

$$\hat{h}(k) = x(1,k-1)x(2,k-1). \tag{228}$$

Note that the EKF assumes knowledge of the parameters υ_i's just as the LMMSE estimator assumes the knowledge of channel correlations.

Now, we assess the performance of the above EKF algorithm for channel estimation in fixed gain AF relay systems. A pilot symbol is inserted every fifth symbol, i.e., $T_p = 5$. Analogous to assumptions in Section 6.5, we assume mobile relay with $f_1 T_s = f_2 T_s$ =0.01. Therefore, we get $\upsilon_1 = J_0(2\pi f_1 T_s)$ and $\upsilon_2 = J_0(2\pi f_1 T_s) J_0(2\pi f_2 T_s)$. We consider two different channel models: i) $h_1(k)$ and $h_2(k)$ are indeed first-order Gauss-Markov processes and ii) $h_1(k)$ and $h_2(k)$ are actually based on the fixed-to-mobile and mobile-to-mobile channel SoS models discussed earlier. However, the EKF assumes them as Gauss-Markov processes with υ_is as the parameters. Figure (39) plots the results of channel estimation along with a comparison with the LMMSE estimator performance. We observe that when the underlying channel model obeys the Gauss-Markov assumption, the EKF provides good performance. However, for channels of our interest, where SoS models are more realistic, the EKF's performance is inferior to that of the LMMSE estimator. Therefore, the EKF is not a good candidate for estimating AF relay channels.

The inferior performance of the EKF arises due to several factors. Firstly, though a Gauss-Markov model is reasonable for individual channels $h_1(n)$ and $h_2(n)$ [21], the model is not suitable for estimating $h(n)$. The underlying channel is too fast to give effective recursive estimates. Information from several pilot symbols must be used to enable estimation under such fading conditions. Therefore, LMMSE with block processing performs better. In addition, the presence of non-Gaussian noise in the received signal leads to some loss of optimality in estimation using the EKF, which potentially degrades the performance. The performance of the EKF may be improved by imposing a higher order model on the channels h_1 and h_2 rather than a first order model. However, with a higher order model, the estimator complexity increases. Therefore, this issue is not considered in our work. A detailed analysis of

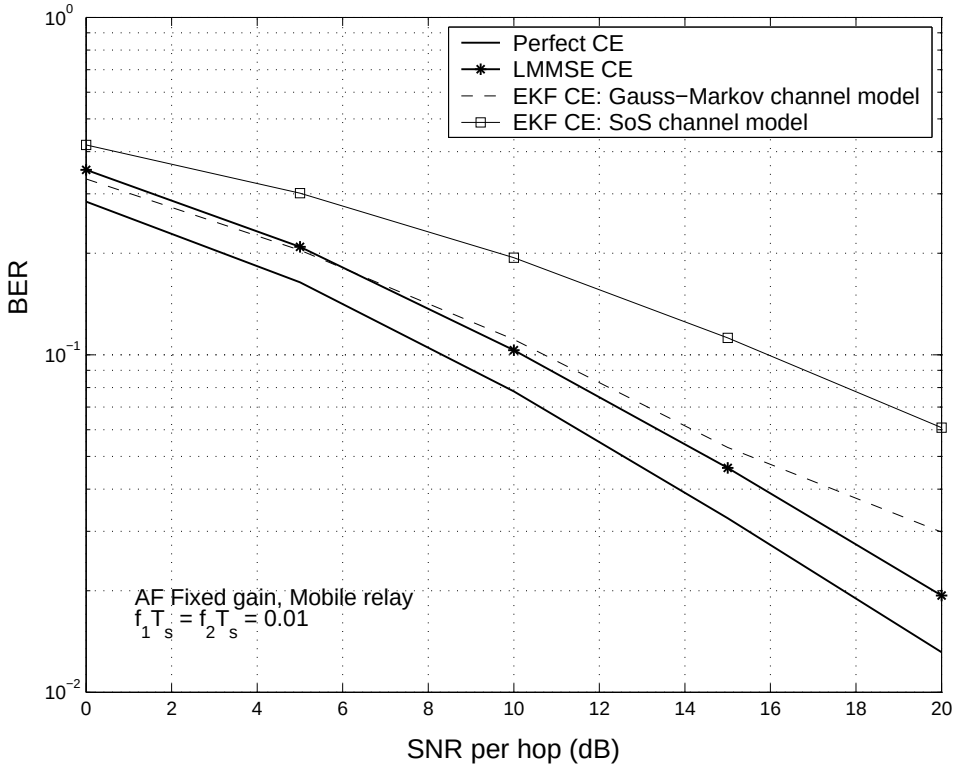

Figure 39: Channel estimation using the Extended Kalman Filter.

these performance vs. complexity tradeoffs may be of interest in future work.

CHAPTER VII

CONTRIBUTIONS AND FUTURE RESEARCH DIRECTIONS

7.1 Contributions to wireless channel modeling and simulation

Wireless channel modeling and simulation related issues are highly relevant for designing wireless communication systems. The knowledge about different channel impairments obtained from channel modeling is a must for developing algorithms for reliable communication. Simulation models complement this by recreating channel impairments in simulations and thus providing a platform for designing and testing different algorithms. Motivated by these facts, here we summarize our research contributions to wireless channel modeling and simulation for different applications.

- **Cellular channels**:

  Several theoretical and SoS simulation models are available in the literature for cellular channels - wireless propagation channels between a BS and a MS. However, we found that a coherent and comprehensive analysis of these different simulation models is not available. Therefore, we provided a rigorous analysis to compare several statistical simulation models for cellular channels. Instead of evaluating different models qualitatively, as often done in the existing literature, quantitative metrics were used to compare different models.

  Our analysis revealed the non-stationary nature of the existing Zheng and Xiao's model (Model IV), thereby justifying the need to resort to quantitative metrics. We identified models that give desired accuracy in simulations by evaluating their auto-correlation and LCR statistics. Our analysis suggests that "just the right amount of randomness" must be added in the simulation models to provide

good performance with minimal complexity. These insights formed the basis of novel simulation models for mobile-to-mobile channels.

- **Mobile-to-mobile channels**:

  Mobile-to-mobile channels with mobility at both the ends of a communication link significantly differ from cellular channels in terms of their temporal properties. A literature survey suggested that theoretical and simulation models for these channels are rare. Therefore, we presented an alternate mobile-to-mobile channel representation by using "double ring" scattering environment where scatterers are placed uniformly on two rings - one around the transmitter and the other around the receiver. This alternate channel representation along with the insights gained from our work on cellular channels enabled us to develop new statistical as well as deterministic SoS simulation models for mobile-to-mobile channels. The SoS model parameters such as random phases and Doppler frequencies were carefully tailored to reproduce the channel statistics in simulations. We demonstrated that our models provide superior performance compared to the existing models, thereby justifying the usefulness of these new models.

- **Amplify and forward relay channels**:

  Future communication systems are likely to deploy relays to improve network coverage and link reliability. For reasons of complexity, AF relays, which simply receive, amplify, and forward a signal, are likely to find widespread acceptance in contrast to DF relays. However, we found that radio channels in such AF relay systems are unique and not well understood. An AF relay channel consists of a cascade of transmitter-relay and relay-receiver fading channels making it different from cellular and mobile-to-mobile channels. Therefore, we characterized the statistical properties of these channels.

The cascading of two links results in the double Gaussian (product of two Gaussians) nature of an AF relay channel. Therefore, the fading is different from the traditional Rayleigh fading. We derived temporal properties like the auto-correlation, the Doppler spread, and the LCR of AF relay channels. These properties show that AF relay channels fade faster compared to cellular and mobile-to-mobile channels. Transmission as well as reception techniques must be designed by taking into account these unique properties of AF relays channels. In addition, we evaluated different kinds of AF relay systems, fixed and variable gain relays, in terms of their outage frequency and outage durations. We showed that variable gain relays tend to perform better because they provide partial compensation of channel fading at the relay. The statistical properties developed by us are useful for channel estimation in AF relay systems.

7.2 Contributions to wireless channel estimation

Coherent reception requires knowledge of the instantaneous channel to compensate fading and perform demodulation. The channel knowledge is acquired by transmitting known pilot symbols and estimating the channel. The problem of channel estimation has been extensively studied for cellular channels. However, the unique nature of AF relay channels makes estimation difficult in relay systems. Therefore, we investigated channel estimation for AF relay channels.

We found that because of the non-Gaussian nature of AF relay channels as well as noise propagation from the relay, design of optimal MMSE estimator is complex. Therefore, we developed a simple but sub-optimal LMMSE scheme to estimate AF relay channels. Design criteria like minimum pilot insertion period and estimator coefficients were provided by applying the properties of AF relay channels for various relay configurations such as stationary as well as mobile relays and fixed gain as well as variable gain relays. We showed that the LMMSE estimator provides better

performance compared to other estimation schemes like linear interpolation and the EKF. We also evaluated the trade-offs in channel estimation for AF and DF systems. We found that DF systems have less stringent requirements on channel estimation because the channels in DF systems fade slowly compared to AF systems.

In addition, an approximate analysis was provided to compute the BER in the presence of imperfect channel estimation. This analysis is useful to evaluate the estimator performance without resorting to time-consuming simulations.

7.3 Future work on mobile-to-mobile channels

Due to a lack of channel measurement capabilities, our contributions have been limited to developing theoretical and simulation models of mobile-to-mobile channels. However, it is important to verify the accuracy of these models in real-world propagation conditions. Therefore, future research efforts may be devoted to collecting channel data and developing models from these measurements. As noted in Chapter II, some efforts in this direction are already underway. Further, there is a need to extend the currently available narrowband, frequency-flat mobile-to-mobile channel models to frequency-selective models for high bandwidth transmissions. In certain applications, MIMO antennas are likely to be deployed in mobile-to-mobile applications. Therefore, it is also necessary to extend the current models to develop MIMO channel models by accurately modeling spatial correlations between multiple antennas.

We have shown the usefulness of our simulation models for computer simulations. The feasibility of porting these simulation models into hardware for real-time channel simulation is also of interest. Hardware channel emulation can increase the usefulness of our simulation models by enabling network level simulations in real-time. In addition, performance vs. complexity trade-offs between statistical and deterministic simulation models should be studied from a network simulation perspective in contrast to the link level analysis presented here.

7.4 Future research on amplify and forward relay channels

It is evident from the results in Chapter V that our study of AF relay channels is still not complete. Often, we found that properties like the auto-correlation and LCR cannot be quantified precisely due to a lack of closed form expressions. Therefore, future research should consider obtaining these properties in closed forms to gain better insights into their behavior. If such closed form properties are not achievable, better and simpler approximations need to be developed. Also, issues like the properties of variable gain relays and differences between uplink and downlink relay channels should be studied in greater detail. In our analysis, we assumed Rayleigh faded transmitter-relay and relay-receiver links due to NLOS propagation. This work needs to be extended for scenarios where the links can be Rician due to the presence of a LOS path.

The discussion in Chapter VI showed that channel estimation in AF relay channels is interesting and non-trivial. We presented different sub-optimal schemes for channel estimation in AF relay channels. Therefore, the problem of optimal MMSE channel estimation is still open for AF relay channels. Future research should be targeted at developing this optimal scheme or alternate sub-optimal schemes with better performance than the schemes discussed here.

The LMMSE estimator presented here assumed accurate knowledge of channel statistics. We briefly studied the estimator performance when these knowledge is not accurate. This issue needs to be addressed in greater detail in future to develop robust estimation schemes.

REFERENCES

[1] "Dedicated short range communications." Available [Online] (02/14/2006): http://grouper.ieee.org/groups/scc32/dsrc/index.html.

[2] "Guidelines for evaluation of radio transmission technologies for IMT-2000," Tech. Rep. ITU-R M.1225, International Telecommunications Union.

[3] "Opportunity driven multiple access." 3G Partnership Project:3G TR 25,924.

[4] "Path research program." Available [Online] (02/14/2006): www.path.berkeley.edu.

[5] "SR5500 wireless channel emulator: Data sheets." Available [Online](02/14/2006): www.spirentcom.com.

[6] "COST 207: Digital land mobile radio communications," Tech. Rep., Office of official publication of European Communities, Luxemborg, 1989.

[7] "Digital mobile radio: Evoluation towards future generation systems, COST 231 final report," Tech. Rep., COST Secretriat, Brussels, Belgium, 1998.

[8] Acosta, G., Tokuda, K., and Ingram, M. A., "Measured joint Doppler-delay power profiles for vehicle-to-vehicle communications at 2.4 Ghz," *Proc. IEEE Global Telecommun. Conf.*, vol. 6, pp. 3813–3817, 2004.

[9] Akki, A. S., "Statistical properties of mobile-to-mobile land communication channels," *IEEE Trans. Veh. Technol.*, vol. 43, pp. 826–831, Nov. 1994.

[10] Akki, A. S. and Haber, F., "A statistical model for mobile-to-mobile land communication channel," *IEEE Trans. Veh. Technol.*, vol. 35, pp. 2–7, Feb. 1986.

[11] Alamouti, S. M., "A simple transmit diversity technique for wireless communications," *IEEE J. Sel. Areas Commun.*, vol. 16, pp. 1451–1458, Oct. 1998.

[12] Anderson, J. B., Rappaport, T. S., and Yoshida, S., "Propagation measurements and modeling for wireless communication channels," *IEEE Communications Mag.*, vol. 33, pp. 42–49, Jan. 1995.

[13] Anghel, P. A. and Kaveh, M., "Exact symbol error probability of a cooperative network in a Rayleigh fading environment," *IEEE Trans. Wireless Commun.*, vol. 3, pp. 1416–1421, Sept. 2004.

[14] Baddour, K. E. and Beaulieu, N. C., "Autoregressive models for fading channel simulation," *Proc. IEEE Global Telecommun. Conf.*, pp. 1187–1192, Nov. 2001.

[15] Boyer, J., Falconer, D. D., and Yanikomeroglu, H., "Multihop diversity in wireless relaying channels," *IEEE Trans. Commun.*, vol. 52, pp. 1820–1830, Oct. 2004.

[16] Byers, G. J. and Takawira, F., "Spatially and temporally correlated MIMO channels: Modeling and capacity analysis," *IEEE Trans. Veh. Technol.*, vol. 53, no. 3, 2004.

[17] Cavers, J. K., "An analysis of pilot symbol assisted model for Rayleigh fading channels," *IEEE Trans. Veh. Technol.*, vol. 40, pp. 686–693, Nov. 1991.

[18] Chizhik, D., Foschini, G., and Valenzuela, R. A., "Capacities of multi-element transmit and receive antennas: Correlations and keyholes," *IEEE Electron. Lett.*, vol. 36, no. 13, pp. 1099–1100, 2000.

[19] Clarke, R. H., "A statistical theory of mobile-radio reception," *Bell Syst. Tech. J.*, pp. 975–1000, July 1968.

[20] Dohler, M., *Virtual Antenna Arrays.* King's College London, London, UK, 2003. PhD Disseration.

[21] Dong, M., Tong, L., and Sadler, B., "Optimal insertion of pilot symbols for transmissions over time-varying flat fading channels," *IEEE Trans. Signal Proc.*, vol. 52, pp. 1403–1418, May 2004.

[22] Durgin, G., *Space-Time Wireless Channels.* Upper Saddle, NJ: Prentice Hall, 2002.

[23] Foschini, G. and Gans, M., "On limits of wireless communications in a fading environment when using multiple antennas," *Wireless Pers. Commun.*, pp. 311–335, Nov. 1998.

[24] Gavrilovich, C. D., "Mobile communication system with moving base station." United States Patent - 5,729,826, Mar. 1998. Available [Online](02/14/2006): www.carucel.com.

[25] Gavrilovich, C. D., "Broad communications on the highways of tomorrow," *IEEE Commun. Mag.*, pp. 146–154, Apr. 2001.

[26] Gesbert, D., Bolcskei, H., Gore, D. A., and Paulraj, A. J., "Outdoor MIMO wireless channels: models and performance prediction," *IEEE Trans. Commun.*, vol. 50, pp. 1926–1934, Dec. 2002.

[27] Goldsmith, A., *Wireless Communication.* New York: Cambridge University Press, 2005.

[28] Gradshteyn, I. S. and Ryzhik, I. M., *Tables of Integrals, Series and Products*. Academic Press, 1980.

[29] Gudmundson, M., "Analysis of handover algorithms microcellular for radio," *Proc. IEEE Vehicular Technol. Conf.*, pp. 537–542, May 1991.

[30] Harrold, T. J. and Nix, A. R., "Intelligent relaying for future personal communication systems," *IEE Colloquium on capacity and range enhancement technique for 3G mobile communications and beyond*, pp. 9/1–9/5, Feb. 2000.

[31] Harrold, T. J., Nix, A. R., and Beach, M. A., "Propagation studies for mobile-to-mobile communications," *IEEE Veh. Technol. Conf.*, vol. 3, pp. 1251–1255, Fall 2001.

[32] Hasna, M. O. and Alouini, M. S., "A performance study of dual-hop transmissions with fixed gain relays," *IEEE Trans. Wireless Commun.*, vol. 3, pp. 1963–1968, Nov. 2004.

[33] Hayes, M. H., *Statistical Signal Processing*. New York: John Wiley & Sons, 1996.

[34] Hoeher, P. and Steingass, A., "Modeling and emulation of multipath fading channels using a controlled randomness," *Proc. ITG-Fachtagung "Wellenausbreitung bei Funksystemen und Mikrowellensystemen*, pp. 209–220, May 1998.

[35] Hoeher, P., "A statistical discrete-time model for the wssus multipath channel," *IEEE Trans. Veh. Technol.*, vol. 41, pp. 461–468, Nov. 1992.

[36] Jakes, W. C., *Microwave Mobile Communications*. Piscataway, NJ: IEEE Press, 1993.

[37] Karagiannidis, G. K., Zogas, D. A., Sagias, N. C., Tsiftsis, T. A., and Mathiopoulous, P. T., "Multihop communications with fixed-gain relays over generalized fading channels," *Proc. IEEE Global Telecommun. Conf.*, vol. 1, pp. 36–40, Dec. 2004.

[38] Koltz, S., Kozubowski, T. J., and Podgorski, K., *The Laplace Distribution and Generalizations*. Boston, MA: Birkhauser, 2001.

[39] Kovacs, I. Z., Eggers, P. C. F., Olesen, K., and Petersen, L. G., "Investigations of outdoor-to-indoor mobile-to-mobile radio communication channels," *Proc. IEEE Veh. Technol. Conf.*, vol. 1, pp. 430–434, Sept. 2002.

[40] Laneman, J. N., Tse, D., and Wornell, G. W., "Cooperative diversity in wireless networks: Efficient protocols and outage behavior," *IEEE Trans. Inform. Theory*, vol. 50, pp. 3062–3080, Dec. 2004.

[41] Laneman, J. N., Wornell, G. W., and Tse, D., "An efficient protocol for realizing cooperative diversity in wireless networks," *Proc. IEEE Intl. Symp. Inform. Theory*, p. 194, 2001.

[42] Lee, W. C. Y., *Mobile Communications Engineering*. New York: McGraw Hill, 1982.

[43] Linnartz, J. P. M. G. and Diesta, R. F., "Evaluation of radio links and networks," Tech. Rep. UCB-IT-PRR-96-16, University of California, Berkeley, PATH Research, California, 1996.

[44] Mandayam, N. B., Chen, P. C., and Holtzman, J. M., "Minimum duration outage for cellular systems: a level crossing analysis," *Proc. IEEE Veh. Technol. Conf.*, vol. 2, pp. 879–883, May 1996.

[45] Martin, U., "Modeling mobile radio channels by echo estimation," *FREQUENZ*, vol. 3, pp. 198–212, Sept. 1994.

[46] Maurer, J., Fugen, T., Olesen, K., and Wiesbeck, W., "Narrow-band measurement and analysis of the inter-vehicle transmission channel at 5.2 Ghz," *Proc. IEEE Veh. Technol. Conf.*, vol. 3, pp. 1274–1278, May 2002.

[47] Nabar, R. U., Boelcskei, H., and Kneubhueler, F. W., "Fading relay channels: Performance limits and space-time signal design," *IEEE J. Sel. Areas Commun.*, vol. 22, pp. 1099–1109, Aug. 2004.

[48] Pabst, R., Walke, B. H., Schultz, D. C., Herhold, P., Yanikomeroglu, H., Mukherjee, S., Viswanathan, H., Lott, M., Zirwas, W., Dohler, M., Aghvami, H., Falconer, D. D., and Fettweis, G. P., "Relay-based deployment concepts for wireless and mobile broadband radio," *IEEE Commun. Mag.*, vol. 42, pp. 80–89, Sept. 2004.

[49] Papoulis, A. and Pillai, S. U., *Probability, Random Variables and Stochastic Processes*. New York: McGraw-Hill, 2001.

[50] Patel, C. S. and Stuber, G. L., "Channel estimation for amplify and forward relay based cooperation diversity systems," *IEEE Trans. Wireless Commun.*, 2005.

[51] Patel, C. S., Stuber, G. L., and Pratt, T. G., "Simulation of Rayleigh faded mobile-to-mobile communications," *Proc. IEEE Veh. Technol.*, vol. 1, pp. 163–167, Oct. 2003.

[52] Patel, C. S., Stuber, G. L., and Pratt, T. G., "Comparative analysis of statistical models for the simulation of Rayleigh faded cellular channels," *IEEE Trans. Commun.*, vol. 53, no. 6, 2005.

[53] Patel, C. S., Stuber, G. L., and Pratt, T. G., "Simulation of Rayleigh faded mobile-to-mobile communications," *IEEE Trans. Commun.*, vol. 53, no. 11, 2005.

[54] Patel, C. S., Stuber, G. L., and Pratt, T. G., "Statistical properties of amplify and forward relay fading channels," *IEEE Trans. Veh. Technol.*, vol. 535, no. 1, 2006.

[55] Patel, C. S., *Channel modeling and estimation for OFDM based mobile-to-mobile communications*. Georgia Institute of Technology, Atlanta, GA, 2003. MS Thesis.

[56] Patzold, M., *Mobile fading channels*. West Sussex, UK: John Wiley & Sons, 2002.

[57] Patzold, M., Killat, U., and Laue, F., "On the problems of Monte Carlo method based simulation models for mobile radio channels," *Proc. IEEE 4th Int'l Symp. on Spread Spectrum Techniques & Applications*, pp. 1214–1220, Sept. 1999.

[58] Pätzold, M., Killat, U., and Laue, F., "A deterministic model for a shadowed Rayleigh land mobile radio channel," *Proc. of 5th IEEE Int'l Symp. on Personal, Indoor and Mobile Communications*, vol. 3, pp. 1202–1210, Sept. 1994.

[59] Pätzold, M., Killat, U., and Laue, F., "A deterministic model digital simulation for Suzuki processes with application to a shadowed Rayleigh land mobile radio channel," *IEEE Trans. Veh. Technol.*, vol. 45, pp. 318–331, May 1996.

[60] Pätzold, M., Killat, U., Laue, F., and Li, Y., "A new and optimal method for the derivation of deterministic simulation models for mobile radio channels," *Proc. IEEE 46th Veh. Technol. Conf.*, pp. 1423–1427, May 1996.

[61] Pätzold, M. and Szczepanski, A., "Methods of modeling of specified and measured power delay profiles," *Proc. IEEE 51st Veh. Technol. Conf.*, pp. 1787–1792, May 2000.

[62] Pop, M. and Beaulieu, N., "Limitations of sum-of-sinusoids fading channel simulators," *IEEE Trans. Commun.*, vol. 49, pp. 699–708, Apr. 2001.

[63] Proakis, J. G., *Digital Communications*. New York: McGraw-Hill, 1998.

[64] Ramaswami, R. and Sivarajan, K. N., *Optical Networks*. San Francisco, CA: Morgan-Kauffman, 2002.

[65] Rappaport, T. S., *Wireless Communications: Principles and Practice*. Upper Saddle River, NJ: Prentice-Hall, 1996.

[66] Sandell, M., *Design and analysis of estimators for multi-carrier modulation and ultrasonic imaging*. Lulea University of Technology, Sweden, 1996. PhD dissertation.

[67] Schafhuber, D., Matz, G., and Hlawatsch, F., "Simulation of wideband mobile radio channels using subsampled ARMA models and multistage interpolation," *Proc. 11th IEEE-SP Workshop on Statistical Signal Processing*, pp. 571–574, Aug. 2001.

[68] Scharf, L., *Statistical Signal Processing: Detection, Estimation and Time Series Analysis*. New Jersey: Addison Wesley, 1991.

[69] Sendonaris, A., Erkip, E., and Aazhang, B., "User cooperation diversity - Part I: System description," *IEEE Trans. Commun.*, vol. 51, pp. 1927–1938, Nov. 2003.

[70] Sendonaris, A., Erkip, E., and Aazhang, B., "User cooperation diversity - Part II: Implementation aspects and performance analysis," *IEEE Trans. Commun.*, vol. 51, pp. 1939–1948, Nov. 2003.

[71] Simon, M. K., *Probability Distributions Involving Gaussian Random Variables: A Handbook for Engineers and Scientists*. Boston: Kluwer Academic Publisher, 2002.

[72] Simon, M. K. and Alouini, M. S., *Digital Communication over Fading Channels: A Unified Approach to Performance Analysis*. New York: John Wiley and Sons, 2000.

[73] Steele, R., *Mobile Radio Communications*. London, UK: Pentech Press, 1992.

[74] Stüber, G. L., *Principles of Mobile Communications*. Netherlands: Kluwer Academic Publishers, 2001.

[75] Telatar, I., "Capacity of multi-antenna Gaussian channels," *Eur. Trans.Telecommun.*, vol. 10, pp. 585–595, Nov. 1999.

[76] Toh, C. K., *Ad-hoc Mobile Wireless Networks: Protocols and Systems*. Upper Saddle, NJ: Prentice-Hall, 2001.

[77] Tong, L., Sadler, B. M., and Dong, M., "Pilot-assisted wireless transmissions: general model, design criteria, and signal processing," *IEEE Signal Proc. Mag.*, vol. 21, pp. 12–12, Nov. 2004.

[78] Tse, D. and Vishwanath, P., *Fundamentals of Wireless Communication*. New York: Cambridge University Press, 2005.

[79] Uysal, M. and Mheidat, H., "Maximum-likelihood detection for distributed space-time block coding," *Proc. IEEE Veh. Technol. Conf.*, vol. 4, pp. 2419–2423, Sept. 2004.

[80] Vatalaro, F. and Forcella, A., "Doppler spectrum in mobile-to-mobile communications in the presence of three-dimensional multipath scattering," *IEEE Trans. Veh. Technol.*, vol. 46, pp. 213–219, Feb. 1997.

[81] Wang, R. and Cox, D. C., "Channel modeling for ad-hoc mobile wireless networks," *Proc. of IEEE Veh. Technol. Conf.*, vol. 1, pp. 21–25, May 2002.

[82] Wang, R. and Cox, D. C., "Double mobility mitigates fading in ad-hoc wireless networks," *Proc. IEEE AP-S Int'l Symp.*, vol. 2, pp. 306–309, 2002.

[83] Xiao, C. and Zheng, Y. R., "A statistical simulation model for mobile radio fading channels," *Proc. IEEE Wireless Commun. & Networking Conf.*, vol. 1, pp. 144–149, Mar. 2002.

[84] Young, D. and Beaülieu, N., "The generation of correlated Rayleigh random variates by inverse discrete fourier transform," *IEEE Trans. Commun.*, vol. 48, pp. 1114–1127, 2000.

[85] Zheng, Y. R. and Xiao, C., "Improved models for the generation of multiple uncorrelated Rayleigh fading waveforms," *IEEE Commun. Lett.*, vol. 6, pp. 256–258, Aug. 2002.

[86] Zheng, Y. R. and Xiao, C., "Simulation models with correct statistical properties for Rayleigh fading channelss," *IEEE Trans. Commun.*, vol. 51, no. 6, pp. 920–928, 2003.

[87] Zheng, Y. R., Xiao, C., and Beaulieu, N., "Statistical simulation models for Rayleigh and Rician fading," *Proc. IEEE Int'l Commun. Conf.*, vol. 65, pp. 3524–3529, 2003.

[88] Zogas, D. A., Karagiannidis, G. K., Sagias, N. C., Tsiftsis, T. A., Mathiopoulous, P. T., and Kotsopoulous, S. A., "Dual hop wireless communications over Nakagami fading," *Proc. IEEE Veh. Technol. Conf.*, vol. 4, pp. 2200–2204, May 2004.

VITA

Chirag Patel was born in Baroda, India, on January 4, 1979 to Meeta and Suresh Patel. He spent initial 22 years of his life at his birthplace Baroda while completing his school and undergraduate engineering studies. He received Bachelor of Engineering (Electronics) degree from Maharaja Sayajirao University of Baroda in 2001 and was awarded the University Gold Medal for securing the 1st rank in the final year of the B. E. degree. He received his M.S. degree from Georgia Institute of Technology, Atlanta in August 2003. From August 2001 to April 2006, he worked under the tutelage of Professor Gordon Stüber, at the Wireless Systems Lab, Georgia Institute of Technology, Atlanta, USA, for his doctoral research. He received the Doctor of Philosophy degree in Electrical and Computer Engineering from Georgia Institute of Technology in May 2006. He spent the Summer of 2005 at Corporate R&D Division of Qualcomm, Inc. His research interests include wireless channel modeling and estimation and statistical signal processing. In his spare time, he enjoys cricket, music and current affairs.